

https://dspace.org/

The effects of dilatancy in unbound granular pavements on the load carrying capacity predicted by the South African Mechanistic-Empirical Design Method

Nxumalo, Winston Nhlanhla

2014-09-03
http://hdl.handle.net/10539/15375

Downloaded from a DSpace repository. https://dspace.org/



UNIVERSITY OF THE WITWATERSRAND

School of Civil & Environmental Engineering

Master of Science Research Project Report

"The effects of dilatancy in unbound granular pavement materials on the load carrying capacity predicted by the South African Mechanistic-Empirical Design Method"

Name: Winston Nxumalo

Student number: 0303157H

Email: nxumalo@jaws.co.za

Course Code: CIVN7019

Course Coordinator: Dr. I Luker

THE EFFECTS OF DILATANCY IN UNBOUND GRANULAR PAVEMENTS ON THE LOAD CARRYING CAPACITY PREDICTED BY THE SOUTH AFRICAN MECHANISTIC-EMPIRICAL DESIGN METHOD

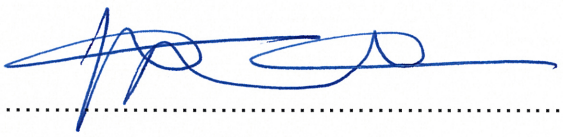
Winston Nhlanhla Nxumalo

A research report submitted to the Faculty of Engineering and the Built Environment, University of the Witwatersrand, Johannesburg, in fulfillment of the requirements for the degree of Master of Science in Engineering by 50 % coursework and 50 % research.

Johannesburg, 2014

DECLARATION

I declare that this research report is my own unaided work. It is submitted for the Degree of Master of Science to the University of the Witwatersrand, Johannesburg. It has not been submitted before for any degree or examination to any other University.



.....

Winston Nhlanhla Nxumalo

24th day of May year 2014

SUMMARY

In South Africa the use of relatively thin (< 50 mm) asphaltic concrete surfaces is a popular method of providing a good all-weather surfacing for flexible pavements. A typical layered pavement structure consists of the surfacing, then the base and subbase structural layers, followed by one or two selected layers on top of the insitu subgrade material. Traffic loading is applied on the pavement through the vehicle's tyres resulting in induced repeated dynamic stresses and strains. A well designed pavement transfers these induced dynamic stresses and strains from the surface of the pavement to an insitu subgrade material such that predetermined failure criteria are prevented for a specified period. In South Africa the South African Mechanistic Empirical Design Method (SAMDM) was developed for pavement analysis and design.

The SAMDM was developed in the late 1960s and early 1970s. The SAMDM has gained substantial popularity in South Africa over other methods such as the CBR method and the AASHO method. It has been found that as a design tool the SAMDM provides the pavement designer with a reasonable level of confidence in the pavement structure and the estimated pavement design life. However, despite the SAMDM's popularity, the method is still subject to much scrutiny and criticism. For example the SAMDM is too sensitive to variability of input parameters. This research report provides a brief review of the SAMDM as a design tool and highlights the method's key components and its development. The report then focuses on the dilatancy of granular materials under shear stresses.

Granular materials subjected to shear stresses dilate as the particles move over each other. The volume expansion is localised to the zone of influence under the wheel load. The surrounding material does not expand, and this typically results in an increase in confining stresses developed within the material, leading to an increase in the material's stiffness. The principles and theory of dilatancy were investigated to evaluate the influence that dilation has on the load carrying capacity predicted by the SAMDM. This report discusses in detail the concept of granular material dilation developed by Rowe (1962) in the fundamental stress-dilatancy theory and subsequent developments and improvements to the theory are also highlighted. The literature published after Rowe's publication is generally found to cement the fundamental principles first introduced by Rowe.

Following the literature review, laboratory investigations were conducted with the aim of determining quantitative results for the shear and dilation properties of two locally sourced granular materials. The shear and dilation properties were then used as input parameters in the finite element analyses carried out. The laboratory testing program was conducted at the University of the Witwatersrand soils laboratory. The two gravel materials were obtained from the Blue Platinum Quarry in Lanseria. Standard laboratory tests, comprising: the sieve

analysis, Atterberg tests, specific gravity tests, compaction tests and CBR tests were carried out on the two materials to classify them according to the TRH 14 (CSRA, 1985) system. The materials were classified as a G4 (Material 1 in this report) and G1 (Material 2). In addition to the standard tests, the laboratory's large shear box was used to test the materials' shear resistance properties and obtain the shear parameters cohesion c, peak friction angle ϕ_p and critical friction angle ϕ_{cv}. Also measured were the dilation properties: the angle of dilatancy ψ and the mobilised shear resistance at the onset of dilation. It was found that at the onset of dilation an average of 64 % of the peak shear strength is mobilised, while approximately 90 % of the peak friction angle was mobilised. It was also demonstrated that very small shear displacements are required to mobilise the majority of the peak shear strength and peak friction angle in granular materials.

The influence of dilatancy on the load carrying capacity of a typical flexible pavement predicted by the SAMDM was then evaluated. Differences in the principal stresses and strains predicted from finite element analyses using the simple linear elastic model and the more complex elastic plastic model which incorporates dilatancy were compared. Using two different FEA packages (SIGMA/W and PLAXIS) it was demonstrated that the higher order elastic plastic constitutive model did not yield the stresses and strains required in the SAMDM which were significantly different to those computed using the first order linear elastic model. There was agreement between the linear elastic model results of both FEA packages. In both FEA packages, the elastic-plastic model with yielding of the soil according to the Mohr-Coulomb failure criterion calculated a lower major principal stress when using SIGMA/W and a higher major principal stress calculated with PLAXIS in the base layer compared to the linear elastic model of each model respectively. The linear elastic model (both PLAXIS and SIGMA/W) and the elastic plastic model (PLAXIS) predicted tensile minor principal stresses in the subbase layer while the elastic plastic model in PLAXIS predicted zero stresses at the same location due to its tension cut-off formulation which results in stress redistribution to ensure that no tension zones are predicted in the soil. The tension cut-off formulation was found to have a significant impact on the stresses and strains predicted by the PLAXIS FEA package. Incorporating dilation into the stress-strain computation affected the resultant stresses and strains to a lesser degree.

The accuracy of the predicted stresses and strains is important for calculating the correct factor of safety (FoS) and number of load repetitions before failure. Variations in the dilatancy angle (ψ) affect the calculated principal stresses and strains and thus influence the predictions of the FoS and load repetitions before failure. Variations of the principal stresses due to small increments in ψ were therefore evaluated. It was found that small variations in ψ affect the major and minor principal stresses predicted by the two FEA packages to different

degrees. Gradual increases in ψ up to 20 % led to gradual increases in σ_1 values predicted by SIGMA/W while increasing ψ led to decreasing values of σ_1 predicted by PLAXIS. Similarly, gradual increases in ψ led to gradual increases of the predicted σ_3 values in the base layer in SIGMA/W and gradual decreases in PLAXIS. The results indicate that the effect of small variations in the angle of dilatancy on the predicted major and minor principal stresses: 1) depends on the FEA package used to calculate the stresses; 2) depends on the formulation of the constitutive model which is selected for the analysis; and 3) is in general very small and possibly negligible. It is therefore concluded that in the elastic plastic model which incorporates dilatancy of soil, the calculated stresses are not highly sensitive to small variations in the dilatancy parameter ψ.

Consideration of the influence which small variations in ψ have on the FoS and predicted load repetitions before failure demonstrated that variations in ψ up to 20 % have small effect on both the calculated factor of safety and the predicted number of load repetitions before failure of the base layer. Gradually increasing ψ resulted in gradual decreasing of both the calculated factor of safety and the number of load repetitions in the PLAXIS FEA package, while it resulted in gradual increase of both the FoS and the load repetitions from the SIGMA/W results. In SIGMA/W a 20 % increase in ψ resulted in an increase of 0.21 % and 1.02 % for the calculated factor of safety and the number of load repetitions respectively. In the PLAXIS package a 20 % increase in ψ led to a decrease of the calculated factor of safety and the number of load repetitions of 0.41 % and 3.16 % respectively. It was thus concluded that the SAMDM is not overly sensitive to small variations in the dilatancy input parameter.

Comparison of the calculated FoS and load repetitions to failure using the stresses computed in the elastic plastic model formulation of the SIGMA/W and PLAXIS FEA packages illustrated that the formulation of the constitutive model used in the selected FEA package has a large effect on the FoS and predicted load repetitions to failure. The formulation of the elastic plastic model in PLAXIS, which incorporates dilatancy and a tension cut-off function, calculated major and minor principal stresses which, using the transfer functions of the SAMDM, predicted load repetitions which were orders of magnitude (up to 17 times) higher than those predicted using the SIGMA/W package. Incorporating a tension cut-off formulation in the FEA model, appears to have had a significant effect on the calculated stresses and strains and also overcame the computation of inadmissible stresses and strains which lead to FoS values which are less than one and predict almost immediate failure of the pavement layer.

...to Nairobi, her mother and my entire family....

And in loving memory of KutloManyaka.

I thank GOD, the creator of all heaven and earth!

I also extend my sincerest gratitude to HIM for bringing the following people into my walk who have made this work possible; My supervisor Dr Irwin Luker, the Chief Lab Technician, Mr. Norman Alexander, Mrs. Thembi Mtselu – Faculty administrator, Thabiso at AfrisamJukskei Quarry and the staff of Afrimat Blue Platimum Quarry.

CONTENTS

TITLE PAGE i

DECLARATION ii

SUMMARY iii

DEDICATION vi

ACKNOWLEDGEMENTS vii

CONTENTS viii

LIST OF FIGURES xi

LIST OF TABLES xiii

LIST OF SYMBOLS xiv

LIST OF ABBREVIATIONS xvi

CHAPTER 1 1

INTRODUCTION 1

1.1. Background to research 1

1.2. Problem Statement 2

1.3. Objectives of research 3

1.4. Scope and limitation of the research 3

1.5. Composition of the research report 4

CHAPTER 2 5

LITERATURE REVIEW AND THEORY 5

2.1. Introduction 5

2.2. The South African Mechanistic-Empirical Design Method (SAMDM) 8

2.3. Pavement Loading 15

2.4. Pavement analysis 20

2.5. Granular materials 22

2.6. Dilatancy 45

LITERATURE REVIEW SUMMARY AND FINDINGS 59

CHAPTER 3 62

INVESTIGATIONAL WORK 62

3.1. Sample Preparation 62

3.2. Methodology 63

3.3. Results 67

CHAPTER 4 85

INFLUENCE OF DILATANCY ON THE LOAD CARRYING CAPACITY PREDICTED BY SAMDM 85

4.1. Influence of dilatancy on the calculation of stresses and strains 85

4.2. Influence of varying the angle of dilation ψ on SAMDM input stresses 95

4.3. Influence of variations in ψ on the factor of safety (FoS) and predicted load repetitions 99

CHAPTER 5 103

CONCLUSIONS AND RECOMMENDATIONS 103

5.1. Conclusions 103

5.2. Recommendations 107

REFERENCES 108

BIBLIOGRAPHY 117

APPENDIX 1 ..... A1

APPENDIX 2 ..... A2

LIST OF FIGURES

Figure 1-1: Typical layered pavement structure (after Theyse & Kannemeyer, 2010)..... 1
Figure 1-2: Tyre influence zone (This study) 2
Figure 1-3 2
Figure 2-1: Loops 5 and 6 of the AASHO Road Test Layout (Highway Research Board, 1961) 6
Figure 2-2: Aerial view of one loop during testing (Highway Research Board, 1961)..... 6
Figure 2-3: Basic procedure of mechanistic design analysis 20
Figure 2-4: Relation between measured values of maximum dry density (Vibratory) expressed in terms of space occupied by solids and Grading Factor for original materials investigated plus two metalliferous Ore with gradings that have Abundance, Sufficient Amount, or Lack of Fines (after Semmelink and Visser, 1994) 26
Figure 2-5: General multi-layer elastic system (after Yoder & Witczak, 1975) 29
Figure 2-6: Secant resilient modulus model (Theyse, 2007).....32
Figure 2-7: Tangent resilient modulus model (Theyse, 2007).....32
Figure 2-8: FEA (After Kim *et al.*, 2009) 33
Figure 2-9: Nonlinear stress-strain behaviour (Geo Slope International, 2007).....35
Figure 2-10: Elastic-perfectly plastic constitutive relationship (Geo Slope International, 2007)..36
Figure 2-11: The Mohr-Coulomb yield surface in principal stress space (c = 0) (Brinkgreve *et al.*, 2002).....37
Figure 2-12: Stress strain relationship in primary loading for standard drained triaxial test (Brinkgreve *et al.*, 2002).....39
Figure 2-13: Definition of tangent stiffness modulus in oedometer test (Brinkgreve *et al.*, 2002) 40
Figure 2-14: Successive yield loci for various values of the hardening parameter γ^P. (Brinkgreve *et al.*, 2002).....41
Figure 2-15: Hysteresis loop for non-elastic permanent deformation behaviour (after Wolff, 1996; Lekarp *et al*., 2000b and Theyse, 2007) 44
Figure 2-16: Stress-strain behaviour of dense sand in plane compression (a) at low stress (b) at high stress (Bolton, 1986) 45
Figure 2-17: Illustration of interface dilation using serrated edges sliding past each other (after Rowe, 1962) 46
Figure 2-18: Geometric packing (elevations) of rods considered by Rowe (a) parallel stack (b) uniform spheres in face centered cubic packing (after Rowe, 1962) 48
Figure 2-19: Simple wedge analysis (after Rowe, 1962) 48
Figure: 2-20: Imaginary plane of particle interlock (Rowe, 1962).....50

Figure 2-21: Typical data of stress ratio R =σ'_1/σ'_3 and volumetric strain plotted against axial strain for Sand O and Sand L at σ'_3 = 100 kPa (After Guo & Su, 2007) 55
Figure 2-22: Measured shear strength of (a) Sand O and (b) Sand L for different void ratios at σ'_3 = 100 kPa (after Guo and Su, 2007).....56
Figure 2-23: Relationships between friction angle ϕ_p and ψ_{max} (after Guo & Su, 2007).....56
Figure 2-24: Contributions to shear resistance of granular materials (a) alternative conceptual model proposed by Guo and Su (2007) (b) revised from Rowe (1962).....56
Figure 3-1: Laboratory shear box test set-up schematic.....65
Figure 3-2: Sieve analysis results for materials BPQ 1 and BPQ 2.....69
Figure 3-3: Penetration curve - BPQ 1 69
Figure 3-4: Penetration curve BPQ 2 69
Figure 3-5: USDA soil matrix textural classification (Davis & Bennet, 1927) 70
Figure 3-6: USDA full soil sample textural classification (Davis & Bennet, 1927).....70
Figure 3-7: Material 1-Shear resistance vs. Shear displacement.....74
Figure 3-8: Material 2-Shear resistance vs. Shear displacement.....74
Figure 3-9: Material 1- Peak Shear Strength & Residual Shear Strength vs. Normal Stress……..74
Figure 3-10: Material 2- Peak Shear Strength & Residual Shear Strength vs. Normal Stress....74
Figure 3-11: Material 1: Vertical displacement vs. Shear displacement.....76
Figure 3-12: Material 1: Rate of dilation vs. Shear displacement.....76
Figure 3-13: Material 2 - Vertical displacement vs. Shear displacement.....77
Figure 3-14: Material 2 - Rate of dilation vs. Shear displacement.....77
Figure 3-15: Shear resistance mobilised at onset of dilation.....79
Figure 3-16: Development of shear band in laboratory specimens (Shibuya *et al.*, 1997) 80
Figure 3-17: Simple shear condition assumed in direct shear box test (Shibuya et al., 1997)....81
Figure 3-18: Directions of principal stress and strain increments and the angle of dilatancy ψ in simple shear (Shibuya et al., 1997) 82
Figure 3-19: Sketch of shear displacement (u) and vertical displacement (v) 83
Figure 4-1: Principle of super-positioning in dual tyre loading.....86
Figure 4-2: Axisymmetric analysis for dual tyre loading.....87
Figure 4-3: Pavement model geometry 88
Figure 4-4: Finite Element Mesh generated in PLAXIS 90
Figure 4-5: Finite Element Mesh generated in SIGMA/W 90
Figure 4-6: Variation of major principal stress with angle of dilation 98
Figure 4-7: Variation of minor principal stress with angle of dilation 98
Figure 4-8: Effect of varying ψ on the calculated FoS and predicted number of load repetitions to failure.....100

LIST OF TABLES

Table 2-1: Factor of Safety limiting criteria (Maree, 1978) 10
Table 2-2: Results from Jooste (2004) showing the influence of variation in assumed pavement layer material types and properties on predicted base layer structural capacity 13
Table 2-3: Legally permissible axle loads on South African public roads (CSRA, 1996) 15
Table 2-4: Recommended interim vertical contact Load/Stress values for mechanistic design analysis (De Beer *et al.*, 1999) 17
Table 2-5: Stress dilatancy relationships 54
Table 2-6: Summary of proposed relationships for describing the evolution of ϕ_f (Been and Jefferies, 2004) 54
Table 3-1: Data logger output calibration constants 66
Table 3-2: Properties of test samples 68
Table 3-3: Material 1 (BPQ 1) Shear box test moisture and achieved compaction results 71
Table 3-4: Material 2 (BPQ 2) Shear box test moisture and achieved compaction results 72
Table 3-5: Summary of material shear strength properties 72
Table 3-6: Typical shear strength parameter for unbound granular materials (SANRAL, 2013) 73
Table 3-7: Shear displacement at onset of dilation (This study) 75
Table 3-8: Material dilation properties 78
Table 4-1: Input parameters required in SAMDM obtained from FEA analysis 86
Table 4-2: Constitutive models used in finite element analysis 88
Table 4-3: FEA results PLAXIS (This study) 91
Table 4-4: FEA results SIGMA/W (This study) 92
Table 4-5: FEA results - PLAXIS vs. SIGMA/W (This study) 93
Table 4-6: FEA ψ input variation for base layer only (This study) 96
Table 4-7: Effect of variations in ψ on the calculated major and minor principal stresses in base layer only 97
Table 4-8: Variation in FoS and predicted load repetitions to failure due to variations in ψ 100

LIST OF SYMBOLS

α	Geometric angle of packing
β	Angle of deviation of the tangent at contact points from the direction of the applied force
e	Void ratio
e_o	Initial void ratio
ε	Strain
ε_v	Volumetric strain
$\dot{\epsilon}_1$	Rate of major principal strain change
$\dot{E}$	Ratio of internal work done (work in/work out)
E	Elastic Modulus
ν	Poisson ratio
γ	Shear strain
ψ	Angle of dilation
ψ_{sp}	State parameter (= e - e_0)
σ	Normal stress (kPa)
σ'_1	Major principal effective stress
σ'_3	Minor principal effective stress
τ	Shear stress (kN/m^2)
π	Pi constant (= 3.14)
ϕ'	The angle of shearing resistance
ϕ'_{max}	Maximum angle of shearing resistance representing the peak strength of dense sand in the Coulomb theory
ϕ'_{cv}	Critical state angle of shearing resistance occurring at strains where shearing occurs at constant volume

ϕ'_f	Angle of friction accounting for reduced value of ϕ' corrected for energy due to expansion
ϕ'_μ	True friction angle between surfaces of the sand particles
M_R	Resilient Modulus

LIST OF ABBREVIATIONS

2D	Two Dimensional
3D	Three Dimensional
AASHO	American Association of State Highway Officials
AASHTO	American Association of State Highway and Transportation Officials
ARD	Apparent Relative Density
BRD	Bulk Relative Density
CAPSA	Conference on Asphalt Pavements in South Africa
CBR	California Bearing Ratio
CC	Coefficient of Curvature
CSRA	Committee of State Road Authorities
CU	Coefficient of Uniformity
DCP	Dynamic Cone Penetrometer
FoS	Factor of Safety
FEA	Finite Element Analysis
FWD	Falling Weight Deflectometer
HVS	Heavy Vehicle Simulation
LHS	Left Hand Side

LL	Liquid Limit
LS	Linear Shrinkage
LVDTs	Linear Variable Differential Transducers
MLLE	Multi-Layer Linear Elasticity
MDD	Maximum Dry Density
NP	Non Plastic
PL	Plastic Limit
PN	Pavement Number
RHS	Right Hand Side
SAMDM	South African Mechanistic – Empirical Design Method
SG	Specific Gravity
SIM	Stress-In-Motion
SN	Structural Number
SR	Stress Ratio
SRD	Solid Relative Density
TMH	Test Method for Highways
TRH	Technical Recommendations for Highways
TRRL	Transport and Roads Research Laboratory

VRSPTA	Vehicle Road Surface Pressure Transducer Array

CHAPTER 1

INTRODUCTION

1.1. Background to research

Pavement design is the process of determining the most economical combination of layer thicknesses and material types which enables a pavement, whether flexible, rigid or composite, to support the design traffic loading. In South Africa the use of relatively thin (< 50 mm) flexible asphaltic concrete surfaces is a popular method of providing a good all-weather surfacing for flexible pavements (De Beer *et al.*, 1999). These granular pavements typically comprise a thin bituminous surfacing, a base of unstabilised gravel or crushed stone and a granular or cemented subbase supported by the insitu subgrade. One or two selected layers normally constructed with granular material are included in the pavement subgrade structure in cases where the insitu subgrade material does not have adequate strength to support the subbase and base layers directly. Figure 1-1 shows the typical layer configuration of a flexible pavement.

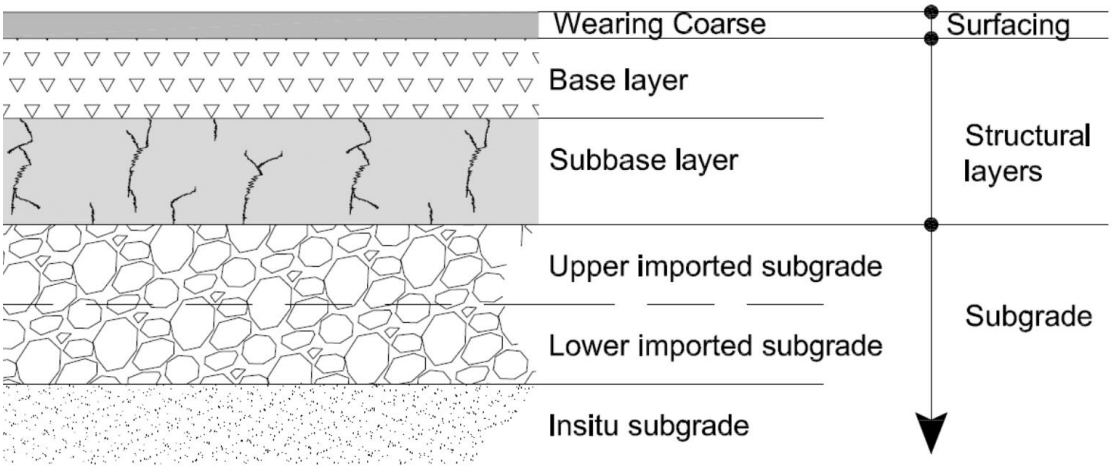


Figure 1-1: Typical layered pavement structure (after Theyse & Kannemeyer, 2010)

When vehicles travel on a flexible pavement repeated dynamic stresses are induced. These stresses are vertical contact stresses (z direction), Longitudinal Contact Stresses (in direction of moving wheel) and Lateral Contact Stresses (orthogonal to moving wheel). The pavement is designed to transfer these repeated dynamic stresses from the surface of the pavement to an insitu subgrade material such that predetermined failure criteria are prevented for a specified period. To achieve this, the South African Mechanistic-Empirical Design Method (SAMDM) was developed in the late 1960s and early 1970s.

1.2. Problem Statement

The literature review undertaken in Chapter 2 of this research report suggests that the SAMDM, despite its popular use in road pavement design and rehabilitation, is too sensitive to the variability of input parameters in predicting pavement life. Observations and monitoring of constructed flexible pavements in South Africa indicate that pavements often last much longer than the estimates for pavement life predicted using the SAMDM (Theyse & Kannemeyer, 2010).

Dilation of granular materials under shear stress is one of the mechanisms in a structural unbound granular pavement which may influence the accuracy of predicted pavement layer life. Granular materials subjected to shear stresses dilate as the particles move over each other. This volume increase is limited to the material within the dilating zone under the wheel load, shown in Figure 1.2. The material beyond the dilating zone imposes passive reactive confining stresses on the dilating material, increasing its stiffness. Dilatancy is investigated in this report to evaluate its influence on the load carrying capacity predicted by the SAMDM.

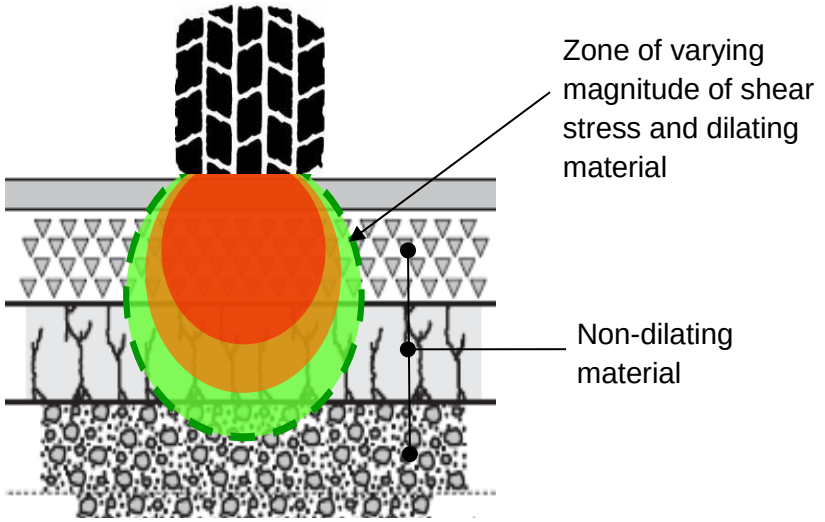


Figure 1-2: Tyre influence zone (This study)

1.3. Objectives of research

This research is aimed at studying the effect of dilation in unbound granular pavement materials on the load carrying capacity of flexible pavements which is predicted by the South African Mechanistic-Empirical Design Method (SAMDM).

1.4. Scope and limitation of the research

The scope of the research undertaken is:

1. to provide a brief review of the SAMDM as a design tool and to highlight the method's key components and development, including pavement analysis, structural analysis and the transfer functions;
2. to describe granular material dilation;
3. to conduct laboratory experimental investigations to provide quantitative values of granular material dilatancy; and
4. to evaluate the effects which dilation has on:
    i. the stresses and strains, calculated using finite element analysis packages, which are then used in the SAMDM to predict the pavement response and
    ii. the prediction of the Factor of Safety (FoS) and load carrying capacity for a typical pavement.

This research focuses on the dilation of granular materials used in unbound pavement layers in South Africa. It does not address any other materials used in the construction of road pavements such as the bituminous asphalt layers, bitumen treated bases and cement treated layers. It is also not concerned with other aspects of road design such as geometric design, construction methods and economic analysis.

1.5. Composition of the research report

The research report consists of five chapters;

Chapter 1 provides an overview of the research. In this chapter the background to the research is given followed by the problem statement in which the dilation of granular material under shear stress is identified as the core focus. The objectives of the research and then the scope and limitations of the study are also discussed.

Chapter 2 contains a literature review covering (i) the development of the South African Mechanistic Empirical Design Method, (ii) pavement loading studies in South Africa and (iii) structural analysis of pavements in which the constitutive (material) models of two commercial software packages are described. This chapter also includes sections covering topics on the states of stress in granular pavement materials, failure of granular materials and a description of the development of the theory of dilatancy. A summary of the findings from the literature survey concludes the chapter.

Chapter 3 describes the laboratory investigational work that was carried out in this study. Standard laboratory tests to characterise the material which were conducted are described, followed by the methodology for the large shear box tests conducted. The chapter then presents the results for the standard laboratory tests leading to classification of the material, followed by the shear box test results in which the materials' shear resistance and dilation properties are given.

Chapter 4 presents evaluation of the influence that the dilatancy of granular pavement materials has on the load carrying capacity predicted by the SAMDM. Firstly the differences in the principal stresses and strains predicted from finite element analysis using the simple linear elastic model and the more complex elastic plastic model which incorporates dilatancy are described. Then the sensitivity of the SAMDM to small variations of the angle of dilation (ψ) is considered by evaluating i) variations of the principal stresses due to small increments in ψ and ii) the influence of variations in ψ on the calculated Factor of Safety (FoS) and the predicted number of load repetitions before failure.

Chapter 5 provides the overall conclusions from the research and recommends further development and research towards improving the SAMDM's ability to accurately predict induced stresses and strains and determine expected pavement layer structural capacity that is more accurate and agrees with observed overall pavement bearing capacity.

CHAPTER 2

LITERATURE REVIEW AND THEORY

2.1. Introduction

At the first Conference on Asphalt Pavements in South African (CAPSA) held in 1969, papers indicate that researchers and designers were no longer content with the limitations of the methods that were available at the time for pavement design and analysis (Ackerman, 1969; Brown, 1969; Burt, 1969; Dehlen, 1969; Marais, 1969). There were two methods that were in general use in South Africa up to the early 1970s, these were the California Bearing Ratio (CBR) design method and the method based on the American Association of State Highway Officials (AASHO) road test results.

The CBR method was developed during and after the Second World War by the U.S. Army Corps of Engineers. It was originally developed for the design of airport pavements having unbound granular bases (Porter, 1943), and was later adjusted and applied to road pavement design (Van Vuuren *et al.*, 1974).

The AASHO road test method is based on results from the AASHO road tests that were conducted near Ottawa in Illinois, U.S.A from October 1958 until December 1960. These road tests consisted of a series of experiments that were carried out by AASHO to determine traffic contribution to the deterioration of different highway pavement types. The tests consisted of six two lane loops shown in Figure 2-1 and Figure 2-2. Each lane was subjected to repeated cycles of loading by a specified vehicle. The pavement type and number of layers within each loop were varied in order to observe the deterioration caused in different pavements by various vehicle loads. The results from the AASHO road tests were then used to develop a pavement design guide that was first issued in 1961 as the “AASHO Interim Guide for the Design of Rigid and Flexible Pavements” (Highway Research Board, 1961). It was later updated in 1972 (AASHTO, 1972) and 1993 (AASHTO, 1993).

The AASHO road test method was adopted in South Africa for the design of the national roads (Ackerman, 1969). The method was a marked improvement on the CBR method, however it only overcame some and not all of the short-comings of the CBR method.

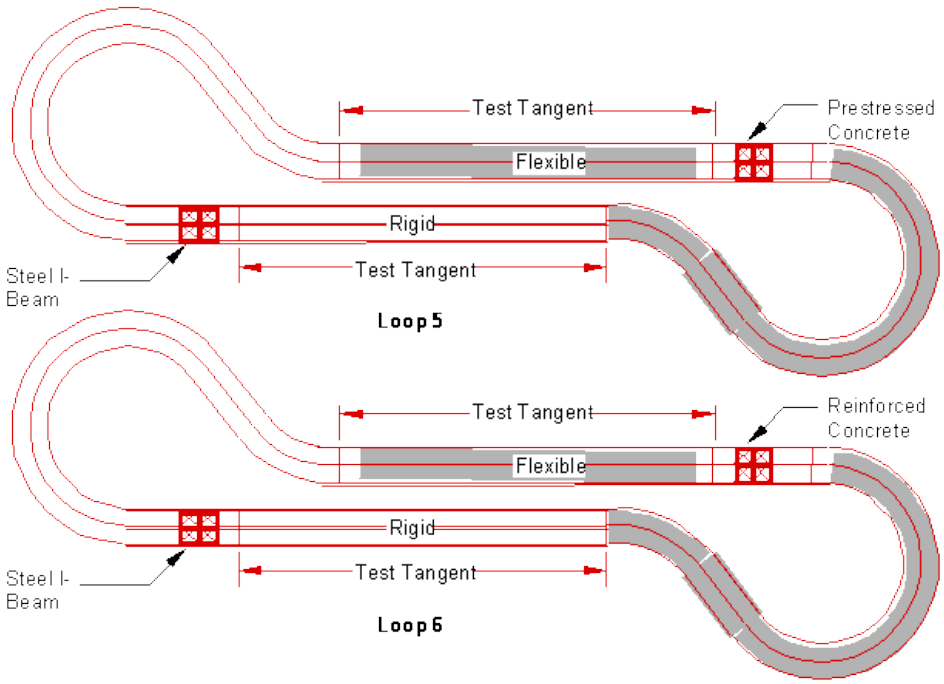


Figure 2-1: Loops 5 and 6 of the AASHO Road Test Layout (Highway Research Board, 1961)

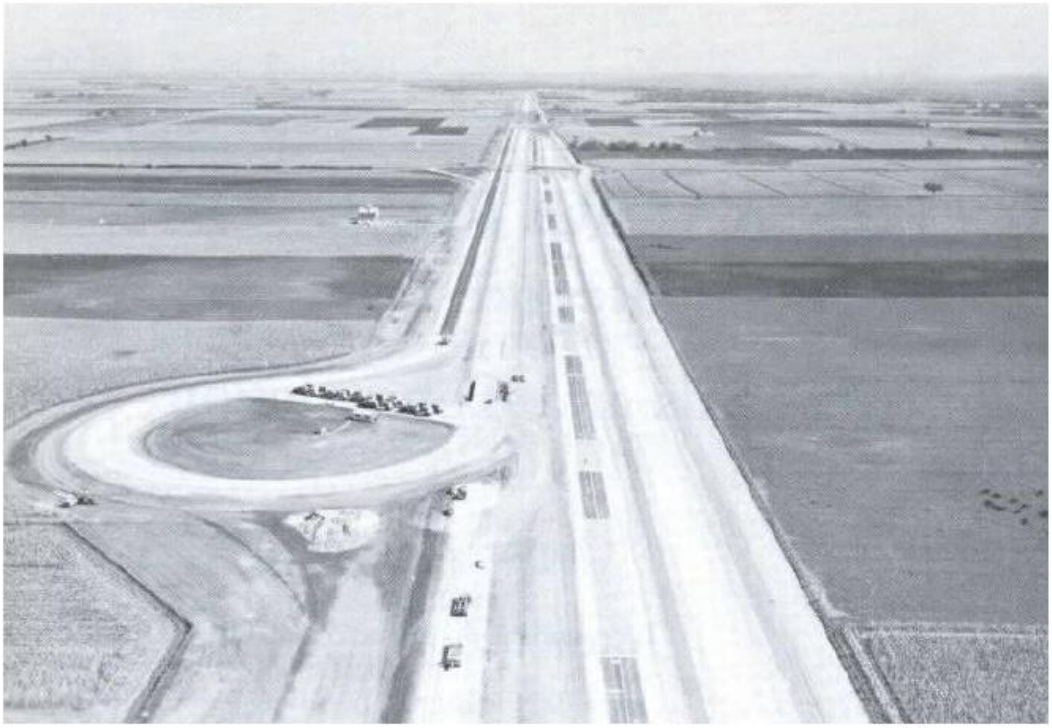


Figure 2-2: Aerial view of one loop during testing (Highway Research Board, 1961)

Both the CBR and AASHO road test methods are empirical and yield values for the thickness of cover required over the subgrade in order to limit the subgrade deformation under traffic. Dehlen (1969) discusses the dangers associated with this design approach and states that while the subgrade was adequately protected, the methods could possibly result in pavement structures which were structurally unbalanced i.e. the surfacing or base would be overstressed in compression, tension or shear. Brown (1969) also discussed the limitations of these largely empirical pavement design procedures. The main limitation of the CBR method was that in its basic form the procedure did not account for different strength characteristics of pavement materials or the effect of load repetitions. The method was also unable to accommodate pavement layers that had been stabilised either with cementitious or bituminous materials and could not be adapted for environments that differed from the environment in which it was empirically developed. The AASHO design procedure, similarly, could not distinguish between material strengths or account for the number of load repetitions.

The need for a rational design procedure became apparent, mainly due to the recognition of the limitations already mentioned, but also: (i) the relatively large number of premature pavement failure occurrences; (ii) the increased knowledge of fatigue behaviour of asphalt mixes and (iii) the increased incidence of heavy loads on national roads (Dehlen, 1969).

In the early 1970s South African pavement research, as in many other countries, was aimed at developing a rational approach to pavement design, similar to structural design procedures, where critical stresses and strains, throughout the pavement system, are limited to acceptable values, hence resulting in a structurally balanced pavement structure and averting premature pavement failure. Brown (1969) concluded that this rational method should limit the stresses in the base layer and lower selected layers and also limit the strains in the subgrade.

2.2. The South African Mechanistic-Empirical Design Method (SAMDM)

The first simplified mechanistic design procedure in South Africa was developed by Van Vuuren, Otte and Paterson during 1974 and published at the Second Conference on Asphalt Pavements held in 1974 (Van Vuuren *et al.*, 1974). The first comprehensive statement of the state of the art on the mechanistic design of pavements in South Africa was presented by Walker, Paterson, Freeme and Marais at the 1977 International Conference on Structural Design of Asphalt Pavements (Walker *et al.*, 1977). A detailed historical development of the SAMDM, from its first publication in 1974 until 1995 (when the SAMDM was updated for the purpose of revising the TRH4 1985: Catalogue of pavement design), is given by Theyse *et al.* (1996). Following the publication of the first simplified SAMDM procedure in 1974, research publications have been concerned with material and pavement behaviour models, design traffic, desired service levels, the economics of roads and the mechanistic design analysis which predicts the pavement bearing capacity through use of "transfer functions" (described in a following paragraphs).

The latest version of the SAMDM, comprehensively described in RP/19/83 (Freeme,1983), has been calibrated against the experience of road engineers from various road authorities in South Africa, and the method is still under review.

The SAMDM has received wide acceptance and use in South Africa, however the method is also subject to substantial scrutiny and criticism. The procedure of the SAMDM is to use a mathematical model of the pavement structure (for example Multi-Layer Linear Elasticity (MLLE)) to predict stresses and strains in the material caused by standard wheel loads. Salient values of these stresses and strains are then converted by so called "transfer functions" into predictions of the response of the pavement to many applications of the loads i.e. bearing capacity. The SAMDM is described in detail in Part 2.4 of this report. Jooste (2004) relates the problems associated with the SAMDM to the empirical element of the method, particularly the transfer functions used to predict the pavement response to applied stresses. Theyse and Kannemeyer (2010) attribute the shortcomings identified by Jooste to the incorrect calculation of the stress condition in unbound pavement layers. There are two methods in South Africa which are used to predict the plastic strain (permanent deformation) in pavements under repeated loading by relating the stresses applied onto the pavement to the yield strength of the unbound granular pavement material. These are the Factor of Safety (FoS) method by Maree (1978) and the Stress Ratio (SR) method by Theyse (2000).

A brief discussion of the permanent deformation and the damage model for unbound granular pavement layers under repeated loading follows here and precedes the description of both the FoS and Stress Ratio methods. Failure models of granular materials are discussed further in Part 2.5.3 of this report.

Theyse and Kannemeyer (2010) report that the dominant mode of distress for unbound granular pavement layers is the permanent deformation or plastic straining of the material which results in ruts observed on the surface. The plastic strain behaviour is often described by the plastic shakedown theory which is formulated in terms of the permanent deformation response of unbound granular materials under cyclic loading at a fixed load magnitude (Werkmeister, 2003; Theyse, 2007; Theyse & Kannemeyer, 2010). While the plastic shakedown theory provides a valid description of the plastic strain behaviour under repeated loading, it is not a useful model unless limiting criteria are set for the shakedown, particularly the plastic creep limit (Theyse & Kannemeyer, 2010).

Maree (1978) introduced the Factor of Safety (FoS) method defined by:

$$FoS = \frac{\sigma_1^y - \sigma_3}{\sigma_1^a - \sigma_3} \qquad \text{Eq. 2.1}$$

In terms of the Coulomb parameters this is:

$$FoS = \frac{K\left[\left(\sigma_3(\tan^2\left(45° + \frac{\phi}{2}\right) - 1)\right) + 2c\tan\left(45° + \frac{\phi}{2}\right)\right]}{\sigma_1^a - \sigma_3} \qquad \text{Eq. 2.2}$$

Where:

ϕ = angle of internal friction (°)

c = cohesion (kPa)

σ_1^y = effective triaxial yield strength of material (kPa)

σ_1^a = effective applied major principal stress in pavement (kPa)

σ_3 = effective applied minor principal stress in pavement (kPa)

K = constant: 0.65 for saturated conditions
0.80 for moderate moisture conditions
0.95 for normal moisture conditions

In Eq. 2.2 above ϕ is the peak friction angle representing the effective strength of a sand or gravel in the Mohr Coulomb theory.

Maree set the limit for the factor of safety in relation to the TRH 4 (CSRA, 1996) road classification Categories A, B or C and the (E80) design traffic (Table 2-1).

Table 2-1: Factor of Safety limiting criteria (Maree, 1978)

Road Category	Equivalent (E80) design traffic	Recommended Factor of Safety (FoS)
A	More than 10 million	1.6
	1 to 10 million	1.5
B	3 to 30 million	1.4
	0.1 to 1 million	1.3
C	0.1 to 1 million	1.2
	Less than 0.1 million	1.0

The FoS method is based on the Mohr-Coulomb theory incorporating shear strength parameters, cohesion (c) and angle of internal friction (ϕ) which are obtained from shear box or triaxial shear test results.

The FoS method safeguards against the rapid shear failure of unbound base layers by setting minimum requirements in terms of the ratio between the imposed shear stress and the shear strength of the material. Using a slightly different formulation, derived from the original FoS formulation, Theyse (2000) defined the second method for predicting plastic strains, termed the Stress Ratio (SR) method, which defines the inverse of the FoS as the critical parameter controlling the permanent deformation of unbound granular pavements.

Two alternative equations which define the Stress Ratio (SR) in slightly different ways were developed by Theyse (2000) and are given below. Eq. 2.3 defines the stress ratio in terms of the deviator stress (σ_1 - σ_3) while Eq. 2.4 defines the stress ratio in terms of the major applied principal stress (σ_1). Both equations are given first in terms of the yield strength (σ_1^y) should the yield strength be known and also in terms of the Mohr-Coulomb shear strength parameters.

$$SR = \frac{\sigma_1^a - \sigma_3}{\sigma_1^y - \sigma_3} = \frac{\sigma_1^a - \sigma_3}{\left(\sigma_3(\tan^2\left(45° + \frac{\phi}{2}\right) - 1)\right) + 2c\tan\left(45° + \frac{\phi}{2}\right)} \quad \text{Eq. 2.3}$$

$$SR = \frac{\sigma_1^a}{\sigma_1^y} = \frac{\sigma_1^a}{\left(\sigma_3\tan^2\left(45° + \frac{\phi}{2}\right)\right) + 2c\tan\left(45° + \frac{\phi}{2}\right)} \quad \text{Eq. 2.4}$$

Theyse and Kannemeyer (2010) report that plastic strain results by Maree (1978) and later by Theyse (2008) showed that the number of load repetitions which could be sustained by a pavement had a definite relationship with the stress ratio. But, when models based on this relationship were implemented in the SAMDM, counter-intuitive and inadmissible stress conditions (FoS < 1 and SR > 1) were calculated in the unbound granular pavement layers, which resulted in the design model predicting almost immediate failure of the pavement layers. However, Theyse and Kannemeyer (2010) report that roads, based on the designs in which counter-intuitive stress conditions were predicted, were constructed and provided good service for many years. The FoS and Stress Ratio (SR) models are based solely on stresses caused by external loads from traffic. Both models do not account for internally developed stresses such as the residual compaction stress, vertical overburden stress and equal all round internal suction pressure from matric suction (Theyse and Kannemeyer, 2010).

Theyse and Kannemeyer (2010) argue that the fundamentals of the SAMDM approach are valid and confirmed by recent research and that it is in fact not the fundamentals of the method which are inaccurate but the incorrect application of the method and assessment of the stress condition by not considering the actual effective stress condition in the pavement layers. They recommend a new approach to an accurate assessment of stresses which they suggest would lead to the successful implementation of the Stress Ratio (SR) method. The approach incorporates the effective stress condition developed in the pavement layer structure and the following stress components:

i. vertical overburden stress in combination with residual horizontal compaction stress;

ii. equal all round internal suction pressure resulting from matric suction in the partially saturated granular material;

iii. the three dimensional stresses caused by the external wheel load.

Theyse and Kannemeyer (2010) also mention that the stiffness of the components of the pavement structure increases under increasing confinement pressure and decreases under increasing shear stress, but the approach which they propose does not explicitly account for the effects of the increasing confinement pressure on the predicted stresses in the pavement, nor for the factors which would cause an increase in confinement pressure.

De Beer *et al.* (1999) gave an overview of the existing South African flexible pavement network with its associated research needs and the mechanistic pavement analysis and its evaluation issues. They give data showing typical rural pavement types and lengths in South Africa at the end of 1997. The data indicated that a very large potential for the design of mainly flexible asphaltic surfacings existed, because only 17.2 % of the total actual road network in South Africa, which included both provincial and national roads, was paved.

Considering that a service level requirement for national and provincial roads would require a surfaced road, this meant that there existed a potential that up to 80 % of the national and provincial road network in South Africa either needed to be rehabilitated or redesigned and reconstructed. Therefore a refined SAMDM method that results in more cost effective pavement design by accounting for all stresses present in the pavement mechanism is warranted.

De Beer *et al.* (1999) also published a list of research needs identified, and for the SAMDM the following are listed.

i. A definition and determination of appropriate traffic loading and tyre/pavement contact stresses to serve as inputs to SAMDM.

ii. A definition and determination of appropriate material input values for the prediction of traffic-associated cracking and plastic deformation in hot mix asphalt layers.

iii. Material inputs and models for the prediction of environmentally associated distress such as shrinkage cracking in asphalt surfacing.

iv. The relation of pavement design properties to asphalt mix design properties.

De Beer *et al*. (1999) found that opinions and roads needs studies had shown that there is little relation between material properties shown by laboratory test results, the mechanistic pavement designs and the surface distress types observed on South African roads. They also found that the traditional 20 kN dual load, 520 kPa, load/stress idealisation is outdated due to the increase in legal axle loads and the level of overloading on South African roads. De Beer *et al.* (1999) also concluded: 1) that studies indicated that more advanced mechanistic analysis methods incorporating advanced materials and load/stress models were not available; 2) they should be developed; and 3) that an improved mechanistic method should be developed for the prediction of pavement performance. The latter should be done by an improvement of both the material modeling (constitutive models), and the definition of the tyre/pavement contact stress.

Jooste (2004) illustrated the sensitivity of the predicted load carrying capacity of a typical pavement designed by the SAMDM to variation in the material input parameters. A typical design example was used, with a base case scenario using material parameters sourced from published values for specific material types. Variations were then considered by carrying out the same analysis using different material property inputs and then comparing the predicted number of load repetitions before failure for the base layer. The following variations were considered.

V1 Support stiffness for the base was changed by decreasing the subbase modulus from 450 MPa to 400 MPa, resulting in a decreased confining stress.

V2 Poisson's ratio of the granular base layer was changed by increasing it from 0.35 to 0.38, resulting in an increase in confining stress.

V3 The base material was changed from Pretoria Norite to Saldana Granite (increasing the cohesion and friction angle values from 53 kPa to 58 kPa and 55.1 ° to 56.7 ° respectively).

V4 The base material type was changed from Pretoria Norite to a Quartzite (decreasing the cohesion and friction angle values from 53 kPa to 48 kPa and 55.1 ° to 53.1 ° respectively).

The following results were obtained:

Table 2-2: Results from Jooste (2004) showing the influence of variation in assumed pavement layer material types and properties on predicted base layer structural capacity

	Base Case	Variation 1 (V1)	Variation 2 (V2)	Variation 3 (V3)	Variation 4 (V4)
Allowable Loads in base layer (Millions)	10.7	4.2	54.5	33.1	3.7

What is pertinent to note is the comparison of the base case to variations V1 and V2. Both these cases are small variations in material property inputs which result in a change in the confining stress. The decrease in the confining stress, by reducing the subbase elastic modulus, leads to a significantly reduced predicted load carrying capacity (in this case by 60.7 %). However, increasing Poisson's ratio (ν) from 0.35 to 0.38, which would have the effect of increasing confining stress, leads to an enormous increase in the predicted load carrying capacity of 409 %.

Variations V3 and V4 involve changes to the cohesion and friction angles. Small increases in the cohesion and friction angle (V3) lead to a 209.3 % increase in the predicted load capacity and small decreases in the values (V4) lead to a 65.4 % decrease in the predicted number of loads.

From the identified needs above it is deduced here that despite the SAMDM method being a widely used and accepted design tool for flexible pavements in South Africa, and the fact that the existing pavements designed using this method are currently providing satisfactory levels of service, there is a significant need to improve both the method and our understanding of the problem being modeled. When a material exhibits shear-induced dilatancy, in terms of the (simple) elastic model, it implies a value of Poisson's ratio greater than 0.5. This is a clear indication that including dilation in the material model that produces stresses and strains used in the SAMDM may cause the SAMDM to predict higher numbers of allowable loads, which would be closer (according to Theyse, 2010) to observed behaviour of roads. The method is clearly sensitive to variation of input material properties (Jooste, 2004) and does not adequately account for the state of effective stress present in the pavement on the mechanism that is ultimately responsible for the plastic deformation observed as rutting in pavement distress (Theyse & Kannemeyer, 2010).

2.3. Pavement Loading

The Road Traffic Act 1996 (Act No. 93 of 1996) and the Road Traffic Regulations made in terms of this Act legislate the maximum load limits of vehicles that may be used on South African public roads. Table 2-3 shows the maximum legally permissible axle loads adopted from Regulation 240 of the above act which is concerned with protecting the pavement by limiting the legal maximum mass of vehicles to values that the road pavement can support without being overstressed.

Table 2-3: Legally permissible axle loads on South African public roads (CSRA, 1996)

Type of axle	No. of tyres (per axle)	Load per axle (kN)*
Single axle (steering)	2 or 3	76
Single axle (non-steering)	2 or 3	78
Single axle	4 or more	88
Tandem axle	4 or more	88
Tridem axle	4 or more	78.3

* g = 9.8 m/s^2

Table 2-3 shows that there are different types of axle and tyre configurations, resulting in varying loads being applied on the pavement. The distribution of axle types and the wheel configuration, and the magnitude and the number of loads applied to a pavement, constitute the traffic spectrum. Current practice in South Africa is to convert the cumulative damaging effect of all individual axle loads from the traffic spectrum into a number of equivalent standard axle loads that result in the same condition of deterioration. The procedures on how to collect information required and the steps that must be followed are given by the Committee of State Road Authorities (CSRA, 1991; CSRA, 1996). It is standard practice to use a standard axle load of 80 kN which is adopted from the AASHO road test method. Therefore for mixed traffic the total equivalent axle loads (E80s) is the number of 80 kN loads which would cause the same damage as the actual spectrum of axle loads imposed (CSRA, 1991). As shown on Table 2-3 the maximum legally permissible axle load is 88 kN which is 10% higher than the design load. However, TRH 16 (CSRA, 1991) states that the 80 kN standard axle load for design does not have to bear any relation to the legal axle load and may be used without regard to the legal limit even if the legal limit is changed.

The loads which are applied by traffic onto a pavement can be characterised by the following parameters (Hoffman, 2008).

- Tyre Load
- Axle and tyre configurations
- Repetition of loads
- Distribution of traffic across the pavement
- Vehicle speed

The tyre loads are the loads at the actual tyre to pavement contact interface. For most analyses it is assumed that the tyre load is uniformly applied over a circular area and that the tyre inflation and contact pressure are the same. The relationship between the radius of the assumed tyre contact area and the tyre inflation pressure is based on the Burmister model (Yoder & Witczak, 1975) and the relationship is given by:

$$a = \sqrt{\frac{P}{p\pi}} \qquad \text{Eq. 2.5}$$

Where a = equivalent load radius of the tyre footprint

P = Tyre load (kN)

p = Tyre pressure (kPa)

Perret (2002) investigated the effect of loading conditions on pavement responses of stress and strain calculated using a linear elastic model. Pavement responses to variations in: the shape of the load surface; the value of the applied mean vertical pressure; the distribution of vertical load pressure on the load surface; and the application of transversal load were investigated. Perret (2002) found the shape and total size of the load surface to be the most important parameters which influence the stress and strain distributions. The shape influenced the relationships between longitudinal and transverse responses at the top and bottom of the bituminous layer and the size of the contact surface was found to influence the mean vertical pressure that the tyre caused through the pavement.

De Beer *et al.* (1999) investigated the actual tyre/pavement contact stress using results from a locally developed Stress-In-Motion (SIM) system known as the Vehicle-Road-Surface-Pressure-Transducer-Array (VRSPTA). The VRSPTA measures the actual tyre pavement contact stresses, namely σ_{zz} (vertical contact stress) in the z - direction, τ_{zy} (lateral contact stress) in y - direction and τ_{zx} (longitudinal contact stress) in the x - direction. They presented two sets of results measured using the VRSPTA on a light

commercial (Hi-Ace) vehicle and a typical 7 - axle truck. The measured vertical contact stresses were found to range between 700 kPa and 900 kPa for the commercial light vehicle with an average tyre inflation of 645 kPa and the measured vertical contact stresses for the 7 axle truck ranged from 650 kPa to 1250 kPa.

Research using the VRSPTA illustrated that actual contact stresses are greater than inflation pressures, depending both on the inflation pressure and the tyre load. De Beer *et al.* (1999) also found that the distribution of the stresses was not uniform and demonstrated that the actual contact stresses exceed the current design value of 520 kPa by a factor of up three. They recommended that the values shown in Table 2-4 be used to replace the standard circular disc of 520 kPa uniform contact stress.

Table 2-4: Recommended interim vertical contact Load/Stress values for mechanistic design analysis (De Beer *et al.*, 1999)

Road Category (TRH4,1996)	Circular Vertical Contact Stress (kPa)	Circular Load Radius (mm)
A	950	91.5
B	850	96.7
C	750	103.0
D	650	110.6

Be Deer *et al.* (1999) also discussed the prevalence of overloading in South Africa. Increased truck tyre loading and inflation pressures, and hence the three dimensional contact stresses, have a significant influence on the service life of the pavement. They stated that in 1997 about 35 % of the 90000 heavy vehicles that were weighed in South Africa were overloaded in terms of the load legislation (National Road Traffic Act 1996). They therefore also recommended that a 100 kN load in addition to the current standard 80 kN load be included in the loading criteria in the design of South African pavements.

Further research on tyre/pavement interface contact stress using Stress-in-Motion (SIM) technology was conducted on the National Route (N3) in South Africa, De Beer *et al.* (2004). The paper highlights the use of SIM technology on heavy vehicles using the N3 route at the traffic control center in Heidelberg between February and March 2003. De Beer *et al.* (1999) found that the steering axle tyres (inflated at 850 kPa) were inflated approximately 10 to 13 % higher than the rest of the tyres on the heavy vehicles.

Morton *et al.* (2004) also published results on measured tyre inflation pressure and axle loading data from a random sample measured between February and March 2004 at the Heidelberg traffic control center. A total sample of 1095 axles was weighed. Morton *et al.* (2004) found that approximately 10 % of all axles measured were overloaded and also that the inflation of the tyres on the steering axle had peaks of 800 kPa and 40 % of all tyres measured were inflated between 800 kPa and 825 kPa, thus agreeing with the findings by De Beer *et al.* (2004). Morton *et al.* (2004) concluded that changes in the stress patterns under heavy loads and high tyre inflation pressures have not been adequately incorporated in design methods and practice, while large quantities of available traffic data are not utilised in the pavement design procedure.

Wide base ("super-single") tyres have gradually been replacing conventional dual tyres in the trucking industry, mainly because of their efficiency and economy. De Beer *et al.* (1997) published results which indicated that super-single pneumatic tyres apply higher vertical and transverse contact stresses across larger contact areas with the pavement. Kim *et al.* (2005) examined the effects of super-single tyre loading on pavements, particularly on the stresses and strains generated in the subgrade. The investigation was carried out using plane strain two-dimensional (2D) and three-dimensional (3D) static and dynamic finite element analyses and also the Multi-Layered Linear Elastic (MLLE) theory. Kim *et al.* (2005) used two software packages to analyse a flexible pavement subjected to loading from wide based tyres; namely ABAQUS (ABAQUS, 1997) for the 2D and 3D static and dynamic FEA and ELSYM 5 (Ahlborn, 1969) for the MLLE analysis. Kim *et al.* (2005) found that the super-single tyres induce higher vertical plastic strain than dual tyres and also found that super-single tyres in single axle configurations produce higher vertical plastic straining than tandem or tridem axle configurations. They concluded the following.

- According to the comparison of conventional and super-single tyres under elastic-plastic conditions, super-single tyres induce approximately four times larger permanent strain than conventional tyres. Therefore, design of pavements using load equivalency factor values for dual tyres leads to overestimation of the pavement design life.
- Single axle loadings with super-single tyres induce the largest vertical plastic strains at the top of the subgrade of all axle configurations considered (about 1.5 times larger than the tridem axle configuration).
- Repeated super-single tyre loadings induce approximately four times larger permanent vertical strains in the subgrade for existing roads than dual tyre loadings. This implies that either mitigation of permanent strains in the subgrade

must be pursued or the number of passages of super-single tyres must be limited by appropriate regulation.

2.4. Pavement analysis

2.4.1. *SAMDM Method*

The process flow chart for pavement analysis used in the SAMDM is shown in Figure 2-3. The process starts with the load and material characterisation. The standard design load for South Africa is a 40 kN dual wheel load at 350 mm spacing and a contact tyre pressure of 520 kPa. The materials' characterisation includes definition of layer thicknesses and the elastic properties for each layer. The SAMDM is in essence a critical layer approach where the most critical layer determines the predicted life of the entire pavement (Transportek, 2001). The next step normally involves a static, linear elastic analysis of the multi-layer system, giving stresses and strains at critical positions in the pavement structure.

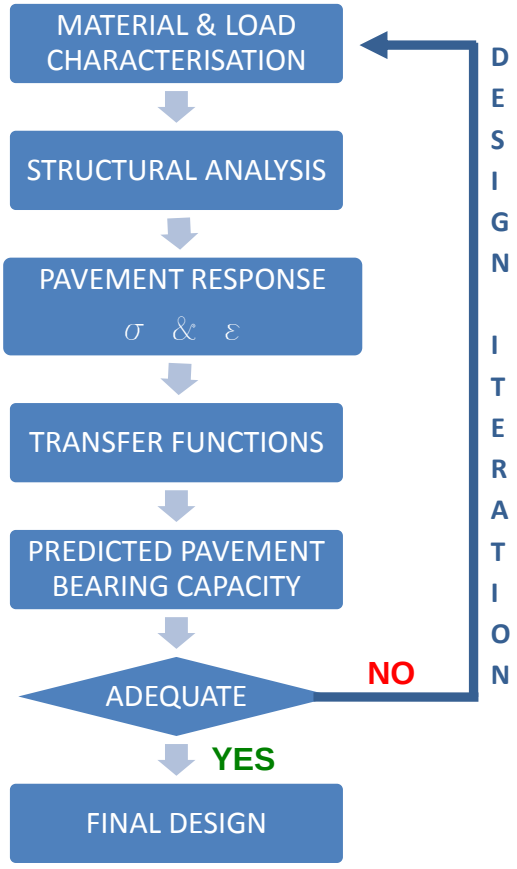


Figure 2-3: Basic procedure of mechanistic design analysis

Multi-Layer Linear Elastic (MLLE) theory or Finite Element Analysis (FEA) is used to obtain these stresses and strains. In this study two commercial FEA packages are discussed in Section 2.5.2. The stresses and strains obtained quantify the pavement response to the applied loading and serve as input to the transfer functions for each distinct material type.

These transfer functions relate the stress or strain condition of the pavement layer to the number of loads that can be sustained at that stress or strain level before a pre-defined terminal condition is reached. The transfer functions were developed from test results obtained in the laboratory and from field tests in which a material sample or a test section was repeatedly subjected to a certain load, stress or strain until the predefined terminal condition was reached. The transfer functions were then obtained from a regression analysis in which a best-fit (linear-logarithmic based) function was fitted to the test data (Theyse *et al*., 1995; 1996).

Theyse *et al.* (1995) describe in detail the procedure for determining transfer functions through the regression analysis of results. In this report they updated the transfer functions using statistical methods and produced transfer functions with various levels of design reliability attached to them. Design reliability levels of 95 %, 90 %, 80 % and 50 % were included to indicate the expected probability of success for the different road classes A, B, C and D as described in TRH 4 (CSRA, 1996). Table A1 (Appendix 1 Page A1.1) gives the results for the transfer functions obtained by Theyse *et al.* (1995) at 50 %, 80 %, 90 % and 95 % probability for (i) continuously graded and gap graded asphalts where the number of load repetitions for the initiation of cracks (or fatigue life) and the tensile strain in the asphalt are represented by N_f and ε_t respectively; (ii) cemented materials (crush initiation (N_{ci}), advanced crushing (N_{ca}), effective fatigue (N_{eff}), stress ratio (σ_v/UCS) where σ_v is the vertical stress on the layer interface where crushing is evaluated and UCS is the unconfined compressive strength of the cemented layer and the strain ratio ($\varepsilon/\varepsilon_b$) where ε is the maximum strain at the bottom of the cemented layer and ε_b the measured strain at breaking point) and (iii) thick asphalt bases and the subgrade. Equations 2.6 to 2.9 provide the transfer functions for granular materials;

$$N_{95\%} = 10^{(2.605122F+3.480098)} \quad \text{Eq. 2.6}$$

$$N_{90\%} = 10^{(2.605122F+3.707667)} \quad \text{Eq. 2.7}$$

$$N_{80\%} = 10^{(2.605122F+3.983324)} \quad \text{Eq. 2.8}$$

$$N_{50\%} = 10^{(2.605122F+4.510819)} \quad \text{Eq. 2.9}$$

Where N is the number of load repetitions and F is the Factor of Safety (FoS) obtained from Eq. 2.1 or Eq. 2.2 on Page 9.

2.5. Granular materials

The structural layers of most roads typically comprise of granular materials (gravels), in either their natural state or after treatment with a stabilizing agent (SANRAL, 2013). Granular materials used in the construction of South African roads are classified in TRH 14 (CSRA, 1985) as follows:

- Crushed stone from fresh, unweathered rock (G1)
- Crushed stone from rock, boulders and/or coarse gravel (G2 & G3)
- Natural gravels (G4, G5 & G6)
- Gravel soils (G7, G8, G9 & G10)

Roads which experience high traffic loading are likely to be constructed using crushed stone granular materials either in the base or subbase as these materials provide a stiff yet adequately flexible layer to resist the high stresses applied by traffic in the upper portions of the pavement structure (SANRAL, 2013). In designing crushed stone layers the designer must strive to minimize the required quantity and handling of material since crushed stone gravels are normally supplied by commercial quarry.

G1 crushed stone is obtained from crushing and processing fresh, unweathered rock to obtain a continuously graded material. It is important for G1 material that the grading is tightly controlled to ensure that the required compaction density, normally 86 % to 88 % of Apparent Relative Density (ARD), can be achieved. Any significant deviation from specified grading, outside the recommended envelopes, negatively affects the chances of achieving the specified density (SANRAL, 2013).

According to Kleyn (2012) G1 crushed stone was developed from single stage crusher-run material when during the late 1950s observant engineers noticed that this material would sometimes after a sudden down-pour and towards the end of its compaction cycle, exhibit a tendency to expel some of its fines (material passing the 75 µm sieve), resulting in the aggregate locking-up into a closely knit matrix, instead of becoming unstable like other granular materials under similar circumstances. This phenomenon was investigated by construction of various test sections and the Heavy Vehicle Simulator (HVS) test program during the 1980s by using in-service G1 base coarse roads. The results showed that the G1 crushed stone base coarse was exceptionally water resistant and that the bearing capacity of the material increases to accommodate an increase in loading up to the crushing point of the aggregate itself, without noticeable traffic moulding. This however came at a price – G1 crushed stone had to be manufactured and constructed to very stringent specifications (Kleyn, 2012). It was therefore concluded that if conditions were just right, the crushed particle fraction could

be packed together so tightly as to approach the state of pre-fracture (i.e. pre-crushed solid rock mass).

Following further research (Kleyn, 2012) in which various Fuller curve grading compositions (Fuller and Thompson, 1907), at which maximum compaction could be attained, were reconstructed and compacted in the laboratory and in field experimental sections, Kleyn (2012) summarises the following observations:

- The aggregate fractions had to be compacted to interlock so as to form an aggregate mix that approaches the condition of the intact parent rock – so called a solid density. This state of interlock is manifested visually on the surface of the layer by a well knitted aggregate mosaic with only the slimmest line of inter-aggregate fines.

- The required final state of particle interlock results in a density much higher than that used in road building, and which cannot be expressed meaningfully in terms of Mod AASHTO density. A more consistent result is obtained when the density is expressed in terms of the Specific Gravity (SG) or “solid density” of the aggregate – Solid Relative Density (SRD).

- Allowance can be made for enclosed voids within the aggregate (Apparent Relative Density or ARD) as well as cracks and fissures on the surface of the aggregate (Bulk Relative Density or BRD). The development of G1 was based on SRD and later on ARD. The difference between these two targets is dependent on the rock type and quality and is in some instances negligible. Indications are that 88 % of SRD is the minimum required compaction for achieving the performance expected from such a layer – equivalent to about 106 % Mod AASHTO density.

- The grading of the aggregate mix is of utmost importance in this process. The conclusion reached was that “there must be just enough of each particle size to fill (all) the inter-particle voids”.

- The aggregate had to be very resistant to general construction impacts and high energy compaction forces that had to be applied to achieve the final state of interlock. No structurally inferior or contaminated material can be tolerated and thus only fresh un-weathered and sound rock must be used.

- The plasticity of the G1 aggregate matrix must be as close as possible to zero – the argument being that the matrix must contain as little material as possible that may affect the particle interlock negatively and thus the shear strength of

the compacted material i.e. the layer must be as moisture insensitive as possible.

Kleyn (2012) then discusses in detail fourteen construction steps required for successful construction of the base course using G1 crushed stone which will not be repeated in the present paper. Of particular interest are steps 10 and 11 (Kleyn, 2012) relating to the slushing process.

According to Kleyn (2012) before the slushing process can begin, rolling must continue until the G1 base layer exhibits no (or very little) movement under the wheel loads of a heavy roller. At this stage the density of the G1 material should be in the order of 85 % of SRD/ARD. If the slushing process is started too early the layer will become unstable and even expel the larger (sandy) fines, which will further complicate the slushing process. When the layer is stable enough the slushing process can commence. This process is initiated by wetting and rolling 40 m to 60 m sections of the layer at a time with heavy static rollers. In the slushing process, the material particle fraction less the 75 µm, is used as a “lubricant” to ease the relative movement between the larger particles towards achieving intimate stone upon stone packing, and resulting in squeezing (slushing) the excess fines out of the matrix in the process. Kleyn (2012) highlights that it was found advantageous to have the percentage material passing the 75 µm sieve slightly higher (2 % - 3 %) than is required to satisfy the Fuller curve grading (Eq. 2.10). The slushing process normally increases the overall ARD by 2 % - 4 %, however the shear strength and performance of the material increases dramatically. Finally the slushed fines are removed from the pavement by brooming with heavy duty hand broom or light mechanical brooms.

G2 and G3 crushed stone are obtained from crushing and processing rock boulders and course gravel. When used as base course, crushed stone gravel materials must be significantly strong (i.e. have good shear resistance) and are required to have a minimum CBR of 80% at 98% Mod AASHTO with stringent grading and plasticity requirements. The largest particle size criterion, i.e. the largest allowable particle size shall not exceed two-thirds of the layer thickness, is particularly important in crushed stone gravels which are used as base material in order to obtain a surface finish that will ensure that a suitable ride quality in the completed road is achieved (SANRAL, 2013).

The natural gravels (G4 to G6) are generally obtained from within the road prism or borrow pits adjacent to the road reserve and these are normally processed after placement on the road being constructed using on-site construction equipment to break down large stones and remove oversize material. It is essential that sufficient

sources of natural materials are available along, or as close as possible to the road alignment to provide the necessary materials within an economical distance (SANRAL, 2013). A useful philosophy when using natural gravels, especially for low volume roads, is to make the pavement design fit the available materials. Subgrade soil is the insitu material encountered and is normally used as it occurs with little alteration. Typical treatment of insitu roadbed material includes scarifying and compaction to 90 % Mod. AASHTO density.

The performance of such granular materials as layers in a pavement is dependent on the composition (grading, particle shape and texture), moisture content, the California Bearing Ratio (CBR) and the compaction achieved on site during construction of the road (Semmelink and Visser, 1994). In their paper, Semmelink and Visser (1994) evaluated the effect of individual properties of the soil on the CBR and the compactability when the soil is used as a road building material. The influence of the following properties on CBR and compactability were evaluated:

- Moisture content;
- Particle shape and texture;
- The Atterberg limits and linear shrinkage (LS);
- Crushing strength and durability of the material;
- Bearing capacity of the underlying material; and
- Factors which influence bearing capacity of the material.

The amount of water used plays an important role in the compaction of unbound granular materials. Too much or too little water will have a detrimental influence on the compaction (Semmelink and Visser, 1994). When the grading complies with the Fuller Equation (Fuller and Thompson, 1907) as shown in Eq. 2.10 such that n = 0.5, the densest aggregate mix can be achieved.

$$\mathrm{P} = 100 \times \left(\frac{d}{D}\right)^{n} \qquad \text{Eq. 2.10}$$

Where

P = percentage passing a sieve with opening side d (mm)
D = maximum stone size (mm)
n = constant

It is often assumed that the shape and texture factors that resist shearing also resist compaction. Particle interlock at the points of interparticle contact is greater for particles with harsh surface texture than for smooth textured particles (Semmelink and

Visser, 1994). At the same relative compaction, angular materials show higher strength characteristics compared to rounded and sub-rounded materials; however it also requires more compactive effort to compact the angular material. Semmelink and Visser (1994) note that the influence of the Atterberg limits and linear shrinkage (LS) on the compactability and bearing capacity is subjective. Plasticity which is a major characteristic of cohesive soils enables the material to suffer deformation without noticeable elastic recovery and without cracking or crumbling.

Semmelink and Visser (1994) also carried out laboratory tests to evaluate the compactability of 21 different untreated road building materials used on roads with heavy and light traffic in South Africa. Figure 2-4 below, shows the relationship between measured values of Maximum Dry Density (Vibratory) with Gradings that have Abundant, Sufficient Amount or Lack of Fines. The maximum dry density was expressed in terms of space occupied by solids.

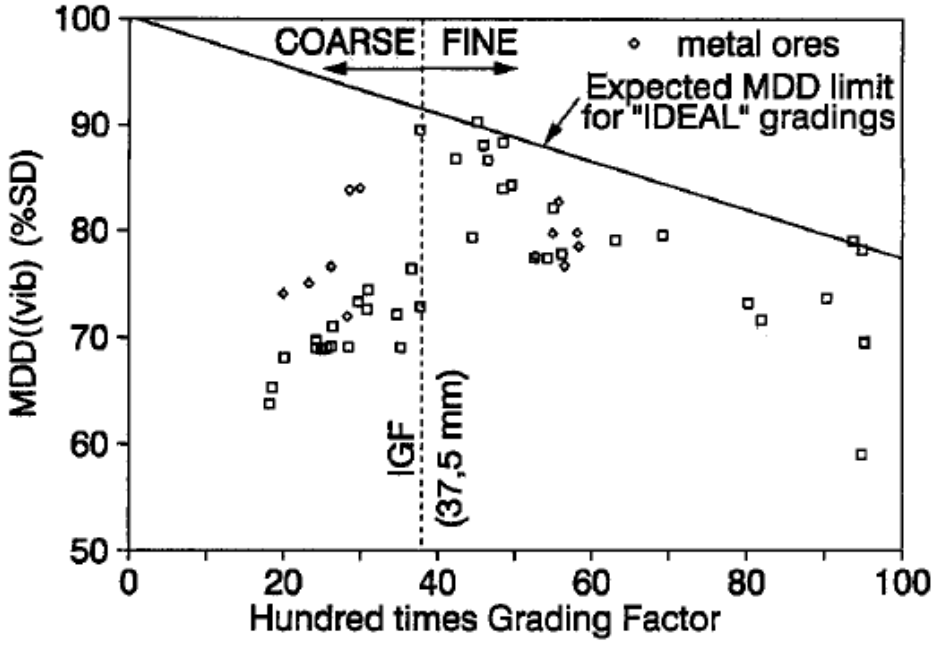


Figure 2-4: Relation between measured values of maximum dry density (Vibratory) expressed in terms of space occupied by solids and Grading Factor for original materials investigated plus two metalliferous Ore with gradings that have Abundance, Sufficient Amount, or Lack of Fines (after Semmelink and Visser, 1994)

The authors (Semmelink and Visser, 1994) highlight that although most untreated materials have gradings on the fine side of the “ideal” grading (i.e. $P = 100 \times [(d / D)^{0.5}]$) there are materials that lack fines (i.e. coarsely graded) that are used. The results (Figure 2-4) show two distinct zones; one where the compacted material is lacking in fines (coarse zone) and the other where the material

contains sufficient or excess fines. The slopes of the data points in the two zones were found to be different and according to Semmelink and Visser (1994) the steeper slope of the coarse zone data points emphasizes the negative influence that a lack of fines can have on the Maximum Dry Density (MDD) that can be achieved. Semmelink and Visser (1994) conclude that this supports the approach of ensuring that the amount of fines in road building materials is slightly higher than required and removing the excess fines by the slushing process as is done for well graded crushed stone bases in South Africa.

The characteristics of unbound granular materials which determine the elastic (transient) deflections in pavements under moving wheel loads are of particular interest because of their effect on the fatigue life of the materials overlaying the granular layer (Wolff, 1996). Granular materials are typically overlain by lightly cemented or asphaltic materials in the pavement structure. Large elastic deformations of the total pavement will cause large deformations in the overlaying cemented or asphaltic materials which result in a reduced fatigue life (load repetitions to cracking) of these layers.

Similarly, the characteristics of unbound granular materials which determine the plastic (permanent) deformations in pavements under wheel loads are also important (Wolff, 1996). The permanent deformations control the rutting and consequently the safety and surface drainage characteristics of the pavements. A pavement is considered to have failed when ruts of 10 mm, 15 mm and 20 mm (Wolff, 1996; CSRA, 1996) have developed on its surface for road categories A, B and C respectively as defined in CSRA (1996). If the pavement is not maintained timeously and correctly, and water is allowed to enter the pavement structure through cracks in the surface, particularly during the later life of the pavement, the failure rut depths of 10 mm, 15 mm and 20 mm can occur (Wolff, 1996).

2.5.1. *States of stress in granular pavement layer materials*

According to Huang (2004) methods of flexible pavement design can be categorised into five categories; 1) empirical methods with or without a soil strength test, 2) methods of limiting shear failure, 3) methods of limiting the deflection, 4) regression methods based on pavement performance or road tests and 5) the popular mechanistic-empirical methods. Methods which fall in the categories listed include the Pavement Number (PN) method (Asphalt Academy, 2009) Dynamic Cone Penetrometer (DCP) Method (Kleyn, 1984; Sampson, 1984; and De Beer, 1991), AASHTO Structural Number (SN) method (AASHTO, 1993), Falling Weight Deflectometer (FWD) SN method (Maree, 1990; and Horak, 2008), the FWD Structural Number (SN) method (Rohde, 1994), the Transport and Roads Research Laboratory (TRRL) Surface Deflection method (Jordaan, 1989) and the Asphalt Institute Surface Deflection method (Jordaan, 1989). The SAMDM falls into category five, the mechanistic-empirical design methods. Methods in this category require the accurate evaluation of stresses and strains to predict the materials' response to the imposed traffic loading.

In general there are two approaches that are used to compute the stresses and strains in pavement analysis, these are;

i. Multi-Layered Linear Elastic (MLLE) Theory and

ii. Finite Element Analysis (FEA) which is further considered as either Two-Dimensonal (2D) FEA or Three-Dimensional (3D) FEA.

The MLLE approach is the most popular and easily understood method. MLLE systems are mathematically exact (Maina *et al.*, 2008) and Figure 2-5 illustrates the general concept of a multilayered elastic stress system. In this method the system is divided into an arbitrary number of horizontal layers (Vokas and Stoll, 1987). The calculation for obtaining the state of stress or strain in a multilayered elastic system is based on several assumptions. Yoder and Witczak (1975) list the assumptions as:

- the material properties of each layer are homogeneous;
- each layer has a finite thickness except for the lower (subgrade) layer and all are infinite in the lateral direction;
- each layer is isotropic;
- full friction is developed between layers at each layer interface;
- surface shearing forces are not present at the surface;
- the stress solutions are characterised by two material properties for each layer i.e. the Poisson ratio (ν or μ) and the Young's modulus (E).

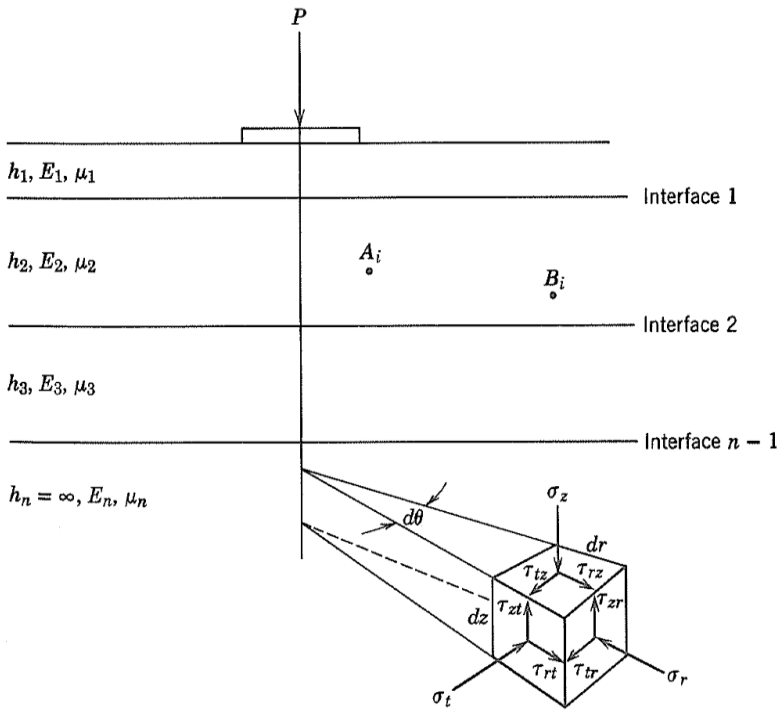


Figure 2-5: General multi-layer elastic system (after Yoder & Witczak, 1975)

Because of the limitations imposed by some of the assumptions used in MLLE theory, these methods are considered as analytical (Maina *et al.*, 2008). The development of analytical methods to compute the state of stresses and strains can be traced back to Boussineq's single layer model (Boussinesq, 1983). Boussinesq produced a series of equations to determine stresses, strains and displacement in a homogenous, isotropic, linear elastic half space with Young's modulus E and Poisson's ratio ν subjected to a static point load P. Boussinesq's equations (Boussinesq, 1983) could be used to analyse stresses due to point loads, line loads, circular and rectangular loads.

While Boussinesq's equations could only be applied to a single layer system, Burmister (1943) presented a method to determine stresses, strains and displacement in a two layered system and then extended the method to a three-layered system followed by a multiple-layered system analysis (Burmister, 1945).

The 2D and 3D finite element methods for computing stresses, strains and displacement are discussed in Section 2.5.2.

The response to stresses on an element of granular material depends on the stress history, the current stress level and the degree of saturation. Granular materials are not perfectly elastic but experience some non-recoverable deformation after each load application (Adu-Ose, 2001 and Wolff, 1996). In the case of transient loads and after the first few load applications, the increment of non-recoverable deformation is much smaller than the increment of resilient (recoverable) deformation (Adu-Ose, 2001). The

engineering parameter used to characterise this behaviour is the resilient modulus (M_R) which is obtained from repeated-load triaxial tests.

Many researchers have developed models for characterising the resilient response of unbound granular pavement materials. According to Adu-Ose (2001) models include:

- the confining pressure model (Seed *et al*., 1955);
- k-θ model (Hicks & Monismith, 1971);
- contour model (Boyce, 1976);
- Uzan model (Uzan, 1985);
- Lytton Model (Lytton, 1995);
- Van Niekerk and Huurman model (Van Niekerk and Huurman , 1995) and
- Lekarp *et al*., 2000

For the repeated load triaxial tests with constant confining stress σ_3 the resilient modulus (M_R) and Poisson ratio (ν) are given (Lekarp *et al.*, 2000) by:

$$M_R = \frac{\Delta(\sigma_1 - \sigma_3)}{\varepsilon_1} \qquad \text{Eq. 2.11}$$

And

$$\nu = -\frac{\varepsilon_3}{\varepsilon_1} \qquad \text{Eq. 2.12}$$

Where:

M_R = Resilient Modulus

ν = Resilient Poisson Ratio

σ_1 = major principal stress

σ_3 = minor principal stress

ε_1 = major principal strain

ε_3 = minor principal strain

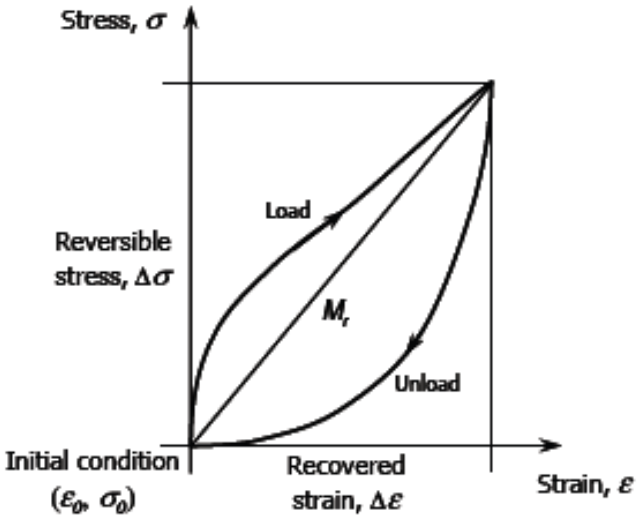
For repeated load triaxial tests in which cyclic confining pressure is applied, Lekarp *et al.* (2000) define the resilient modulus and Poisson's ratio as:

$$M_R = \frac{\Delta(\sigma_1 - \sigma_3)\Delta(\sigma_1 + 2\sigma_3)}{\varepsilon_1\Delta(\sigma_1 + \sigma_3) - 2\varepsilon_3\Delta\sigma_3} \qquad \text{Eq. 2.13}$$

and

$$\nu = \frac{\Delta\sigma_1\varepsilon_3 - \Delta\sigma_1\varepsilon_1}{2\Delta\sigma_3\varepsilon_3 - \varepsilon_1\Delta(\sigma_1 + \sigma_3)} \qquad \text{Eq. 2.14}$$

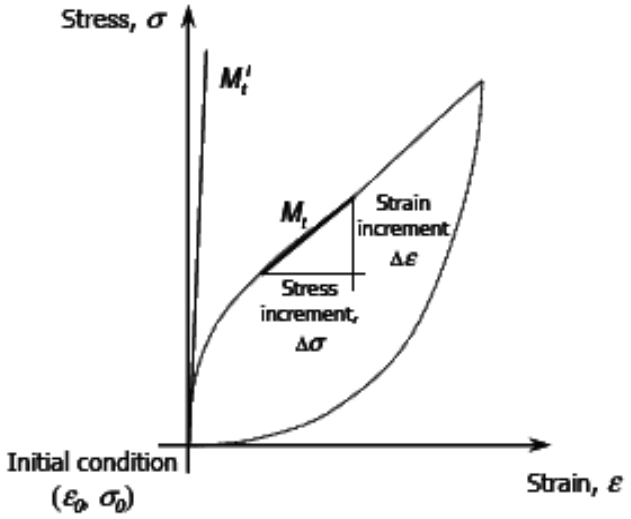
The resilient modulus may be modeled by the secant or tangent modulus shown in Figure 2-6 and Figure 2-7. The secant modulus represents the slope of the hysteresis loop from the initial stress-strain condition to the fully loaded stress-strain condition while the tangent modulus represents the instantaneous slope of the hysteresis loop at any point during the loading cycle.



Secant Resilient Modulus,

$$M_r = \frac{\Delta\sigma}{\Delta\varepsilon}$$

Figure 2-6: Secant resilient modulus model (Theyse, 2007)



Tangent Resilient Modulus,

$$M_t = \lim_{\Delta\varepsilon \to 0} \frac{\Delta\sigma}{\Delta\varepsilon}$$

Figure 2-7: Tangent resilient modulus model (Theyse, 2007)

2.5.2. *Finite Element Analysis*

Finite element analysis (FEA) has presented valuable advances in the analysis of pavement structures to determine the stresses and strains induced in the pavement layer materials. FEA is extremely versatile in the representation of mechanical characteristics (Kim *et al*., 2009). Three different types of analysis models are shown in Figure 2-8, namely axisymmetric, plane strain (Two-Dimensional (2D)) and Three-Dimensional (3D). The advantages and disadvantages are given in detail by Kim *et al*. (2009). However, it is noteworthy to mention that Kim *et al*. (2009) found that the axisymmetric analysis (while limited to modeling single tyre loading distributed evenly over a circular area) yielded results close to the 3D analysis while the 2D analysis gave higher values of stresses and strains.

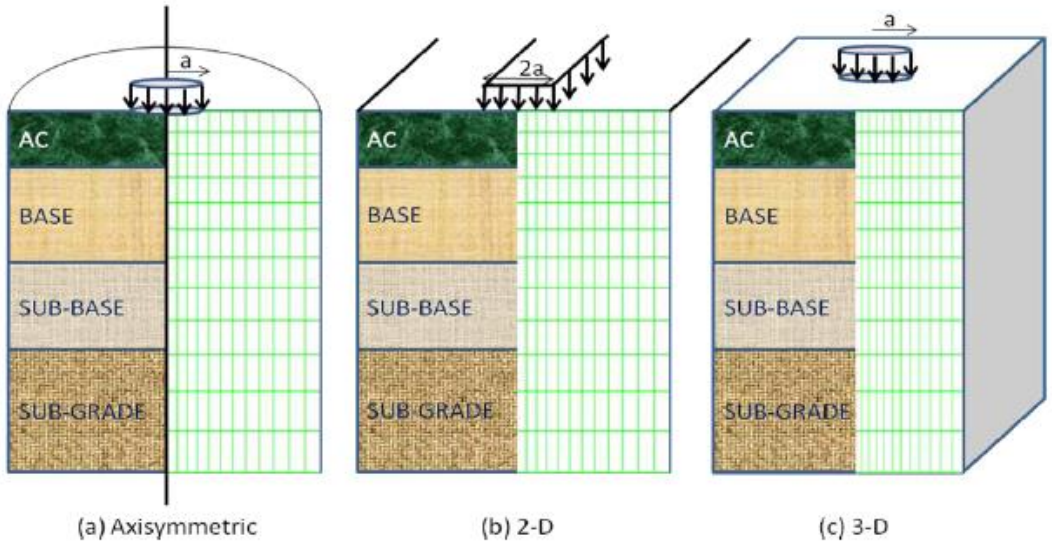


Figure 2-8: FEA (After Kim *et al*., 2009)

The nonlinear stress-strain behaviour of soil can be modeled at several different levels of sophistication using different constitutive (material) models. The constitutive models of two commercial finite element programs, namely SIGMA/W (Geo Slope International Ltd, 2007) and PLAXIS (Brinkgreve *et al*., 2002), are discussed below. The models are described and their limitations are highlighted. Not all the available models are described in detail, only those that were considered for use in this particular investigation.

2.5.2.1. SIGMA/W

SIGMA/W is a finite element software package which is used to perform stress and deformation analyses of earth pressures and applied loads. It may be used to compute stress-deformation relationships with or without changes in pore water pressures that arise from stress state changes. It includes six different soil constitutive models plus

an option for a user defined constitutive model. For each model the behaviour will be different depending on the pore water condition to which the model is applied, i.e. a total stress; effective stress with no pressure change; or effective stress with pore water pressure change (Geo Slope International Ltd, 2007). SIGMA/W supports the following six built-in material models.

Linear elastic model

This is the simplest soil model in SIGMA/W in which stresses are directly proportional to the strains. The proportionality constants are Young's Modulus E, and Poisson's ratio ν. Poisson's ratio can be varied, but because of computational constraints in SIGMA/W it is limited to a maximum value of 0.49. The model requires the following input parameters: E, ν, c and ϕ. The parameters c and ϕ are not used in the solution, but are used in the contour output program of SIGMA/W to show regions of soil where computed stresses have exceeded the yield strength of the material.

Anisotropic elastic model

SIGMA/W also includes an additional model to the linear elastic model which accounts for ground deposits in layers which are stratified and inclined. The anisotropic elastic model allows the possibility of having different stiffness values in two orthogonal directions.

Non-linear elastic hyperbolic model

The stress strain behaviour of soil becomes nonlinear, particularly as failure conditions are approached. A procedure for modeling this soil behaviour which is used in SIGMA/W is by varying the soil modulus.

SIGMA/W uses the formulation presented by Duncan and Chang (1970) to compute the elastic modulus (E). In this formulation the shear stress (σ_1 - σ_3) vs. axial strain curve is hyperbolic (Figure 2-9) and the soil modulus is a function of the confining stress and the shear stress that a soil is experiencing. This non-linear material model requires only soil properties that are obtained quite readily from triaxial tests.

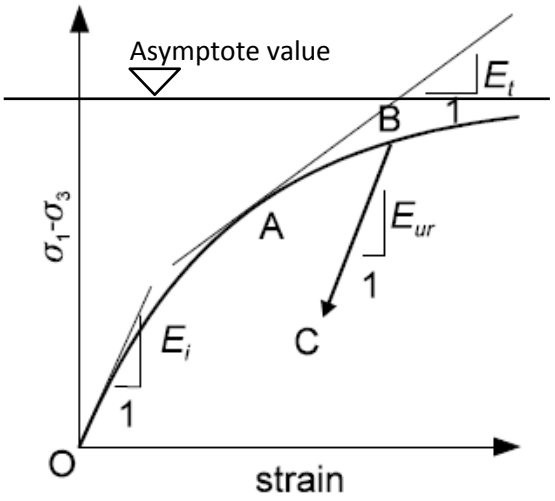


Figure 2-9: Nonlinear stress-strain behaviour (Geo Slope International, 2007)

According to Geo Slope International (2007) Eq. 2.15 and Eq. 2.16, originally derived by Duncan and Chang (1970) give the initial modulus (E_i) and the tangent modulus (E_t). SIGMA/W uses E_i as the unload-reload modulus (E_{UR}).

$$E_i = K_L P_a \left(\frac{\sigma_3}{P_a}\right)^n \qquad \text{Eq. 2.15}$$

$$E_t = \left[1 - \frac{R_f(\sigma_1 - \sigma_3)(1 - sin\phi)}{2c(cos\phi) + 2\sigma_3 sin\phi}\right]^2 E_i \qquad \text{Eq. 2.16}$$

where:

E_i = initial tangent modulus as a function of confining stress,σ_3

E_t = tangent modulus

K_L = loading modulus number

P_a = atmospheric pressure

n = exponent for defining the influence of confining pressure on the initial modulus

ϕ = friction angle

c = cohesive strength of soil

σ_3 = confining stress

σ_1 = major principal stress

R_f = ratio between the asymptote to the hyperbolic curve and the maximum strength (typically between 0.75 and 1.0)

Elastic-plastic model

The Elastic-Plastic model in SIGMA/W describes an elastic, perfectly-plastic relationship. A typical stress strain relationship is shown in Figure 2-10. The stresses are directly proportional to strains until the yield point is reached. Beyond the yield point the stress–strain curve is horizontal. In SIGMA/W, the soil plasticity is formulated using the theory of incremental plasticity (Hill, 1950). The following material properties are required as input: Young's Modulus E, Poisson's ratio ν, cohesion c, friction angle ϕ, and the dilatancy angle ψ. (If the value of the dilation angle is not specified, the dilation angle is considered to be equal to the internal angle of friction). Refer to Section 2.6.1 on Page 45 for definition of the dilatancy angle ψ.

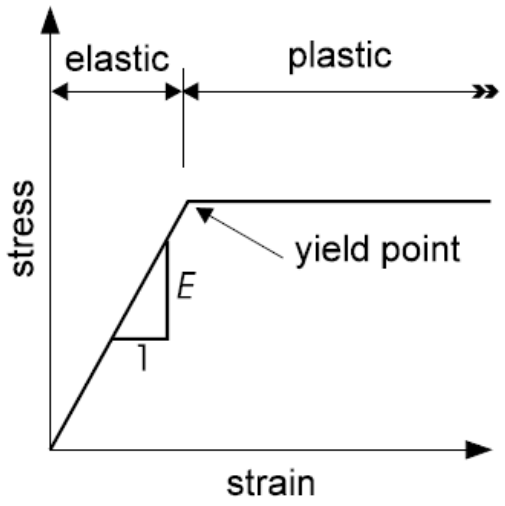


Figure 2-10: Elastic-perfectly plastic constitutive relationship (Geo Slope International, 2007)

Plasticity is the development of irreversible strains. In order to evaluate whether plasticity occurs in a calculation, a yield function is needed. A yield function can be represented as a surface in principal stress space. For example as shown in Figure 2-11

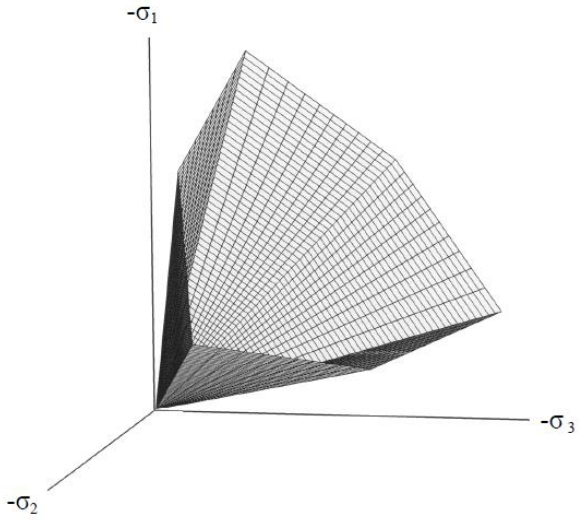


Figure 2-11: The Mohr-Coulomb yield surface in principal stress space (c = 0) (Brinkgreve *et al.*, 2002)

SIGMA/W uses the Mohr-Coulomb yield criterion as the yield function for the elastic-plastic model.

Cam Clay model

The Cam Clay model is a critical state model as well as a hardening elastic-plastic model.

Modified Cam Clay model

The modified Cam Clay model is similar to the Cam Clay model except that the yield function is in the shape of an ellipse instead of a tear drop.

User defined model

The user can create his own constitutive material model.

2.5.2.2. PLAXIS (2D)

PLAXIS supports six material models and an additional user defined model for predicting soil behaviour (Brinkgreve *et al*., 2002). The six models are listed below, however only two, the Mohr Coulomb Model and the Hardening-Soil Model, are described in detail.

Linear elastic model

The linear elastic model in PLAXIS is exactly the same as the one described on Page 34 for SIGMA/W.

Mohr-Coulomb model (perfect plasticity)

A perfectly-plastic model is a constitutive model with a fixed yield surface, i.e. a yield surface that is fully defined by model parameters and not affected by (plastic) straining. For stress states represented by points within the yield surface, the behaviour is purely elastic and all strains are reversible. This model is the same as the elastic plastic model described for SIGMA/W and similarly requires five parameters, namely Young's Modulus E, and Poisson's ratio ν for soil elasticity, the cohesion c, the friction angle ϕ, and the dilatancy angle ψ for soil plasticity.

In PLAXIS, the full Mohr-Coulomb yield condition is defined by six yield functions which are formulated in terms of the principal stresses.

In the formulation of the Mohr-Coulomb model the plastic potential functions contain a third plasticity parameter, the dilatancy angle (ψ). This parameter is required to model positive volumetric strain increments (dilatancy) as actually observed for dense soils.

For c > 0, the standard Mohr-Coulomb yield criterion allows for tension. In reality, soil can sustain no, or very little, tensile stress. This behaviour can be included in a PLAXIS analysis by specifying a tension cut-off. In this case Mohr circles with positive principal stresses are not allowed and the allowable tensile stress (σ_1) is taken to equal zero.

Jointed rock model (anisotropy)

This is an anisotropic elastic plastic model where plastic shearing can only occur in a limited number of shearing directions. This model is used to model the behaviour of stratified or jointed rock.

The hardening soil model (isotropic hardening)

This is a constitutive model formulated in the framework of classical theory of plasticity (Shanz *et al.,* 1999). In the model the total strains are calculated using a stress-dependent stiffness, different for primary loading and un-/reloading, and by using a multi-surface yield criterion. In contrast to an elastic perfectly plastic model, the yield surface of a hardening plasticity model is not fixed in the principal stress space, but it can expand due to plastic straining. The model involves compression hardening to simulate irreversible compaction of soil under primary compression. It can be used to simulate the behaviour of sands and gravels as well as softer types of soil such as clays and silts.

This model provides advanced simulation of soil behaviour. As for the Mohr-Coulomb model, limiting stresses are described by means of Young's Modulus E, and Poisson's ratio ν, cohesion c, the friction angle ϕ, and the dilatancy angle ψ. However, the soil stiffness is described much more accurately by using three different input stiffnesses: the triaxial loading stiffness, E_{50}, the triaxial unloading stiffness, E_{ur}, and the oedometer loading stiffness E_{OED}.

The parameter (E_{50}) is the confining stress dependent stiffness modulus for primary loading in a triaxial test. E_{50} is used instead of the initial modulus E_i for small strain, which as a tangent modulus, is more difficult to determine experimentally (Shanz *et al.,* 1999). E_{50} is given by the equation:

$$E_{50} = E_{50}^{ref} \left(\frac{\sigma_3 + c\ cot\phi}{\sigma^{ref} + c\ cot\phi} \right)^m \qquad \text{Eq. 2.17}$$

E_{50}^{ref} is a reference stiffness modulus corresponding to the reference stress (σ^{ref}). The stiffness depends on the minor principal stress, σ_3, which is the confining pressure in a triaxial test. The amount of stress dependency is given by the power m, and as a secant modulus E_{50}^{ref} is determined from a triaxial stress-strain curve for mobilisation of 50 % of the maximum shear strength σ_p (See Figure 2-12).

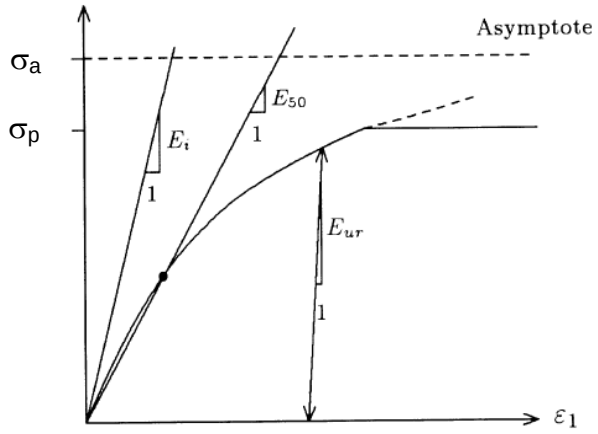


Figure 2-12: Stress strain relationship in primary loading for standard drained triaxial test (Brinkgreve *et al.*, 2002)

The unloading and reloading stiffness, E_{ur}, is given by Eq. 2.18:

$$E_{ur} = E_{ur}^{ref} \left(\frac{\sigma_3 + c\ cot\phi}{\sigma^{ref} + c\ cot\phi} \right)^m \qquad \text{Eq. 2.18}$$

where E_{ur}^{ref} is the reference Young's modulus for unloading and reloading, corresponding to the reference stress σ^{ref}.

Having defined E_{50} and E_{ur} the oedometer stiffness, E_{oed} is defined and given by Eq. 2.19:

$$E_{oed} = E_{oed}^{ref} \left(\frac{\sigma_1 + c\ cot\phi}{\sigma^{ref} + c\ cot\phi} \right)^m \qquad \text{Eq. 2.19}$$

Where E_{oed}^{ref} is a tangent stiffness modulus indicated in Figure 2-13. Hence E_{oed}^{ref} is a tangent stiffness at a reference stress of (σ^{ref}).

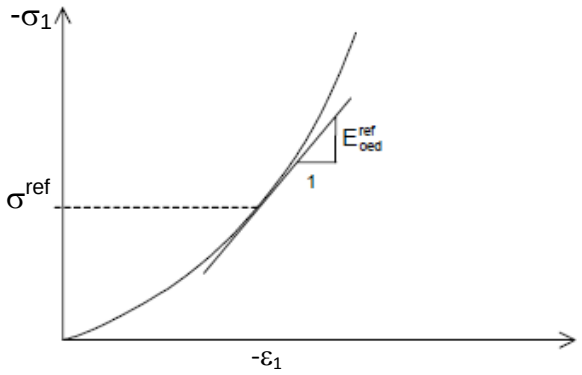


Figure 2-13: Definition of tangent stiffness modulus in oedometer test (Brinkgreve *et al.*, 2002)

In contrast to the Mohr-Coulomb model the Hardening-Soil model also accounts for the stress-dependency of stiffness moduli. This means that the soil stiffness can increase with pressure.

The PLAXIS manual (Brinkgreve *et al.*, 2002) states that the hardening soil model improves on the hyperbolic model (Duncan & Chang, 1970) by far. The hardening soil model uses the theory of plasticity rather than the theory of elasticity. The model also includes soil dilatancy and introduces a yield cap. The yield cap is introduced since the shear yield surfaces shown in Figure 2-14 do not explain the plastic volume strain that is measured in isotropic compression. A second type of yield surface is therefore introduced to close the elastic region in the direction of the p-axis. Without such a yield cap it would not be possible to formulate a model with independent input for both E_{50} and E_{oed}.

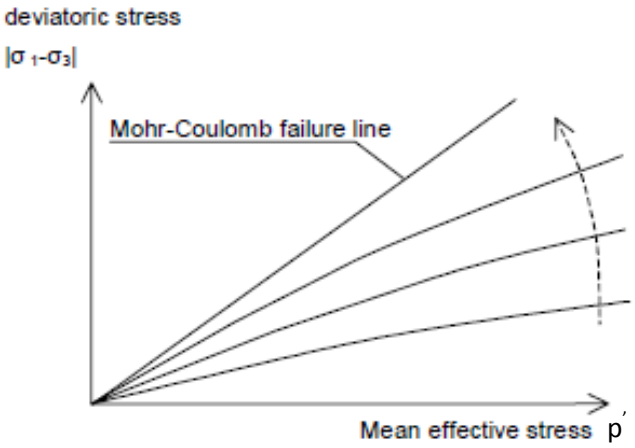


Figure 2-14: Successive yield loci for various values of the hardening parameter γ^P. (Brinkgreve *et al.*, 2002)

Some basic characteristics of the model are:

- Stress dependent stiffness according to a power law. (Input parameter *m*)
- Plastic straining due to primary deviatoric loading. (Input E_{50}^{REF})
- Plastic straining due to primary compression. (Input parameter E_{oed}^{REF})
- Elastic unloading / reloading.
- Failure according to the Mohr-Coulomb model. (c, ϕ, ψ.)

Further information on the hardening soil model is available in Schanz and Vermeer (1995) and Schanz *et al.* (1999).

The soft soil creep model (time dependent behaviour)

This is a second order model formulated in the framework of visco-plasticity. The model can be used to simulate the time dependent behaviour of soft soils such as normally consolidated clays and peat. The model includes logarithmic compression.

Soft soil model

This is the Cam Clay type model that can be used to simulate the behaviour of soft soils like normally consolidated clays and peat. This model performs best in situations of primary compression.

User defined model

PLAXIS allows the user to define a model which is not included above.

Discussion

The two FEA package discussed above are capable of modeling soil behaviour using nine differently formulated constitutive models. With each model, soil behaviour is modeled to varying levels of sophistication and accuracy, so each of the models gives different values of stress and strain. This is later shown in this research by comparing the principal stress and strain results between the linear-elastic and elastic-plastic models, see Section 4.1.5 on Page 91. However, it is current practice (Theyse *et al*., 1996; Transportek, 2001 & Jooste, 2004) to use the first order multi-layered linear elastic model to determine the stresses and strains which serve as input to the transfer functions. Much of the criticism of the SAMDM by Jooste (2004) was of the use of the transfer functions. However, transfer functions are calculated using the input stress and strain values. This means that different principal stresses and strain values obtained from the different material constitutive models discussed will result in the prediction of varied pavement bearing capacity.

2.5.3. *Failure of Granular materials*

Granular materials (G1 to G6) show stress dependent behaviour under repeated stresses and deformation occurs through shear or densification (Maree & Freeme, 1981; Wolff, 1996). The description of each type of material, the required specification and construction requirements are extensively covered by Maree & Freeme (1981), CSRA (1994) and Theyse *et al.* (1995).

Granular base pavements comprising untreated gravel or crushed stone on a granular or cemented subbase with a subgrade of various gravels usually exhibit a distress mode which is largely controlled by the type of subbase. With a granular subbase the distress mode is usually permanent (plastic) deformation from densification and/or shear of the untreated subbase. This deformation may manifest itself either as rutting or as surface roughness (CSRA, 1994).

Wolff (1996) summarises the failure mechanisms whereby shape changes or permanent deformation in granular layers occur as follows.

- Total rupture of material by one or a few load repetitions when the maximum available shear strength is exceeded and gross shear displacements occur.
- Non-recoverable shear strains caused by many repetitions of load substantially less than the rupture load. The permanent deformations due to this creep or progressive deformation behaviour are more in the nature of fatigue properties.
- Densification or compaction of the material in the loaded zone without necessarily any complementary shear deformations.

Wolff (1996) pointed out further that the shape changes caused by the first two mechanisms are dependent on the shearing resistance characteristics of the granular soil. Wolff elaborates that "*shearing resistance characteristics*" does not simply mean the strength at failure for slow rate of strain as would be expressed by a strength envelope obtained from conventional soils tests. It rather means the strength behaviour under the specific forms of dynamic (repeated) loading and insitu confinement and all the strains up to and including rupture.

After examining the measured elastic and plastic strains that were developed in granular pavement layers subjected to repeated loading during Heavy Vehicle Simulation (HVS) testing Wolff (1996) found that the nature of granular materials is such that elastic and plastic strains are introduced by one repetition of stress much smaller than the yield stress of the material as defined by the Mohr-Coulomb failure envelope.

Wolff (1996) then concluded that the stress-strain behaviour of granular materials is non-linear and in-elastic as follows.

- The stress-strain curve of a granular material will not be a straight line with a constant slope, but a curved line with a slope or resilient modulus (M_R) varying with applied stress (See Figure 2-6 and Figure 2-7, Page 32).
- Permanent or plastic strain takes place during each application of stress, (the stress being much smaller than the yield stress of the material), and that these strains accumulate with load repetitions. On the removal of stress, the loading stress-strain curve will not be retraced, but a hysteresis loop will form including the permanent deformation that has taken place during the application of the stress.

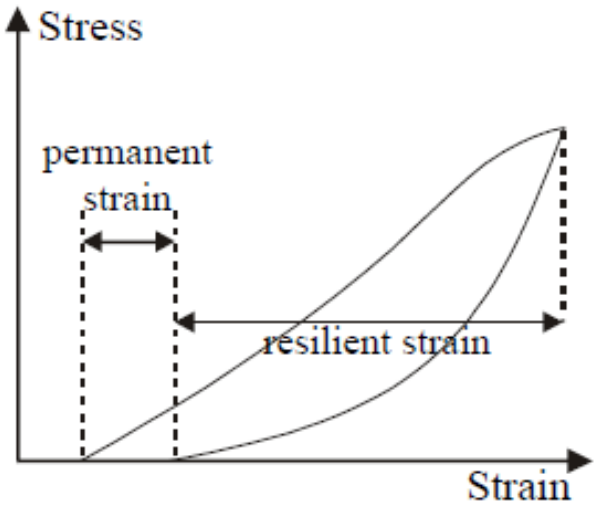


Figure 2-15: Hysteresis loop for non-elastic permanent deformation behaviour (after Wolff, 1996; Lekarp *et al.*, 2000b and Theyse, 2007)

Figure 2-15, shows a general hysteresis loop similar to that observed by Wolff (1996) on HVS tested granular materials. This supported his hypothesis that the permanent deformation that unbound granular materials undergo, when subjected to repeat loading by stresses well below the yield stress of the material as defined by the Mohr-Coulomb failure envelope, is caused by the elasto-plastic behaviour.

2.6. Dilatancy

2.6.1. *Shear strength and dilatancy*

The shear resistance properties of granular materials are affected by many factors including interparticle friction, dilation and particle shape (Guo & Su, 2007). These properties are determined from the results of either direct shear tests or drained triaxial tests, with the drained strength of coarse granular materials being relevant in practice (Craig, 2004). Typical stress-strain behaviour of sand is shown in Figure 2-16 which shows curves relating the principal effective stress ratio (σ'_1/σ'_3) to the major principal strain (ε_1) and the volumetric strain (ε_v) to the major principal strain (ε_1) for: (a) initially dense and (b) initially loose sand specimens.

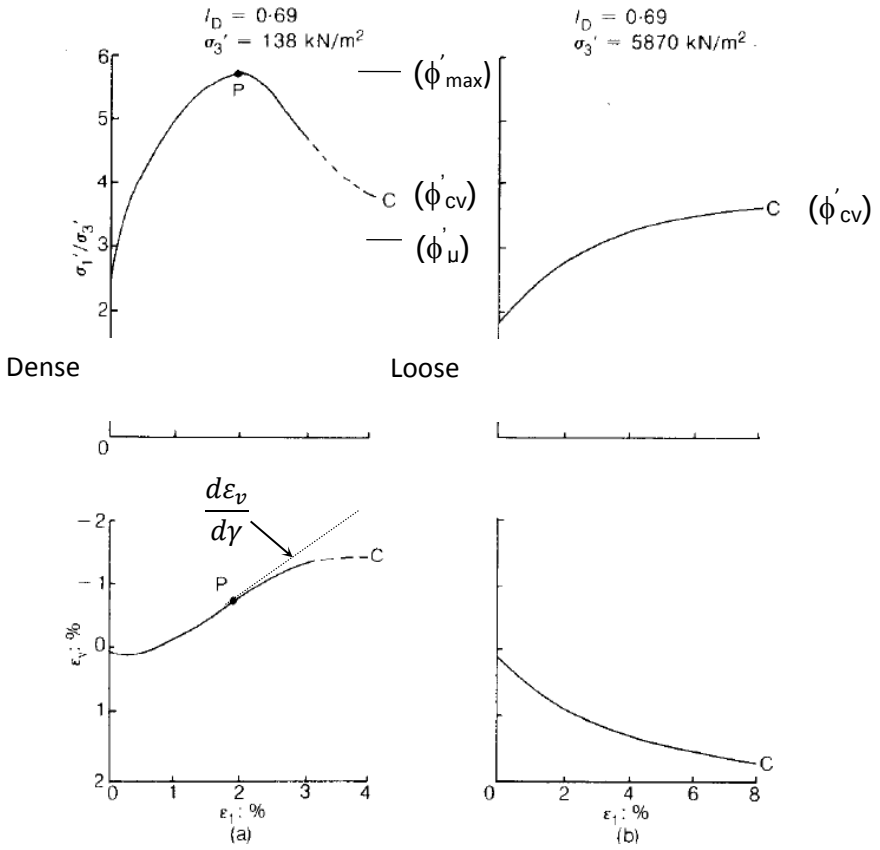


Figure 2-16: Stress-strain behaviour of dense sand in plane compression (a) at low stress (b) at high stress (Bolton, 1986)

In dense sand there is a considerable degree of interlocking between particles and in addition to the frictional resistance at the particle points of contact, this interlocking must be overcome before shear failure can occur. In general the degree of interlocking is greatest in the case of very dense, well graded sands consisting of angular particles (Craig, 2004).

The characteristic stress-strain curve for sand Figure 2-16 which is initially dense shows a peak stress at point P corresponding to the maximum angle of shear resistance (ϕ'_{max}), at a relatively low strain. Thereafter, as the interlocking is progressively overcome, the stress decreases with increasing shear strain until the critical state at point C is reached, corresponding to the critical angle of shear resistance (ϕ'_{cv}) where shearing occurs at constant volume. Rowe (1962) illustrated the process of particle dilation with a simple analogy of two uniform serrated faces in contact (Figure 2-17). The reduction in the degree of interlocking produces an increase in the volume of a specimen, shown as positive dilatancy. The opposite, after the edge peaks just pass each other, is termed negative dilatancy, resulting in a higher degree of particle packing and interlock.

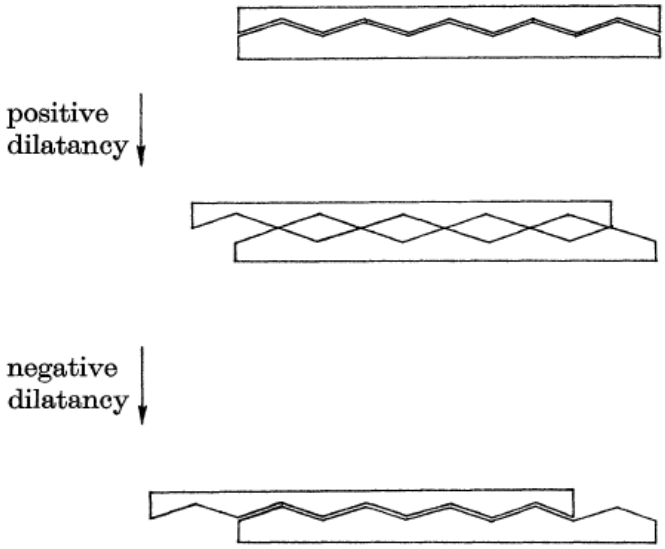


Figure 2-17: Illustration of interface dilation using serrated edges sliding past each other (after Rowe, 1962)

The term dilatancy describes the increase in volume of dense sand during shearing and the rate of dilation is represented by the gradient $d\varepsilon_v/d\gamma$ with the maximum corresponding to the peak shear stress. The angle of dilation (ψ) is given by $\tan^{-1}(d\varepsilon_v/d\gamma)$ which represents the average value of the numerous microscopic planes inclined at various angles between individual particles along which sliding occurs (Craig, 2004).

The kind of dilation that dense sand exhibits is not the dilation associated with an over-consolidated material expanding to its new looser critical state. The behaviour of dense sands and over consolidated materials differs because in dense sands the maximum rate of dilation is achieved at the strain corresponding to the maximum shear stress, whereas in over-consolidated materials dilatancy does not begin until the peak shear stress is reached. Dilation in over-consolidated material is the result of the material

having been pre-stressed at a point in its history, resulting in consolidation of the material remaining after that stress is removed. The dilatant behaviour of over consolidated materials is due to the breaking of interparticle bonds and the formation of a major slip plane along which the material fabric has an opportunity to swell and soften to its new critical state (Terzaghi *et al*., 1996). Instead the dilation in dense sands is that required to free the particles on a shear plane interface to slide over each other such that the material, initially at rest, becomes a flowing shear band (Cleaver *et al.*, 2000).

The term dilatancy was introduced by Reynolds (1885) and following the early work by Taylor (1948), the strength and dilatancy of soils received a great deal of attention in the early 1960s (Bolton, 1986). Bolton reports that this resulted in general agreement among those researching the strength of soil that:

a) secant, rather than tangent ϕ' values should be the basis for discussion;
b) dilatancy towards critical states is central to an understanding of soil behaviour and;
c) both the magnitude of the mean effective stress and soil density affect the rate of dilatancy of soils and therefore the strength parameters of soil.

It was during this period of increased attention to the strength and dilatancy of soil that pioneering work by Rowe (1962) was published. Rowe (1962) conducted experiments on ideal assemblies of rods and uniform spheres to establish expressions for the relationship between the rate of dilatancy and the maximum principal effective stress ratio for any ideal packing. The solution was extended to the case of a random assembly of irregular particles by investigating the conditions under which the mass dilates such that the rate of internal work absorbed in frictional heat is a minimum. This resulted in a fundamental stress-strain relationship which has been adopted extensively in modeling granular material dilatancy by many researchers, including Bolton (1986), Guo and Su (2000), Been and Jefferies (2004).

2.6.2. *Fundamental stress-dilatancy theory*

To measure the strength and volume changes of simple geometric packings of cohesionless uniform particles subject to a deviatoric stress Rowe (1962) used uniform rods. He considered the following packing geometries:

a) two dimensional stress system: uniform rods in parallel stack (Figure 2-18 (a));

b) three dimensional stress system with uniform spheres in face-centered cubic packing (Figure 2-18 (b));

c) uniform spheres in rhombic packing.

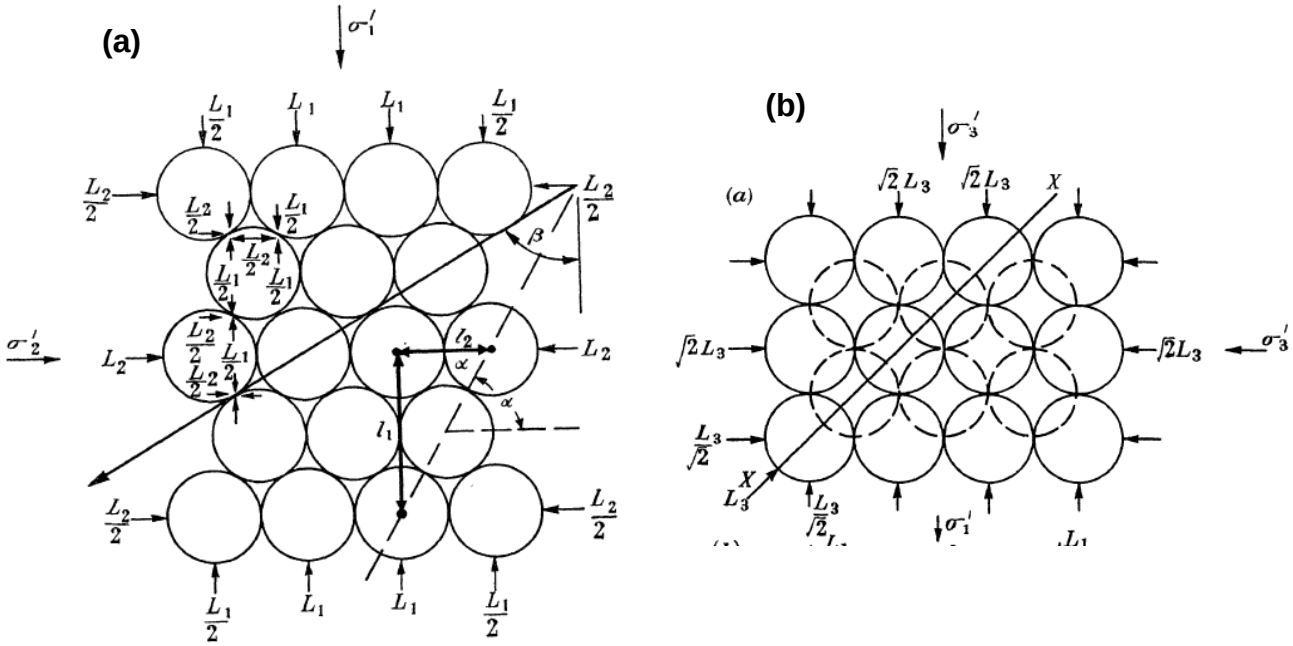


Figure 2-18: Geometric packing (elevations) of rods considered by Rowe (a) parallel stack (b) uniform spheres in face centered cubic packing (after Rowe, 1962)

Rowe considered a wedge ABC subject to a normal force Q and an applied shear force P with sliding occurring in the direction β from that of shear force P (Figure 2-19).

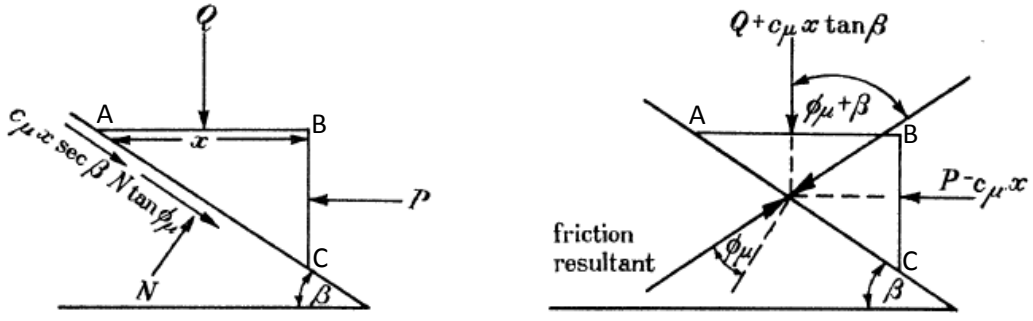


Figure 2-19: Simple wedge analysis (after Rowe, 1962)

With c_μ and ϕ_μ defined as the cohesion and true angle of friction between the mineral surfaces of the particles respectively, resolving the forces gives (according to Rowe (1962)):

$$P = Q\tan\left(\phi_\mu + \beta\right) + \frac{c_\mu x \sec^2\beta}{1 - \tan\beta\tan\phi_\mu} \qquad \text{Eq. 2.20}$$

Now from Figure 2-18 (a)

Letting $L_{1,2}$ = load per rod in directions 1 or 2

β = deviation of the tangent at the contact points from the direction 1

with each rod being supported by two points on each side, from Eq. 2.20 we have,

$$L_1/L_2 = \tan(\phi_\mu+\beta) \qquad \text{Eq. 2.21}$$

And with reference to Figure 2-18 (a)

Let l_1 = length per alternate row in direction 1
Let l_2 = length per rod in direction 2,

such that

$$\tan\alpha = l_1 / l_2, \qquad \text{Eq. 2.22}$$

and σ'_1, σ'_2 = major and minor principal stresses, acting in directions 1 and 2 on Figure 2-18 (a)

Then according to Rowe:

$$\frac{\sigma'_1}{\sigma'_3} = \frac{L_1 l_1}{L_2 l_2} = tan\,\alpha\, tan(\phi_\mu + \beta) \qquad \text{Eq. 2.23}$$

Similarly, using uniform spheres in face centered cubic packing and rhombic packing Rowe (1962) found that whatever the geometrical arrangement of the solids, the stress ratio of major principal effective stress to minor principal effective stress at the peak strength and during subsequent states of deformation resulted in Eq. 2.23. He found further that the expression in Eq. 2.23 can be obtained for any packing if an imaginary plane of particles interlocking at angle α to the direction of the minor principal stress is drawn, together with particles sliding in contact in a direction β to the major principal stress (Figure: 2-20).

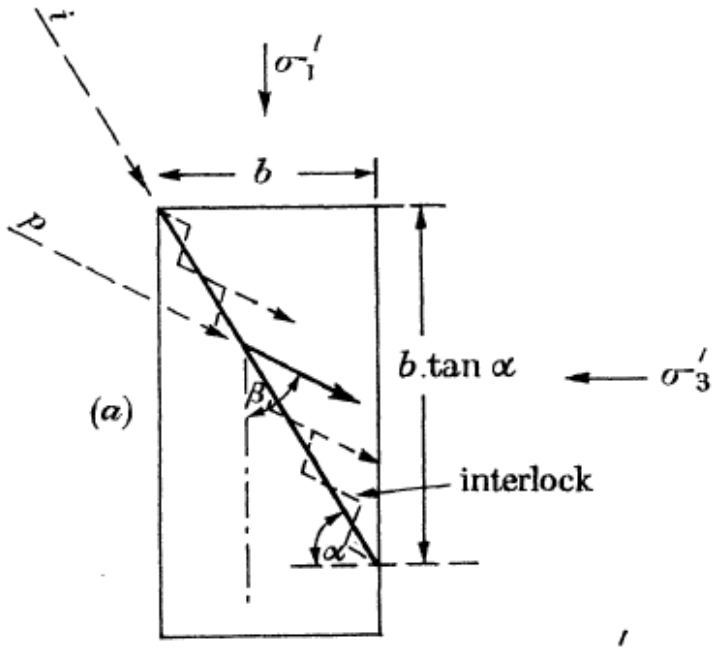


Figure: 2-20: Imaginary plane of particle interlock (Rowe, 1962)

Rowe (1962) then applied the expression in Eq. 2.23 to a random mass of irregular particles postulating from observations that the time for relocation of the particles would be most economically achieved for a given particle arrangement if the individual values of β are such that the rate of internal work done is a minimum.

This is expressed by the condition:

$$d\dot{E}/d\beta = 0 \qquad \text{Eq. 2.24}$$

When

$$\beta = (45° - \frac{1}{2}\phi_{\mu}) \qquad \text{Eq. 2.25}$$

such that

$$\frac{\sigma_1'}{\sigma_3'\left(1 + \frac{d\dot{V}}{V\dot{\epsilon}_1}\right)} = \tan^2\left(45° + \frac{\phi_{\mu}}{2}\right) \qquad \text{Eq. 2.26}$$

Rowe (1962) introduced the assumption that the rate of internal work done is a minimum without further proof, but the validity of this relationship was confirmed by De Josselin de Jong (1976), who by considering the same model of toothed serrated planes as that treated by Rowe (1962) and applying to that model the laws of friction only, without resorting to energy principles, obtained the same result.

The stress-dilatancy expression in Eq. 2.26 accounts for the sum of the energy absorbed in friction and that in dilation. Rowe (1962) concludes that the left hand side of the equation is the stress ratio corrected for the dilation and the right hand side is the stress ratio for an ideal plastic material with friction angle ϕ'_{μ}.

From the observations of experimental data Rowe (1962) found that Eq. 2.26 did not fit the behaviour and thus needed to be modified. This resulted in Eq. 2.27 and Eq. 2.28:

$$\frac{\sigma'_1}{\sigma'_3\left(1+\frac{\mathrm{d}\dot{V}}{V\dot{\epsilon}_1}\right)} = \tan^2\left(45° + \frac{1}{2}\phi_f\right) \qquad \text{Eq. 2.27}$$

Where $\frac{d\dot{V}}{V}$ is the instantaneous unit volume expansion and ϕ_μ in Eq. 2.26 is replaced by ϕ_f, the angle of friction accounting for the reduced value of ϕ' corrected for energy due to expansion.

$$\sigma'_1/\sigma'_3 = \tan\alpha\tan\left(45° + \frac{1}{2}\phi_f\right) \qquad \text{Eq. 2.28}$$

In Eq. 2.27, Rowe related the mobilised stress ratio to the plastic strain rates, in what has become known as stress–dilatancy theory. The relationship is generally included in literature (Bolton, 1986; and Been & Jefferies 2004) in the form:

$$\frac{\sigma'_1}{\sigma'_3} = \left(\frac{\sigma'_1}{\sigma'_3}\right)_{\mathrm{crit}}\left(1 - \frac{\mathrm{d}\varepsilon_v}{\mathrm{d}\varepsilon_1}\right) \qquad \text{Eq. 2.29}$$

Where

σ'_1, σ'_3 are the major and minor principal effective stresses

and

$d\varepsilon_v$, $d\varepsilon_1$ are the volumetric and major principal strain rates of change.

From the work done by Rowe (1962), below is a summary of his findings which today constitute the basic theory on dilatancy.

- The Mohr-Coulomb criterion of failure, based on the theory of plasticity applicable to shear of continuous material, is shown not to have general application to discontinuous assemblies of particles such as sands.
- Whatever the geometrical arrangement of solids subjected to a deviatoric stress system, the stress ratio at the peak strength and during subsequent states of deformation follows the law:

$$\frac{\sigma_1'}{\sigma_3'} = \tan\alpha \tan(\phi_\mu + \beta) \qquad \text{Eq. 2.30}$$

- The slip plane observed in the laboratory and in the field is not the cause of failure at the peak shear stress as assumed by Coulomb. Failure at the peak shear stress is caused by the α-plane corresponding to the average geometry of packing at the instant of collapse of critical groups of particles.
- When the soil is shearing at no volume change i.e. at the critical state, in the completely remoulded state the stress-dilatancy relation modified for energy loss is identical in result with the Mohr-Coulomb theory, indicating that the slip plane observed in the laboratory and field is the later result of failure.
- Experimental results showed that ϕ'_f, the angle of friction accounting for the reduced value of ϕ' corrected for energy due to expansion, increases from ϕ'_μ at the minimum porosity to ϕ'_{cv} for loose packings at maximum porosity. Calculated values of ϕ'_{max} decrease from a maximum at the minimum porosity towards ϕ'_{cv} at the maximum porosity. The difference between the curves of ϕ'_{max} and ϕ'_f is attributed to the energy spent on dilation.

2.6.3. *Further developments and modifications to Rowe's stress dilatancy theory*

Bolton (1986) introduced a relative dilatancy index, which expresses the dilation potential of a soil by a single number, and demonstrated its use in the predictions of the behaviour of sands at failure by comparing his prediction to published data. Bolton (1986) used a similar approach to Rowe (1962) to develop an expression which deviated only slightly from Rowe's in its estimate of ϕ' appropriate to plane-strain shear. The expression is:

$$\phi' = \phi_{crit} + \psi \qquad \text{Eq. 2.31}$$

Where

ϕ_{crit} is the angle of shearing resistance observed in a simple shear test on soil loose enough to be in a critical state, therefore with zero dilation

ψ is the dilatancy angle

Bolton (1986) further showed that the predictions of Rowe's stress-dilatancy relationship (Rowe, 1962) for plane shear can be obtained by modifying Bolton's definition of ϕ' to the form:

$$\phi' = \phi_{crit} + 0.8\psi \qquad \text{Eq. 2.32}$$

Bolton (1986) concluded:

- Secant angles of shearing are required in a rational approach to the strength and dilatancy of sands. The relationship $\phi_{max} - \phi_{crit}$ was shown to be a useful measure of the extra component of strength due to dilatancy in a dense soil.
- A new relative dilatancy index I_R in the form:

$$I_R = I_D(10 - \ln p') - 1 \qquad \text{Eq. 2.33}$$

was defined in terms of relative density, I_D, and the mean effective stress level p'.

Been and Jefferies (2004) applied the stress-dilatancy relationship to study the nature of loose soil behaviour with regard to liquefaction of the soil by using drained triaxial tests. They found that there are several forms of the stress-dilatancy relationship in literature, but all retain the form:

$$\frac{\sigma_1'}{\sigma_3'} = K\left(1 - \frac{\dot{\varepsilon}_v}{\dot{\varepsilon}_1}\right) \qquad \text{Eq. 2.34}$$

where

$$K = \left(\frac{1 + \sin\phi_\mu}{1 - \sin\phi_\mu}\right) \qquad \text{Eq. 2.35}$$

This form relates to Rowe's equation (Rowe, 1962) prior to the modification (Eq. 2.26), since K is based on the true angle of friction between the mineral surfaces of the particles ϕ_μ, where Rowe (1962) observed that the mobilised friction angle for particle slip varied. Been and Jefferies (2004) note that Rowe (1962) introduced ϕ_f such that $\phi_\mu \leq \phi_f \leq \phi_c$, where ϕ_c is the critical state friction angle. However there is limited guidance or data which describe how ϕ_f varies and they note that many models simply assume that K is constant.

Experimental investigations carried out by Been and Jefferies (2004) clearly indicated that ϕ_f varies. They observed that the soil parameter ϕ_f is neither constant nor equal to the critical value in general for dense sand. This led them to seek an understanding of how ϕ_f varies within the stress path of a test and how the evolution of ϕ_f varies with changing initial soil state.

Been and Jefferies (2004) considered four stress-dilatancy theories (Table 2-5), alternative to Rowe's original theory (Rowe, 1962).

Table 2-5: Stress dilatancy relationships

Theory	Source
Cam Clay	Schofield and Wroth (1968)
Modified Cam Clay	Roscoe and Burland (1968)
Nova 1982	Nova (1982)
Li and Dafalias 2000	Li and Dafalias (2000)
Rowe 1962	Rowe (1962)

After plotting the stress dilatancy relationships from the four theories, and using a constant ϕ_f, Been and Jefferies (2004) concluded that the Cam Clay flow rule was the best flow rule for modeling sand behaviour.

Further, Been and Jefferies (2004) examined three proposed relationships (Table 2-6) which describe the evolution of ϕ_f. All three relationships are in terms of the state parameter ψ_{sp} ($e - e_{cs}$), defined as the difference between the current void ratio, e, and the void ratio at the critical state, e_{cs}, at the same mean effective stress, because (according to Been & Jefferies, 2004) ψ_{sp} is the only state variable that can be reasonably determined from current technology. Been and Jefferies (2004) ould not find conclusive evidence that the state parameter ψ_{sp} is an appropriate choice for the state variable controlling ϕ_f. The authors (Been and Jefferies, 2004) conclude that all three relationships are crude engineering approximations to the actual behaviour and that particle arrangement or a fabric tensor is needed in addition to ψ_{sp} to define the state of sand.

Table 2-6: Summary of proposed relationships for describing the evolution of ϕ_f (Been and Jefferies, 2004)

Originator	Relationship
Manzari and Dafalias, 1997	$\phi_f = \phi_{cv} + m\psi$
Li and Dafias, 2000	$\phi_f = \phi_{cv}.\exp(m\psi)$
Jefferies and Shuttle, 2002	$\phi_f = \phi_{cv} - \lvert\psi_i\rvert$

Note: m = constant

More recently Guo and Su (2007) investigated the effect of particle angularity on the shear strength and stress-dilatancy characteristics of granular material through a series of laboratory tests on two materials, Ottawa standard sand (Sand O) and crushed limestone (Sand L). Sand O is a quartzite sand with sub-rounded to rounded particles while Sand L consists of highly angular particles. The focus was placed upon

the shear resistance associated with dilation and interparticle locking. A total of 47 drained triaxial compression tests (24 on Sand O and 23 on Sand L) were performed using the Bishop type triaxial apparatus. Based on the experimental results, Guo & Su proposed an alternative concept of the different components of the maximum friction angle. The results obtained by Guo and Su (2007) are shown in Figures 2-21, 2-22 and 2-23.

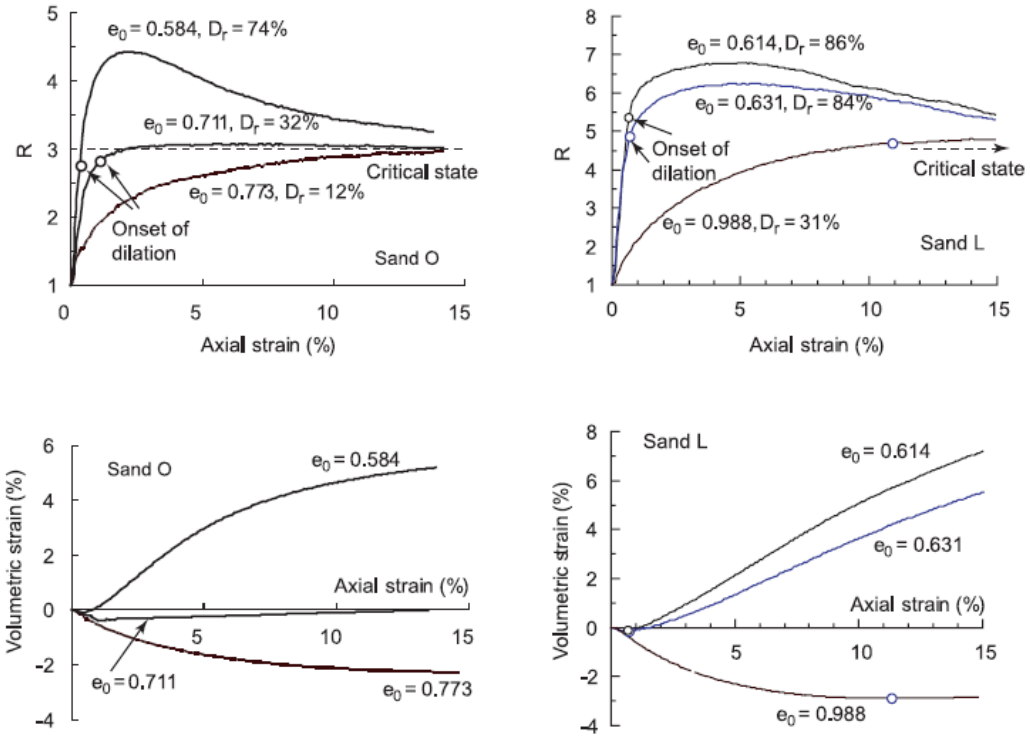


Figure 2-21: Typical data of stress ratio R =σ'_1/σ'_3 and volumetric strain plotted against axial strain for Sand O and Sand L at σ'_3 = 100 kPa (After Guo & Su, 2007)

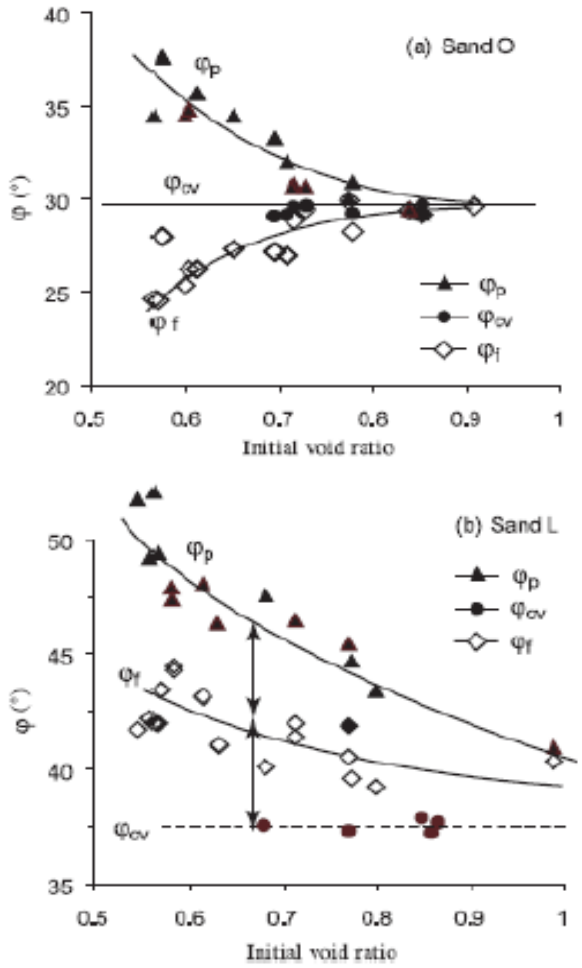


Figure 2-22: Measured shear strength of (a) Sand O and (b) Sand L for different void ratios at σ'_3 = 100 kPa (after Guo and Su, 2007)

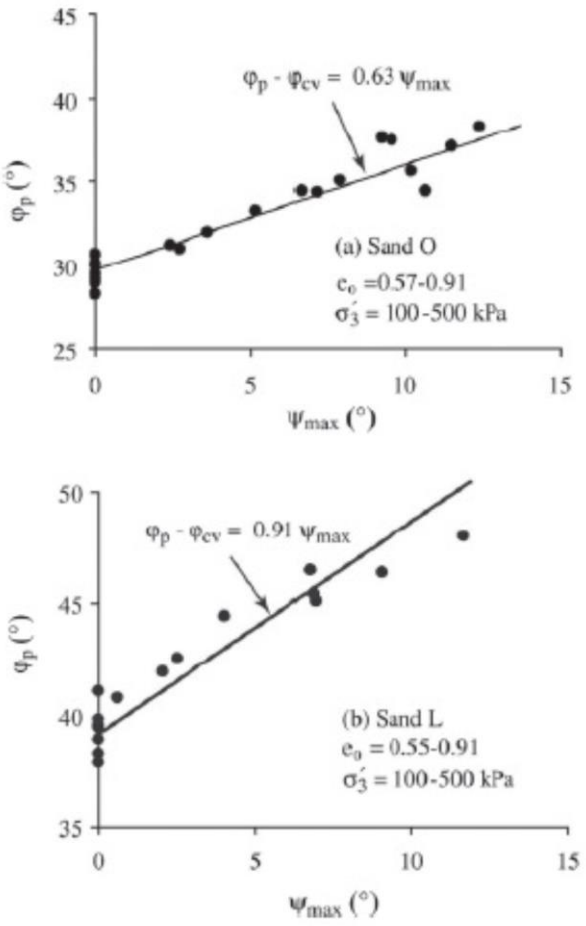


Figure 2-23: Relationships between friction angle ϕ_p and ψ_{max} (after Guo & Su, 2007)

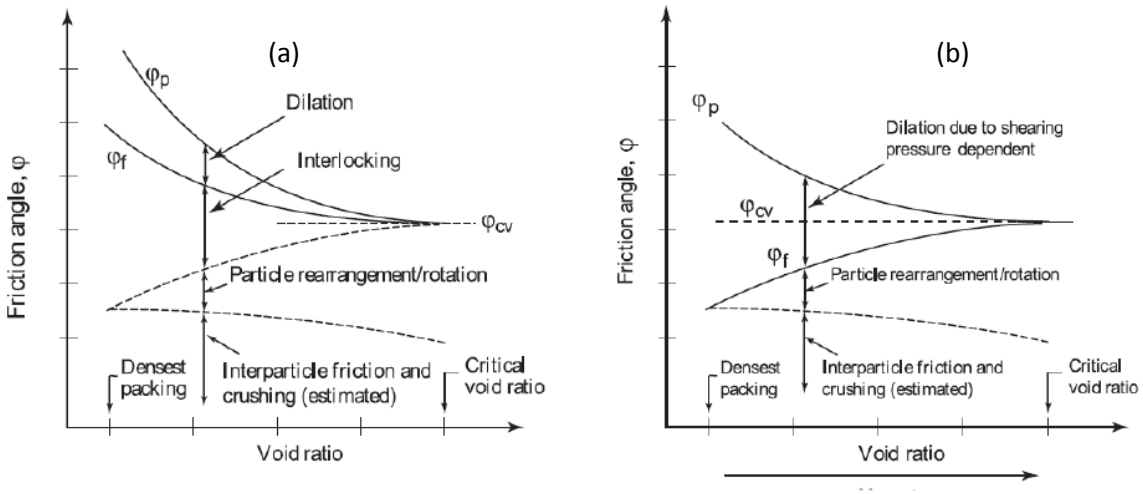


Figure 2-24: Contributions to shear resistance of granular materials (a) alternative conceptual model proposed by Guo and Su (2007) (b) revised from Rowe (1962)

From the results Guo and Su (2007) made the following observations:

- When comparing the response of Sand L with that of Sand O, it was observed that Sand L required relatively larger axial strains to mobilise the maximum shear resistance than Sand O (Figure 2-21) of the same relative density, but post peak strain softening is gentler than that of Sand O. Guo and Su (2007) attribute the differences between the behaviour of Sand O and Sand L to the effects of particle shape. Since the angularity of particles causes more interparticle locking that restrains relative sliding and rotation between particles, a larger shear stress is required for Sand L than for Sand O to break the interlocking owing to particle angularity before relative particle movement can take place, which implies that the mobilised shear resistance is a combination of dilation, interparticle locking and inter-granular friction.

- Examining the results of Figure 2-21 revealed that dilation of Sand O starts at a stress ratio smaller than that at critical state, indicating that the mobilised friction angle at the onset of dilation ϕ_f is smaller than the critical angle ϕ_{cv}. For Sand L however, the experimental data show that the onset of dilation occurs at a mobilised friction angle higher than ϕ_{cv}. Figure 2-22 (a) and (b) show the variation of ϕ_f and the peak friction angle ϕ_p against the initial void ratio e_o. Further comparison between Figure 2-22 (a) and (b) indicates that the higher ϕ_f of Sand L than ϕ_{cv} likely reflects the influence of interparticle locking due to particle angularity.

- By defining the angle of dilation ψ following Rowe (1962) as $\sin\psi = d\varepsilon_v/d\gamma$ with $d\varepsilon_v$ and $d\gamma$ being volumetric and shear strain increment respectively, Guo & Su presented the relationship between the peak friction angle $\phi_p$and the maximum angle of dilation ψ_{max} as shown in Figure 2-23. From these results Guo and Su observed the relationship between ϕ_p and ϕ_c for Sand O and Sand L respectively as:

$$\phi_p - \phi_c = 0.63\,\psi_{max} \qquad \text{Eq. 2.36}$$

and

$$\phi_p - \phi_c = 0.91\,\psi_{max} \qquad \text{Eq. 2.37}$$

Based on the experimental data presented by Guo and Su (2007) and by following the decomposition of shear strength components presented by Rowe (1962), Guo and Su proposed an alternative conceptual model shown in Figure 2-24 (a) which extended Rowe's model (Figure 2-24 (b)) to accommodate the contribution of interparticle locking owing to particle angularity.

LITERATURE REVIEW SUMMARY AND FINDINGS

i. The data and results presented by Jooste (2004) indicate that small changes in pavement layer properties can lead to large variations in predicted structural capacity of the pavement. The findings also suggest that the current design model may be underestimating pavement load carrying capacity by not fully accounting for factors that increase confining stress such as material dilatancy. Jooste illustrated that decreasing the confining stress leads to a reduced predicted load carrying capacity and also that increasing the confining stress by varying the material input properties which affect the confining stress leads to an increased load carrying capacity. In his evaluation, however Jooste did not investigate any relationship that may possibly relate the dependence of the predicted load carrying capacity of a pavement to the changes in confining pressure.

ii. The standard design load of a 40 kN dual-wheel load at 350 mm spacing between centres and a constant tyre pressure of 520 kPa is outdated. Actual tyre/pavement contact stresses are greater than the tyre inflation pressure and exceed the design value of 520 kPa by a factor of up to three times. The prevalence of overloading on South African roads, the increased truck tyre loading and the increasing tyre inflation pressure have a significant influence on the stresses applied by traffic loading onto the pavement. The loading conditions used to evaluate pavement response must be in line with observed stresses, and measurements using the Vehicle-Road-Surface-Pressure-Transducer-Array (VRSPTA) which yields three dimensional contact stresses should be utilized (De Beer *et al*., 1999) Trends and new technology such as the super single-tyres must be incorporated and accounted for in the design of pavements since the stresses induced by these tyres are different to those of the traditional dual tyre.

iii. Granular materials show stress-dependent behaviour under repeated stresses and deformation occurs through shear and densification. These materials are not elastic and experience some non-recoverable deformation after each load application. The theory of linear elasticity is used in the SAMDM to compute the stresses induced in the pavement layer materials by externally applied loads. The assumptions of the theory are highlighted in Section 2.5.1 and include the assumptions that each layer is homogeneous and isotropic. Soil, seldom if ever, exactly fulfills and often seriously violates these assumptions. Yet the engineer has little choice but to use the results of this theory together with engineering judgment.

iv. De Beer (1999) identified that one of the components required for an improved mechanistic method towards the prediction of pavement performance is an improvement of the material constitutive modeling. In this report, two FEA packages, namely SIGMA/W and PLAXIS, are considered and the constitutive models of each are discussed. The models discussed include the first order linear elastic model, elastic-plastic model, anisotropic elastic model, nonlinear elastic hyperbolic model, Cam Clay model and the soil hardening model. These models offer various levels of sophistication, often with a proportional increase in the number of required input parameters. With these models it is possible to incorporate the following criteria for modeling soil behaviour.

- The possibility of having different stiffness values in two orthogonal directions and accounting for ground deposits or layers which are often stratified and inclined.
- Modeling the soil stiffness as a function of the confining stress and the shear strains.
- Including the dilatancy term (ψ) which models the positive volumetric strain increments (dilatancy) actually observed in dense soils.
- Limiting all stresses developed in the model to compression stresses by specifying a tension cut-off and disallowing tensile stresses in the soil structure. In this case Mohr circles with positive principal stresses are not allowed.

The varied formulations of the constitutive models give different principal stress and strain results which can be converted by transfer functions into predictions of road layer life. The calculated stress and strain results therefore influence the predicted pavement layer life. Yet, it is still general practice in the SAMDM to use the first order approximation model of a multilayered linear elastic system. The multilayered linear elastic system is based on several assumptions, discussed in Section 2.5.1 of this report, a number of which are known to be only very gross approximations for actual observed soil behaviour.

v. The stresses used in the SAMDM model are based solely on externally applied loads. Internally developed stresses (e.g. from negative pore pressures and dilation) are not adequately incorporated. Theyse and Kannemeyer (2010) recommended a new approach towards accurate assessment of stresses which incorporates contributions to the effective stress by vertical overburden stress, equal all round internal suction pressure and the three dimensional

stresses associated with the wheel load. This approach, however, does not account for the influence of the increased confining pressure from restrained dilation on predicted stresses.

vi. Dilatancy can be expressed as a property due solely to the geometry of the volumetric expansion necessary before shearing can take place (Bolton, 1986). The shear strength component owing to dilatancy of a dense granular soil is not in addition to the peak frictional angle (ϕ_p) but is a component of ϕ_p and is best represented by the expression:

$$\phi_p = \phi_{cv} + \psi \qquad \text{Eq. 2.31}$$

CHAPTER 3

INVESTIGATIONAL WORK

Two finite element analysis (FEA) packages, PLAXIS and SIGMA/W were discussed in Section 2.5.2 of this report. These packages were used to assess how the incorporation of the dilatancy term in the constitutive model affects the predicted stresses used in the SAMDM for pavement analysis. In order to obtain input parameter values for these FEA packages, direct shear tests were conducted on dilating road building aggregates. Standard laboratory tests were carried out in order to classify the material according to the TRH 14 (CSRA, 1985) system. A large shear box (357 mm x 357 mm x 125 mm deep) was then used to test the materials in direct shear and obtain the shear parameters: peak and residual friction angles, cohesion and dilatancy. The following sections describe the laboratory testing program carried out at the University of the Witwatersrand materials testing laboratory. The following two commercially available materials were sourced from the Blue Platinum Quarry in Lanseria in the North of Johannesburg and used for the purposes of the investigation:

- **Material 1: Blue Platinum Quarry (BPQ 1)**
- **Material 2: Blue Platinum Quarry (BPQ 2)**

Both Material 1 and Material 2 which were used in this investigation are of dolerite origin and are obtained from blasting and crushing operations at the Blue Platinum quarry. The quarry is located approximately 5 km north west of Lanseria Airport and from the 1:250 000 geological maps published by the Government Printer (1981) the local geology of this area is in the Karoo Basin sequence which is characterised by an accumulation nearly eight kilometers thick of mudrock and sandstone, with tillite at the bottom, basalt at the top and coal at about midway (Brink, 1983). Rocks of the Karoo sequence are extensively intruded by dolerite (Brink, 1983) in the form of horizontal sills and vertical dykes. The entire quarry is located on a large dolerite sill.

3.1. Sample Preparation

The following procedure was used to prepare the samples:

a) Material was emptied from the sample bags, mixed and allowed to dry overnight.
b) The material was then sieved through the 26.5 mm sieve and all particles retained in the 26.5 mm sieve were discarded.
c) The material passing the 26.5 mm sieve was then sieved through the 75 μm sieve by washing in a basin and discarding the finer fraction until approximately 150 kg samples were obtained. The fines fraction was removed in order to improve the drainage of the gravels and thus reduce pore pressure build up

during the shear test and also because in practice the process of slushing (Simmelink and Visser, 1994; Kleyn, 2012) is used in which once the layer is placed and compacted, it is saturated and rolled continuously causing excess fines to migrate upwards onto the surface which are then broomed away in preparation for application of the prime coat. The material was then allowed to dry at room temperature for approximately 2 days.

3.2. Methodology

In order to characterise the material according TRH 14 (CSRA, 1985) the following standard laboratory tests were carried out:

- Sieve Analysis

  Summary of Test: A soil consists of discrete particles of various shapes and sizes. The objective of a particle size analysis is to group these particles into standardised separate ranges of particle sizes in order to determine the relative proportions, by dry mass, of each size range (Head, 1992a). Dry sieving of representative samples obtained by the method of quartering was carried out in accordance to TMH 1 (TMH, 1986): Test Method A1 (a). The following sieves were used: 26.5 mm, 19.0 mm, 13.2 mm, 9.5 mm, 4.75 mm, 2.36 mm, 2.00 mm, 0.425 mm, 0.075 mm and the pan.

- Atterberg Indicator Tests

  Summary of Test: The Atterberg limits including the Liquid Limit (LL), the Plastic Limit (PL) and Linear Shrinkage (LS) were carried out according to TMH 1 (TMH, 1986) test methods A2 (LL), A3 (PL) and Head (1992a) – Section 2.7.4 (Linear Shrinkage). The tests were carried out on the fraction passing the 0.425 mm sieve and are used to characterise the fines portion of the material.

- Specific Gravity

  Summary of Test: Soils may be composed of an accumulation of particles which are either of single mineral type, e.g. clean quartz sand, or more likely a mixture of a number of mineral types each with a different density. In this case the specific gravity is a measure of the mean particle density of the fraction of the soil mass passing the 0.425 mm sieve. The specific gravity test was carried out using pykometer bottles as set out in Head (1992a).

- Compaction tests

  Summary of Test: The compaction test provides the following basic data for soils; (i) the relationship between dry density and moisture content for a given degree of compactive effort, (ii) the moisture content for the most efficient compaction and (iii) the value of the maximum dry density so achieved (Head, 1992a). The compaction tests were carried out as set out in TMH 1: Test Method A7 (TMH, 1986). For the tests carried out under this investigation a mould with a diameter of 157.3 mm and a height of 127.0 mm with a detachable collar was used to house the sample. An automated compaction machine with a 4.536 kg tamper with a diameter of 50.8 mm was used to compact the material in three layers according to the Modified AASHTO 55 compaction effort (TMH, 1986).

- Bearing Strength Tests

  Summary of Test: The test is performed by pushing a standard plunger into the soil at a fixed rate of penetration and measuring the force required to maintain that rate. From the resulting load penetration relationship the California Bearing Ratio (CBR Value) can be derived for the soil in the condition at which it was tested (Head, 1992a). The CBR test was carried out as set out in TMH 1: Test Method A8 (TMH, 1986). A surcharge weight of 5 534.1 g was placed on the specimen and a loading rate of 1.2 mm per minute was used.

In addition to the standard laboratory tests which were used to characterise the material the following laboratory test was carried out:

- Direct Shear Test

  Summary of Test: The direct shear test, carried out using the shear box apparatus, measures the immediate or short term shear strength of soil in terms of total stresses. The shear box test is an angle of friction test in which one portion of soil is made to slide along another by the action of a steadily increasing horizontal shearing force, while a constant load is applied normal to the plane of relative movement (Head, 1992b). The apparatus provides no control of drainage and no provision for measuring pore water pressures. It is therefore not suitable for carrying out an undrained test, and its usual application is restricted to drained tests in which effective stresses are equal to total stresses (Head, 1992b). The test was carried out on the two materials using a large hydraulic shear box testing machine, with specimen dimensions 357 mm x 357 mm x 125 mm deep.

  Each specimen was compacted into the shear box using hand tools, and for the BPQ 1 material an average compaction of 101.43 % mod. AASHTO maximum dry density was achieved at an average moisture content of 5.8 %, while for the

material BPQ 2 the average compaction achieved was 84 % of mod. AASHTO maximum dry density at an average of 3.7 % moisture content. After preparation and compaction into the shear box the specimens were consolidated overnight at a normal stress of 3.7 kPa to allow the sample to reach equilibrium before shearing commenced. The samples were then tested under one of three effective normal stresses: 100 kPa, 200 kPa or 400 kPa. The shear load is applied to the lower part of the box, while the upper part is restrained against horizontal movement. During the test the normal and shear loads were measured using calibrated load cells mounted centrally above the soil and on the horizontal loading piston. The horizontal and vertical displacements were measured using Linear Variable Differential Transducers (LVDTs). All data output was captured using an Agilent 34970A data acquisition unit linked to a laptop as shown in Figure 3-1.

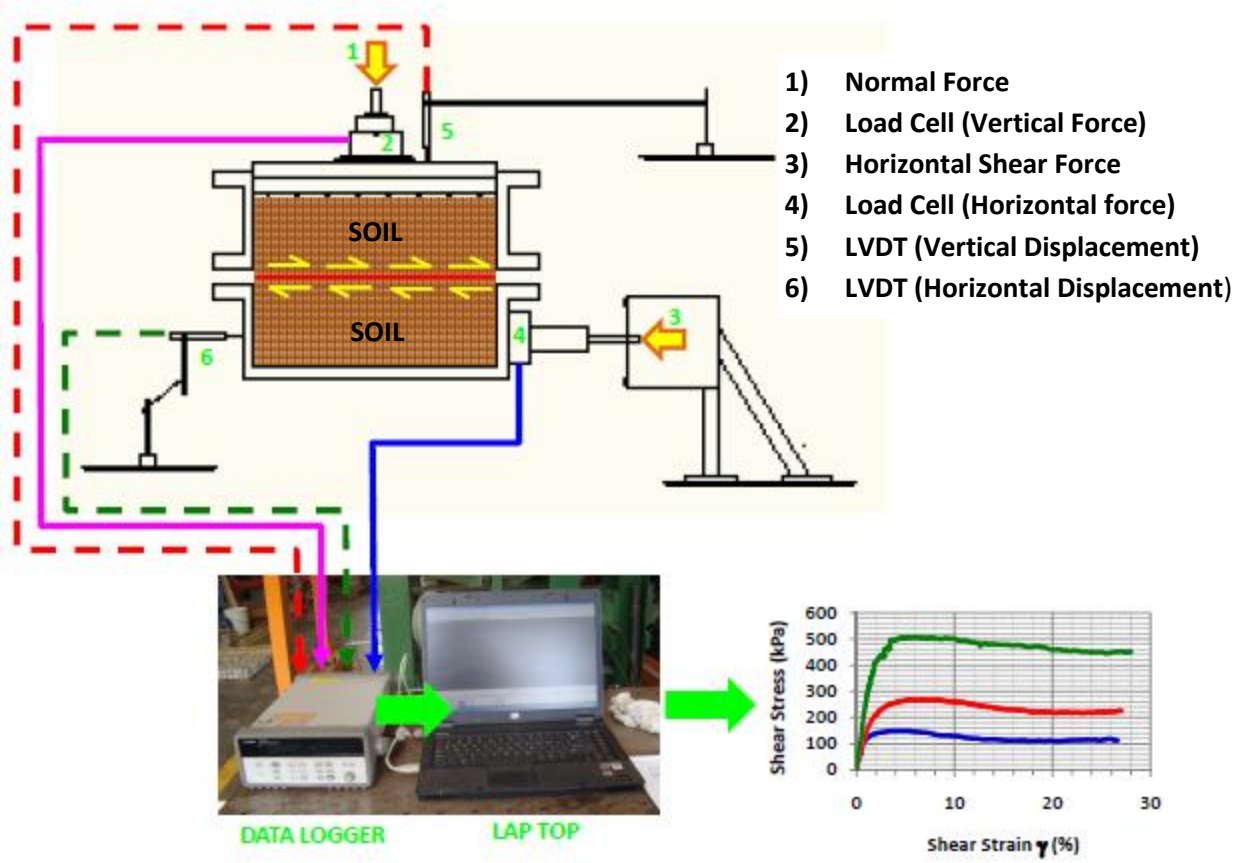


Figure 3-1: Laboratory shear box test set-up schematic

Calibration: The output from the data logger was obtained in units of volts and millivolts for the LVDTs' and load cell measurements respectively. Before commencing with the shear box test, the two LVDTs (LVDT No 587 measuring horizontal displacement and No 1033 measuring Vertical Displacement) and the vertical (921169) and horizontal (44927) load cells were calibrated. Calibration conversion factors were obtained using the least squares straight line fit which yielded the following equation:

$$y = a + bx \qquad \text{Eq. 3.1}$$

Where y = force (kN) or displacement (mm)
a and b are constants
x = voltage (V or mV)

The calibration results are attached in APPENDIX 2 (*Pages A2.1 – A2.4*), and Table 3-1 below presents a summary of the calibration constants for a and b.

Table 3-1: Data logger output calibration constants

	Units	Equipment	Data Logger output Units	Coefficient a	Coefficient b
Horizontal displacement	mm	LVDT No 587	Volt	33.880	7.267
Vertical Displacement	mm	LVDT No 587	Volt	-0.026	0.250
Horizontal Force	kN	Load Cell No. 44927	Millivolt	-350.584	258.942
Vertical Force	kN	Load Cell No. 921169	Volt	26.590	4.480

3.3. Results

3.3.1. *Laboratory tests for classification of soil*

A summary of the gravel and soil properties of the two samples tested in the laboratory is shown in Table 3-2. Figure 3-2 shows the grading curves for both materials superimposed onto the grading envelopes for G1 and G4 materials specified in TRH 14 (CSRA, 1985) and Figure 3-5 provides the plot of both materials on the soil matrix (consisting only the clay, silt and sand particle fractions i.e. < 2.0 mm) classification chart while Figure 3-6 shows the full soil sample (consisting of soil matrix and gravels) classification chart. It was to be expected that both materials are non-plastic (NP) due to the particle fraction responsible for plasticity properties of a soil (i.e. fraction passing the 75 μm sieve) having been removed. The effect of removing material passing the 75 μm sieve is evident as both materials have less than 0.8 % passing the 75 μm sieve (Table 3-2). The grading of both materials is uniform with both Material 1 (BPQ 1) and Material 2 (BPQ 2) grading curves falling within the required grading envelopes for G4 and G1 respectively (See Figure 3-2) until the 2 mm particle diameter size where both grading curves fall below the respective grading envelopes. As noted by Semmelink & Visser (2004) and Kleyn (2012) the grading of granular material is important and has a significant influence on the compactability of the material. Semmelink and Visser (2012) noted that the material fraction passing the 75 μm sieve is used as a lubricant during compaction to ease the relative movement between the larger particles while Kleyn (2012) concluded that there should be just enough of each particle size to fill the interparticle voids in order to achieve the densest interparticle packing. The deficiency in the fine materials which was observed in both BPQ 1 and BPQ 2 means that in the field it would be difficult to achieve the required and specified compaction. This is particularly important in the case of BPQ 1, which according to the TRH 14 classification system (CSRA, 1985) is a G1, since this would adversely affect the slushing process (Kleyn, 2012) and the benefits derived from the slushing process.

According to the plasticity and heave charts, the fine fractions of both material samples classify as low plasticity SILTS (ML) with low heave potential. The soil matrix, which comprises of all particles up to the 2 mm particle diameter size, of both materials BPQ 1 and BPQ 2 is classified as sand and on the full soil sample classification plot BPQ 1 plots as a sandy gravel and BPQ 2 as a gravel (Refer to Figure 3-5 and Figure 3-6).

Figure 3-3 and Figure 3-4 show the penetration data for BPQ 1 and BPQ 2. The summary for the calculated CBR values for the 2.54 mm penetration are included in Table 3-2, and for both BPQ 1 and BPQ 2 the CBR values of 82 % and 147 % at 98 %

Mod AASHTO Dry Density are above the minimum required CBR value of 80 % specified in TRH 14 (CSRA, 1985) for G2, G3 and G4 materials at 98 % Mod AASHTO density.

TRH 14 (CSRA, 1985) specifies a maximum swell of 0.2 % at 100 % Mod AASHTO for G2, G3 and G4 and 0.5 % at 100 % Mod AASHTO for G5. As shown in Table 3-2 the maximum swell measured at 100 % Mod AASHTO for BPQ 1 and BPQ 2 was 0.02 and 0.12 % respectively. Therefore according to swell requirements both meet requirements for classification as either G4 or better.

Table 3-2: Properties of test samples

PROPERTIES		MATERIAL 1 (BPQ 1)	MATERIAL 2 (BPQ 2)
Grading	D_{10} (mm)	0.7	0.425
	D_{30} (mm)	3.9	2.18
	D_{60} (mm)	14	5.7
	Coefficient of Uniformity (CU)	20	13.4
	Coefficient of curvature (CC)	1.6	2.0
	Grading Modulus	2.76	2.61
	Maximum particle size (mm)	19.0	19.0
	Percentage passing 0.075 mm	0.36	0.72
Particle Density	Mg/m^3	2.661	2.656
Atterberg Limits	Liquid Limit	NP	NP
	Plastic Limit	-	-
	Plasticity Index	NP	NP
	Bar Linear Shrinkage	0	0
Compaction	Maximum Dry Density (kg/m^3)	2033	2400
	Optimum Moisture Content (%)	8.6	4.25
CBR	@ 100 % mod AASHTO	112 %	173 %
	@ 98 % mod. AASHTO (2.5 mm)	82 %	147 %
	@ 93 % mod. AASHTO (2.5 mm)	35.7 %	82 %
Swell	@ 100 % mod AASHTO (%)	0.02	0.12
TRH 14 (CSRA, 1985) CLASSIFICATION		**G4**	**G1**

NOTE: NP = Non plastic

Considering the properties discussed above, according to the THR 14 (CSRA, 1985) classification system, Material 1 (BPQ 1) is classified as G4 and Material 2 (BPQ 2) is classified as G1.

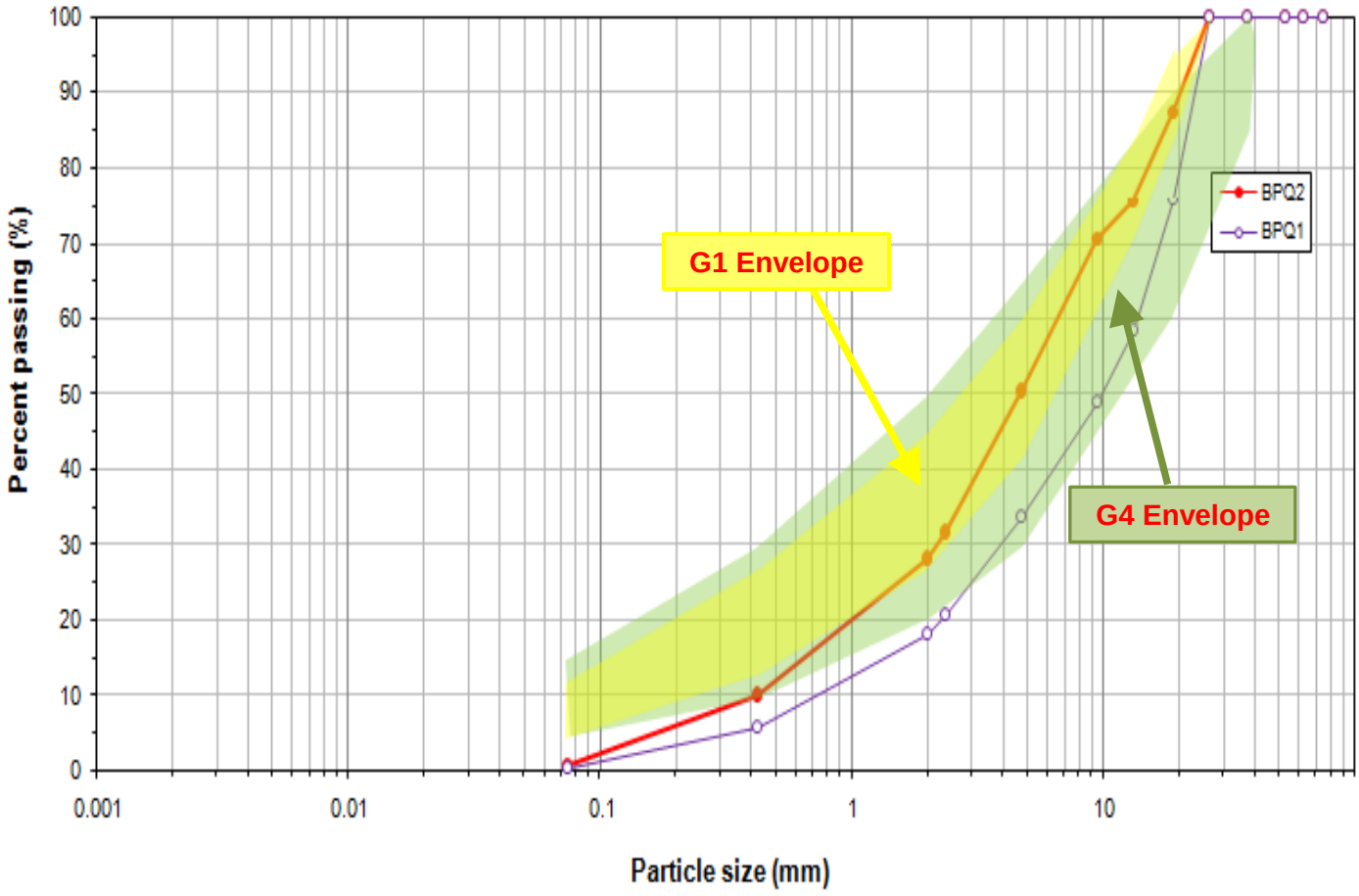


Figure 3-2: Sieve analysis results for materials BPQ 1 and BPQ 2

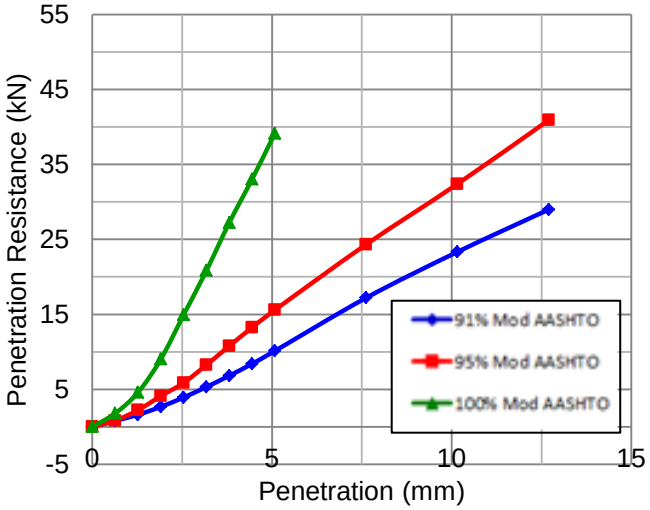


Figure 3-3: Penetration curve - BPQ 1

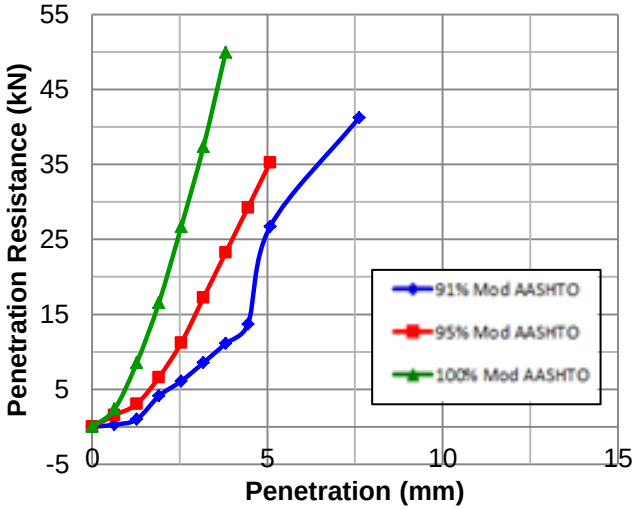


Figure 3-4: Penetration curve BPQ 2

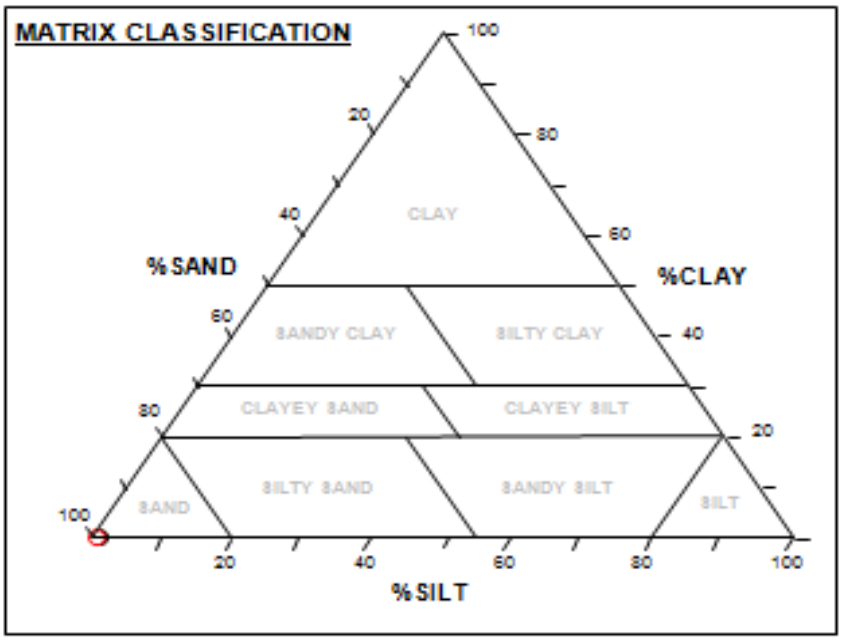


Figure 3-5: USDA soil matrix textural classification (Davis & Bennet, 1927)

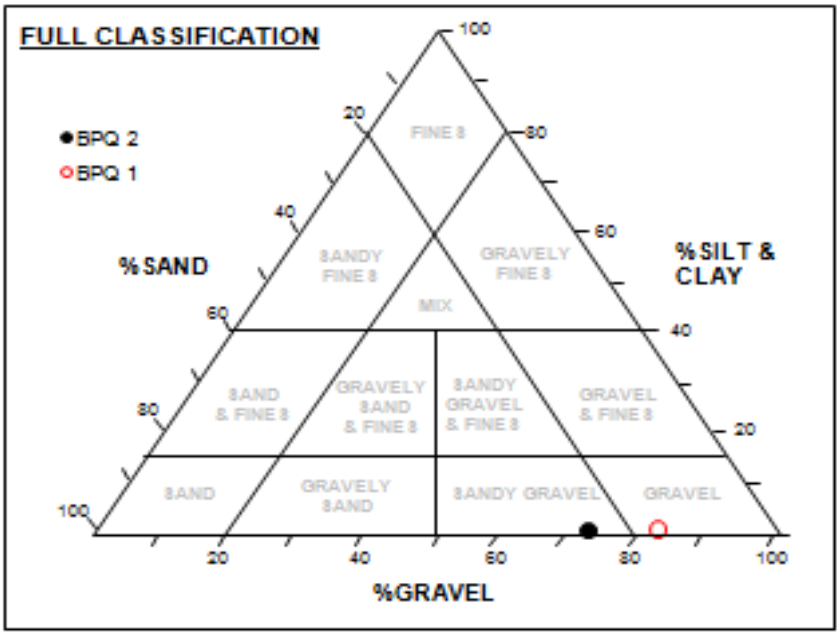


Figure 3-6: USDA full soil sample textural classification (Davis & Bennet, 1927)

3.3.2. *Shear box test results*

3.3.2.1. Material Shear Resistance

The strength of granular material and its performance under shear stress is influenced by the moisture content and the compaction achieved (Semmelink & Visser, 2004). Therefore the moisture condition and compaction under which the materials BPQ 1 and BPQ 2 were tested is important for the interpretation of the shear strength results. Table 3-3 and Table 3-4 below, show the moisture content and the bulk density calculated for the BPQ 1 and BPQ 2 samples, respectively, which were tested in the large shear box at vertical compressive stress of 100 kPa, 200 kPa and 400 kPa.

The Optimum Moisture Content (OMC) for BPQ 1 is 8.6 % and from Table 3-3, the samples were tested at an average Moisture Content (MC) of 5.8 %. The Bulk density as a percentage of the Maximum Dry density (MDD) varied from 94.7 % to 112.3 % with an average of 101.4 %.

Table 3-3: Material 1 (BPQ 1) Shear box test moisture and achieved compaction results

SAMPLE	MOISTURE		COMPACTION		
	Moisture Content [%]	OMC [%]	Bulk Density (BD) [kg/m^3]	Maximum Dry Density (MDD) [kg/m^3]	BD as percentage of MDD [%]
100 kPa	5.0	8.6	1 978.5	2033	97.3
200 kPa	4.8		1 926.5		94.7
400 kPa	7.5		2 282.3		112.3

From Table 3-4, the average moisture content for the three BPQ 2 samples tested is 3.7 % which is very close to the OMC of 4.2 %. The bulk density as a percentage of the MDD was generally very low varying from 78.5 % to 87.5% with an average of 84 %. Compared to the high compaction normally specified for G1, which is typically 88 % Apparent Relative Density (ARD) which is equivalent to about 106 % Mod. AASHTO density (Kleyn, 2012), the compaction which was achieved for the BPQ 2 samples was very low and this will have an influence on the shear strength properties that are discussed in the following paragraph. This clearly indicates that a higher compactive effort would be required to achieve the higher compaction requirements and this is likely influenced by the lack of the fines fraction which was removed from the sample.

Table 3-4: Material 2 (BPQ 2) Shear box test moisture and achieved compaction results

SAMPLE	MOISTURE		COMPACTION		
	Moisture Content [%]	OMC [%]	Bulk Density (BD) [kg/m^3]	Maximum Dry Density (MDD) [kg/m^3]	BD as percentage of MDD [%]
100 kPa	3.4	4.2	2 105.5	2 400	87.7
200 kPa	3.4		1 882.8		78.5
400 kPa	4.3		2 060.3		85.8

During each direct shear box test, the measured quantities were acquired every 5 seconds, providing a detailed record of each test. The measured quantities were the shear force, the normal force, the shear displacement in the horizontal direction and the vertical displacement of the sample due to contraction or dilation of the soil. The shear properties of both materials 1 and 2 are summarised in Table 3-5.

Table 3-5: Summary of material shear strength properties

PROPERTIES	MATERIAL 1 (BPQ 1)		MATERIAL 2 (BPQ 2)	
Peak Shear Strength	Normal Stress (kPa)	Shear Stress (kPa)	Normal Stress (kPa)	Shear Stress (kPa)
	121	183	101	150
	204	261	214	268
	405	498	402	454
Cohesion (c)	**40.5 kPa**		**49.3 kPa**	
Peak Friction Angle (ϕ_p)	**48.3°**		**45.2°**	
Residual Shear Strength	**Normal Stress (kPa)**	**Shear Stress (kPa)**	**Normal Stress kPa)**	**Shear Stress (kPa)**
	119	150	100	113
	200	227	202	218
	403	396	402	403
Critical Frictional Angle (ϕ_{cv})	**40.6 °**		**42.6 °**	

Because the displacements were measured at a very short time interval (5 seconds), it was necessary to smooth out the measured shear stress vs. shear displacement (u) curves in order to obtain meaningful results. A moving average of 20 successive readings limited the scatter and gave sufficiently smooth curves which are represented on Figures 3-7 and 3-8. The cohesion (c), peak friction angle ϕ_p and critical state friction angle ϕ_{cv} are obtained from Figure 3-9 and Figure 3-10 which indicate the peak and residual shear strengths (obtained from Figures 3-7 and 3-8) versus the normal stress.

Table 3-6 below shows typical shear strength parameters of G1 and G4 material in terms of the material saturation level given by SANRAL (2013). The shear strength parameters for BPQ 1 (Cohesion = 40.5 kPa and Friction angle = 48.3°) which according to TRH 14 (CSRA, 1985) classification is a G4 material, compares relatively well with expected strength parameters for a moderately saturated G4 with 50 % moisture. The shear strength parameters for BPQ 1 (Cohesion = 49.3 kPa and Friction Angle = 45.2°), which classified as a G1 according to TRH 14 (CSRA, 1985) classification, however, are well below the expected shear strength parameters for wet material at 80 % saturation moisture. This is likely due to the low compaction (average 84 %) which was achieved.

Table 3-6: Typical shear strength parameter for unbound granular materials (SANRAL, 2013)

MATERIAL	SATURATION LEVEL	SHEAR STRENGTH PARAMETERS	
		Cohesion (kPa)	Friction Angle (°)
G1	Dry (20% Moisture)	90 – 130	53 – 57
	Moderate (50% Moisture)	75 – 100	51 – 55
	Wet (80% Moisture)	50 – 75	50 – 53
G4	Dry (20% Moisture)	75	50
	Moderate (50% Moisture)	40	51
	Wet (80% Moisture)	20	47

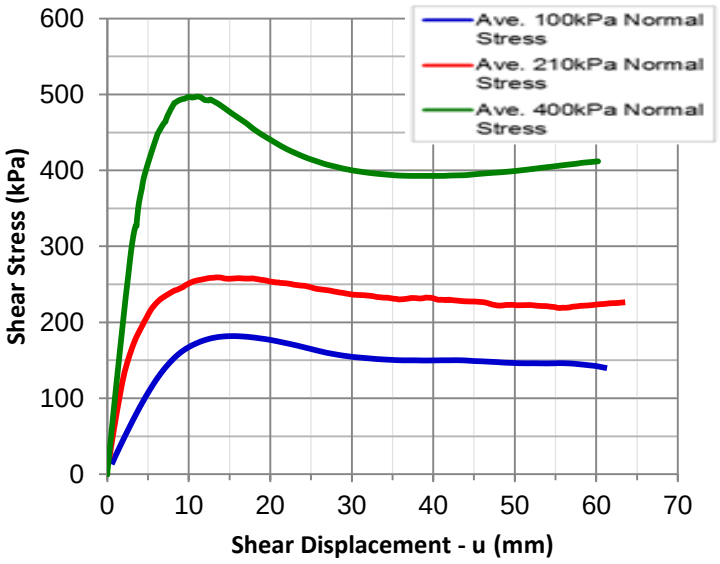


Figure 3-7: Material 1-Shear resistance vs. Shear displacement

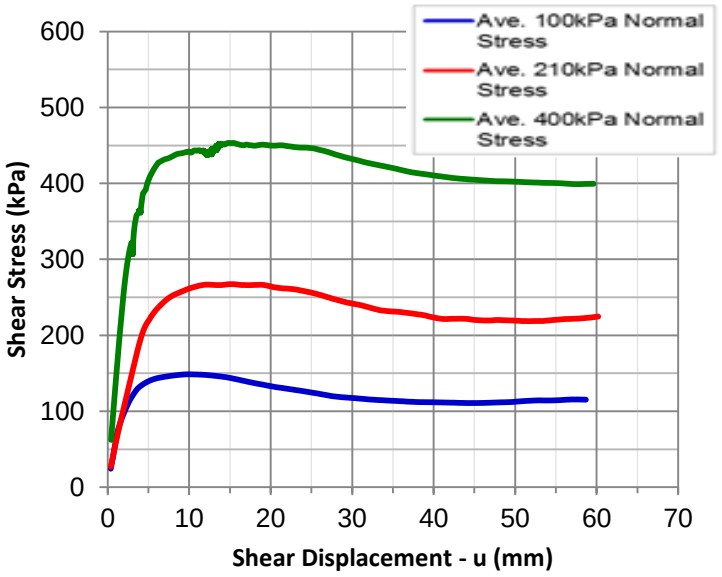


Figure 3-8: Material 2-Shear resistance vs. Shear displacement

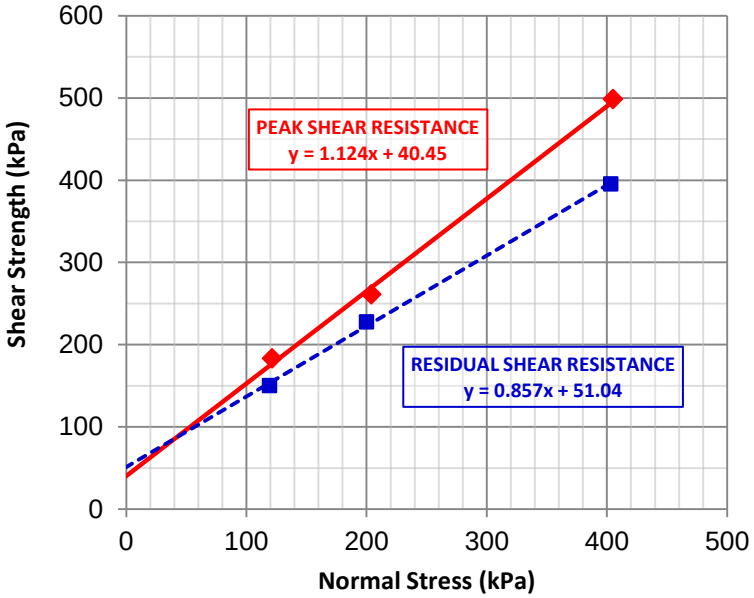


Figure 3-9: Material 1- Peak Shear Strength & Residual Shear Strength vs. Normal Stress

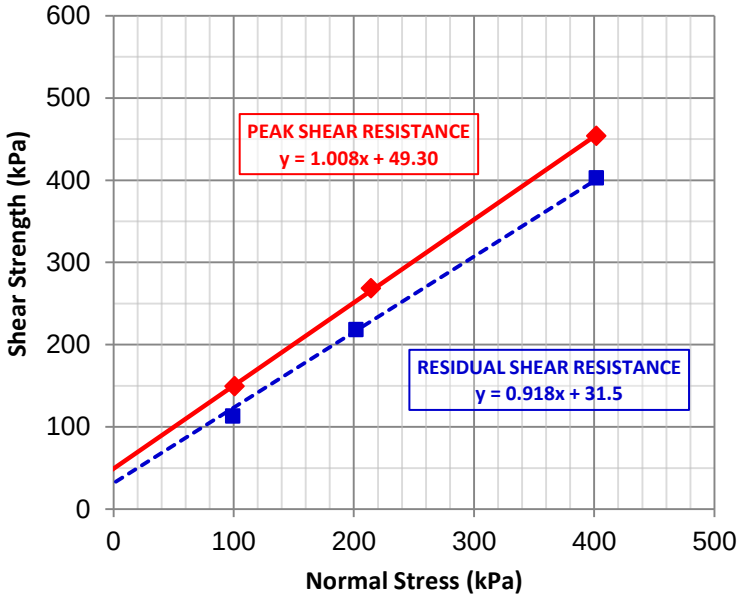


Figure 3-10: Material 2- Peak Shear Strength & Residual Shear Strength vs. Normal Stress

3.3.2.2. Dilation Properties

Results of the dilation (δv) and the rate of dilation ($\delta v/\delta u$) versus the shear displacement (u) for the two materials tested in the laboratory are shown on Figures 3-11 and 3-12 (Material 1) and Figures 3-13 and 3-14 (Material 2). According to Guo and Su (2007) the onset of dilation can be defined from the shear displacement (u) where the rate of dilation given by $\delta v/\delta u$ is equal to zero. The onset of dilation was obtained from Figures 3-11 and 3-13, and the corresponding shear displacement values are given in Table 3-7 below.

Table 3-7: Shear displacement at onset of dilation (This study)

Applied normal pressure (kPa)	Shear displacement at onset of dilation (u) (mm)	
	Material 1 (BPQ 1)	Material 2 (BPQ 2)
100	4.4	0.6
200	3.9	3.7
400	3.9	3.8
Mean Values	**4.1**	**3.7 ***

* 100 kPa result excluded

Evaluation of the results indicates that the dilation began at a mean shear displacement of 4.1 mm (Material 1) and 3.7 mm (Material 2) excluding the 100 kPa results for Material 2. It is noted that the results for the Material 2 sample tested at 100 kPa do not appear to fit the general trend of the other two sets of results tested at 200 and 400 kPa. Significantly higher dilation was recorded (11 mm compared to an average of 6 mm for the 200 and 400 kPa test samples) and the peak dilation rate is recorded at a shear displacement of 0.6 mm compared to an average of 3.1 mm for the 200 kPa and 400 kPa test results.

Figure 3-12 below, shows an average peak dilation rate $\delta v/\delta u$ of 0.22 was observed for Material 1 at a lateral shear displacement between 13 and 15 mm which coincides with the shear displacements where peak shear stress was mobilised in the material (See Figure 3-7, Page 74) as expected. Similarly, Figure 3-14 below, shows the peak rate of dilation $\delta v/\delta u$ for material 2 as 0.18 (excluding the results for the 100 kPa vertical pressure test) which occurred at a shear displacement ranging between 10 and 15 mm. Again this coincides with the shear displacement at which the peak shear stress was mobilised in the material (See Figure 3-8, Page 74) as expected.

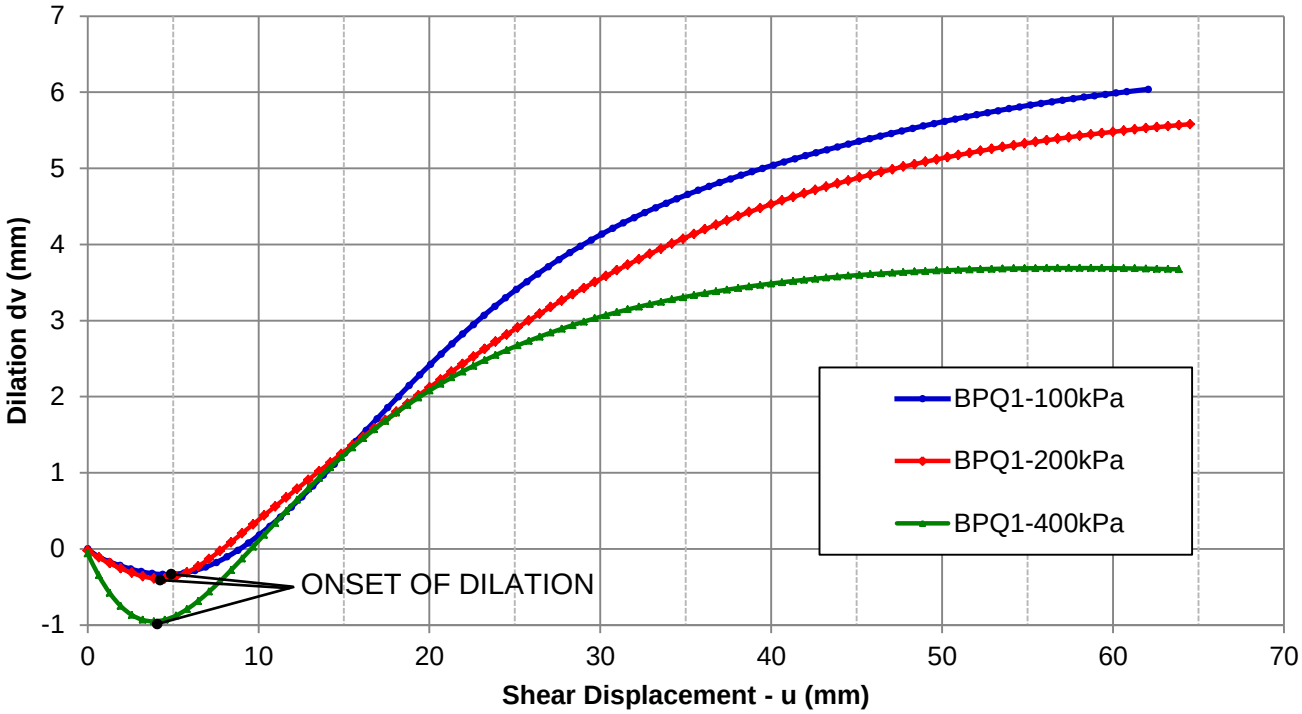


Figure 3-11: Material 1: Vertical displacement vs. Shear displacement

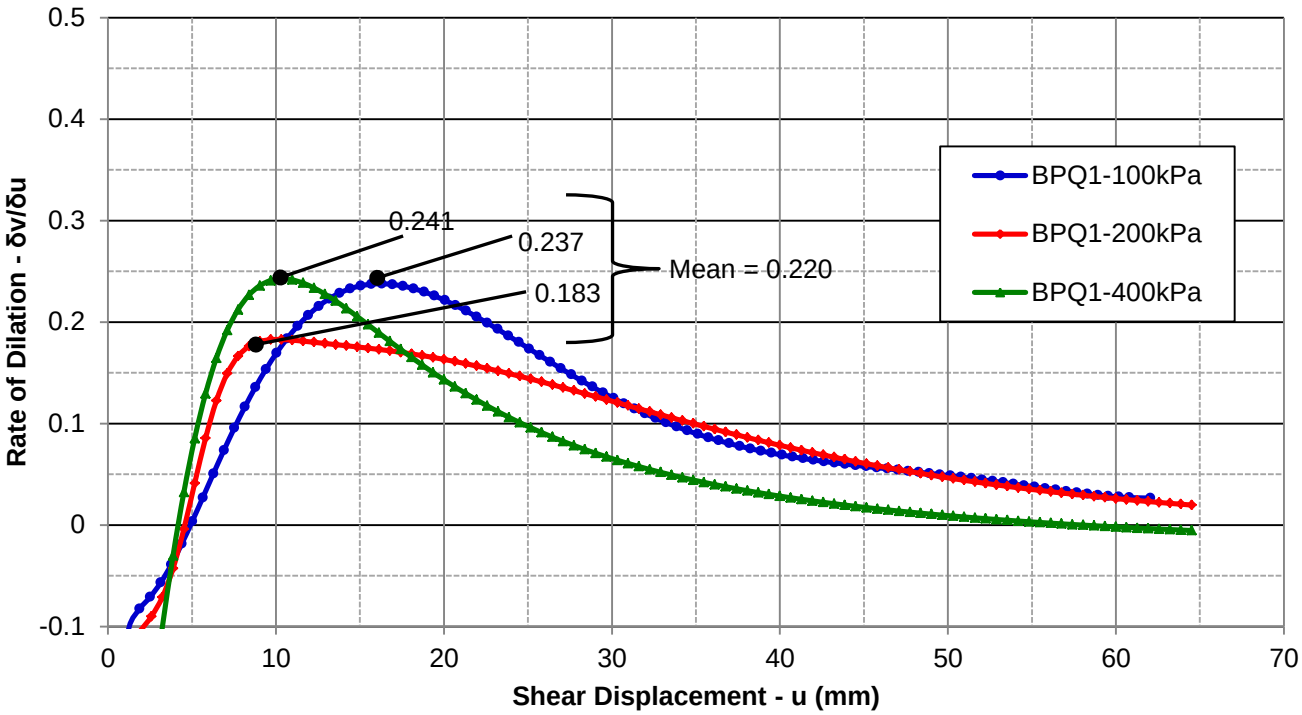


Figure 3-12: Material 1: Rate of dilation vs. Shear displacement

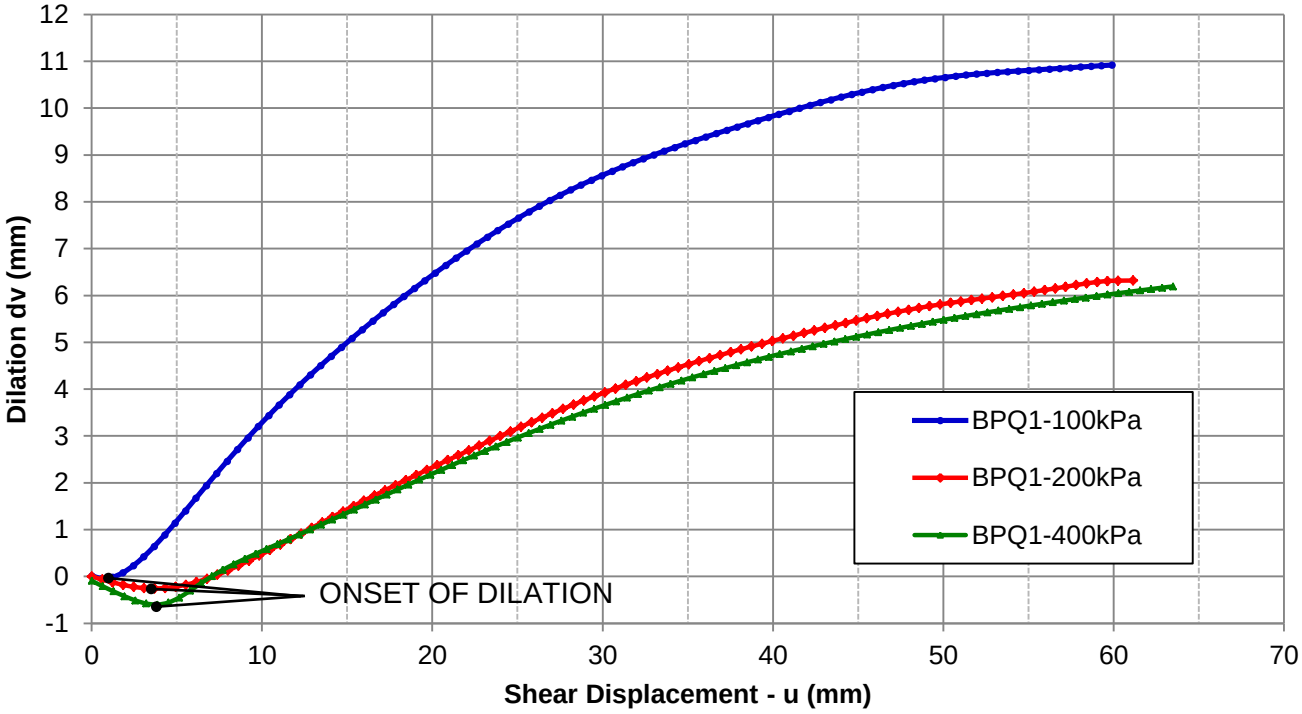


Figure 3-13: Material 2 - Vertical displacement vs. Shear displacement

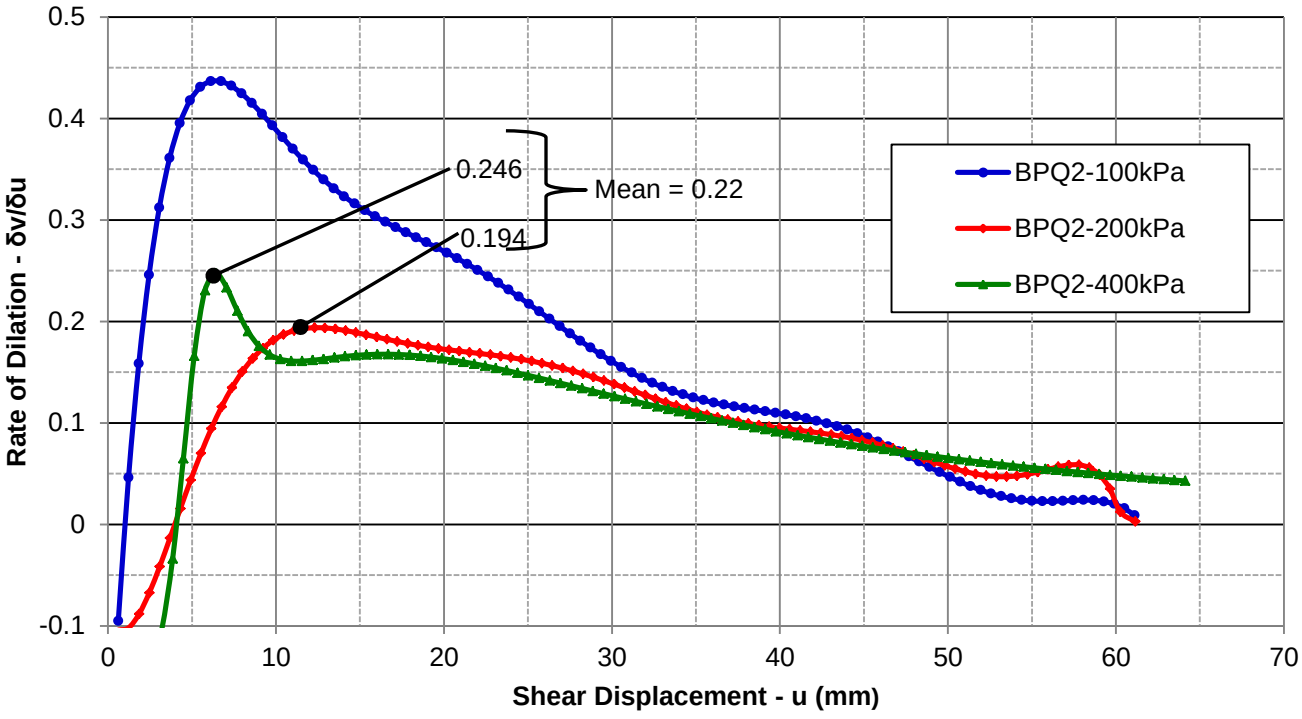


Figure 3-14: Material 2 - Rate of dilation vs. Shear displacement

The dilation properties of the two materials are summarised in Table 3-8. The results included are the shear resistance at the onset of dilation, the friction angle mobilised at the onset of dilation and the angle of dilatancy ψ. The shear resistance at the onset of dilation is determined from the mobilised shear strength (shown on Figures 3-9 and 3-10 on Page 74) corresponding to the shear displacement at the onset of dilation (shown in Table 3-7 on Page 75). Comparing the shear resistance at the onset of dilation to the peak shear resistance indicates that as a percentage the shear resistance at the onset of dilation varied from 54 % to 71 % (average 67 %) for Material 1 and for Material 2 varied from 38 % to 74 % with an average of 60 %. Averaging the two materials, 64 % of the peak shear strength is mobilised at the onset of dilation.

Table 3-8: Material dilation properties

Applied normal stress (kPa)	MATERIAL 1			MATERIAL 2		
	Shear Resistance at onset of Dilation (kPa)	% of Peak Shear resistance	Peak Shear Resistance (kPa)	Shear Resistance at onset of Dilation (kPa)	% of Peak Shear resistance	Peak Shear Resistance (kPa)
100	99	54 %	183	57	38 %	150
200	199	76 %	261	184	69 %	268
400	353	71 %	498	336	74 %	454
Mobilised friction angle (ϕ) at onset of dilation	41.4 °			42.5 °		
ANGLE OF DILATION (ψ)	12.4 °			12.4 °		

The friction angle mobilised at the onset of dilation is obtained from Figure 3-15, below, which shows the shear resistance mobilised at the onset of dilation plotted against the applied normal stress. The tangent of the mobilised friction angle is equal to the slope of the linear curves fitted to the data.

Comparing the results of the friction angle mobilised at the onset of dilation to the peak friction angle indicates that at the onset of dilation approximately 90 % of the peak friction angle is already mobilised in both materials. This illustrates that very small shear displacements are required to mobilise the majority of the friction angle.

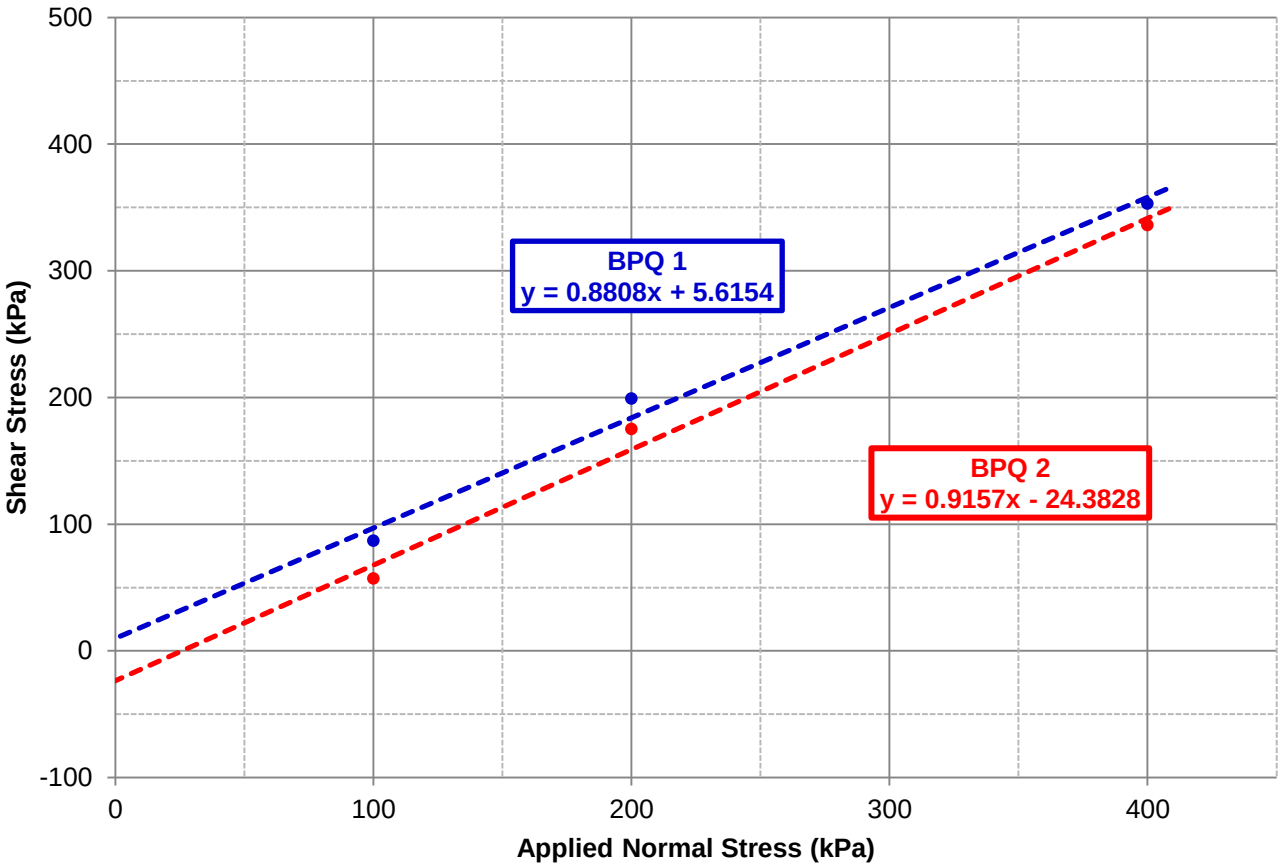


Figure 3-15: Shear resistance mobilised at onset of dilation

Discussion

According to Shibuya *et al*. (1997) interpretation of the direct shear box test results may be misleading when based on externally measured average stresses and a postulated horizontal failure mechanism. They considered the use and interpretation of the direct shear box test as a quasi-simple shear. Figure 3-16 shows the failure modes of laboratory test specimens and the assumed formation of the shear band for plane strain compression, torsional simple shear and the direct shear box.

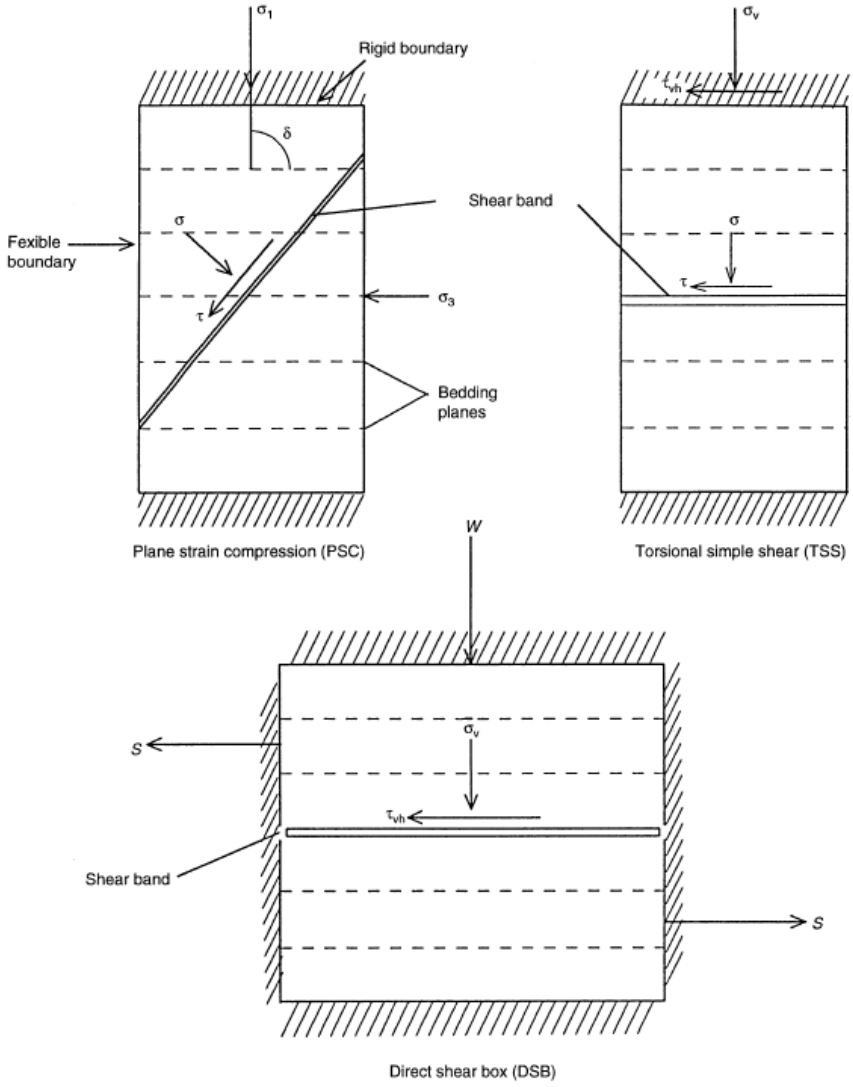


Figure 3-16: Development of shear band in laboratory specimens (Shibuya *et al.*, 1997)

According to Shibuya *et al.* (1997), assuming that failure is accompanied by the development of a shear band of a certain thickness and neglecting the effects of rough end platens, stress and strain are normally assumed to be uniform throughout the plane strain and torsional simple shear tests until shear bands form. Stress and strain non-uniformities are presumed to be significant in the direct shear box test specimen, because the complementary shear stress cannot fully develop on the rigid vertical boundary. In addition, under critical state conditions a single shear band is forced to develop along the horizontal plane at mid-height of the specimen. However by considering supporting test results from Tatsuoka *et al*. (1990), Shibuya *et al*. (1997) found that the simple shear mode of deformation need only be achieved over a very thin element at mid-height, and that it is not necessary for the simple shear deformation to occur throughout the full depth of the direct shear specimen. Figure 3-17 shows an idealised two-dimensional mode of such deformation.

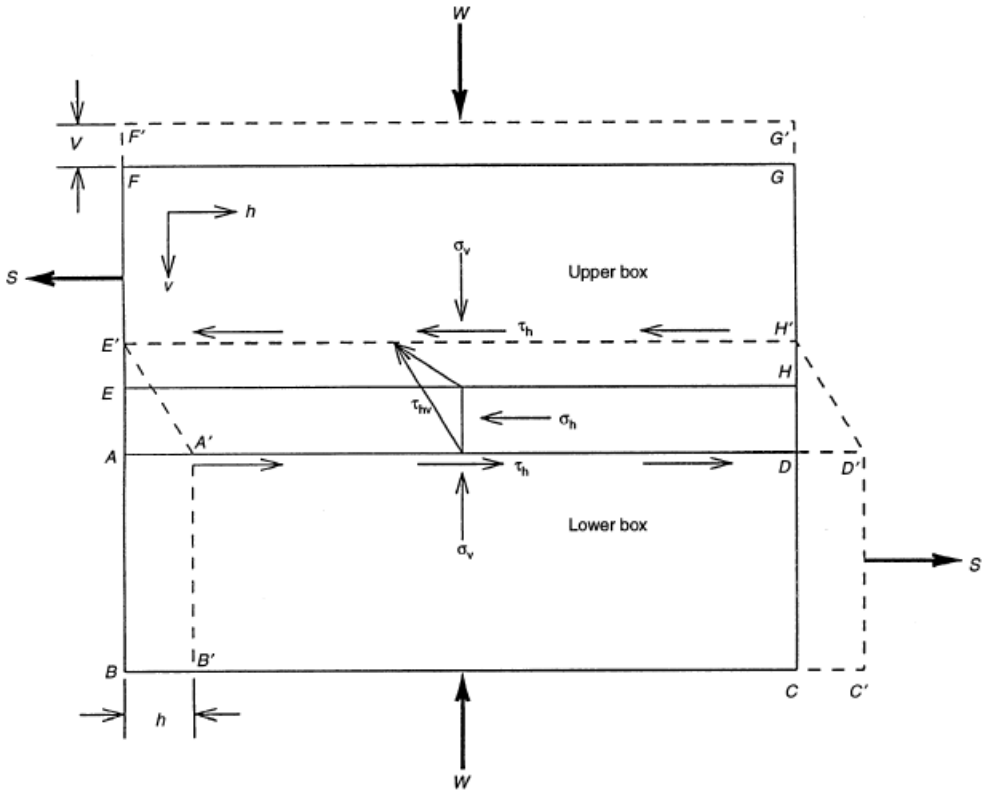


Figure 3-17: Simple shear condition assumed in direct shear box test (Shibuya et al., 1997)

From Shibuya *et al.* (1997) the rectangular specimen BFGC subjected to a constant vertical load W applied through a rigid horizontal platen FG, which is prevented from rotating, the simple shear mode of deformation is seen in the central element AEHD. When the lower half of the specimen, ABCD, is horizontally displaced against the upper portion, EFGH, the horizontal shear stress τ_h develops within the element A'E'H'D'. The shear force S is measured as a result of integration of τ_h along the horizontal plane, for example A'D' or E'H'. From this discussion Shibuya *et al*. (1997) conclude that the average horizontal strain is zero since the rigid box prevents any overall extension of the horizontal planes and since W is kept constant, the vertical strain increment $\delta\varepsilon_v$ is close to zero, except for the deformed element A'E'H'D'.

From Figure 3-18 which shows the directions of the principal stress and strain increments and the angle of dilatancy on Mohr's circles of strain increments, Shibuya *et al.* (1997) also showed that in the idealised simple shear mode of deformation, the mobilised angle of shearing resistance ϕ_{ds} and the angle of dilatancy ψ are defined by the following equations:

$$\phi_{ds} = tan^{-1}\left(\tau_h / \sigma_v\right) \qquad \text{Eq. 3.2}$$

And

$$\psi = \tan^{-1}(-\delta v/\delta h) \qquad \text{Eq. 3.3}$$

Where δh and δv are the horizontal and vertical displacements (with compression taken as positive for δv)

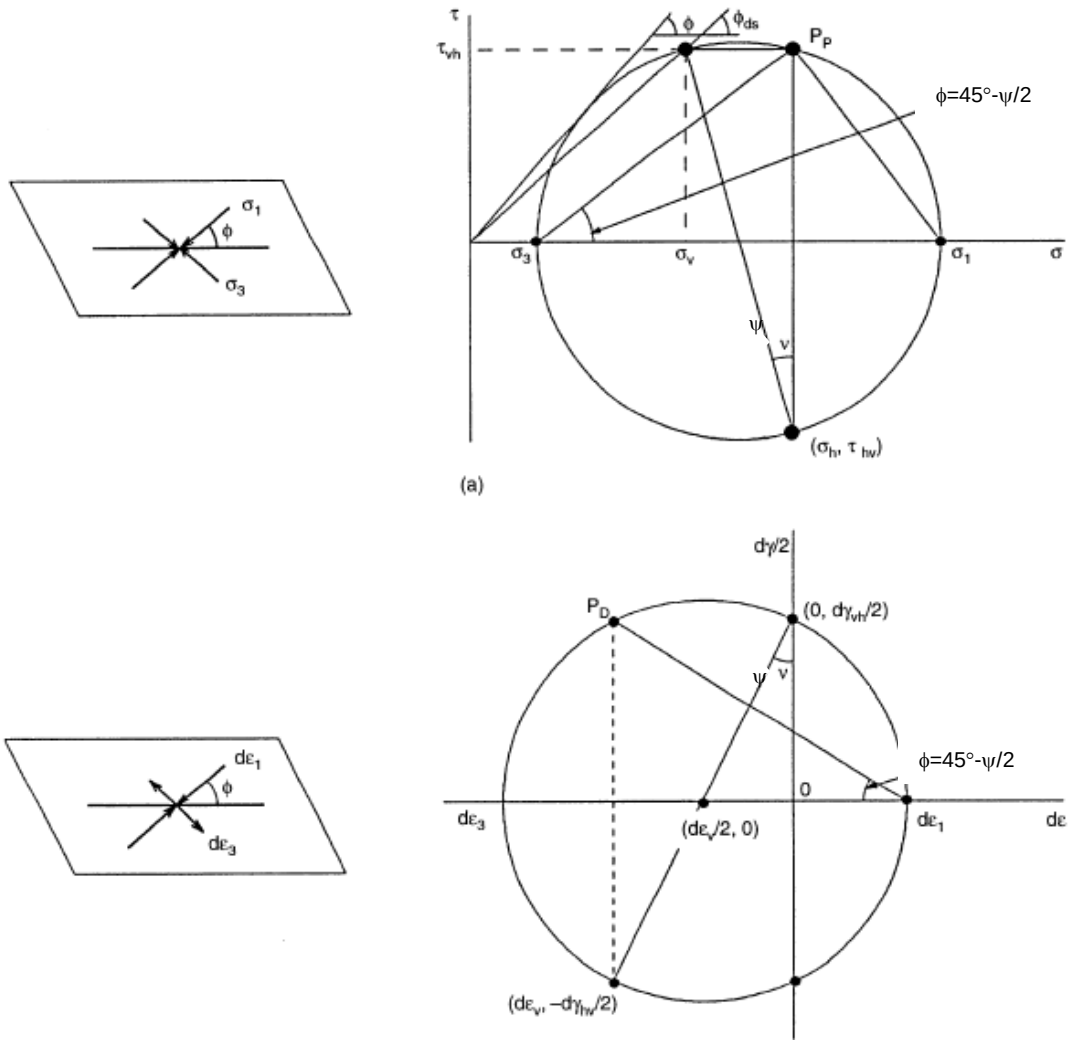


Figure 3-18: Directions of principal stress and strain increments and the angle of dilatancy ψ in simple shear (Shibuya et al., 1997)

It therefore follows that by assuming that the horizontal plane in the shear box is a zero extension line, the angle of dilation can be deduced from the Mohr's circle of strain increments (Shibuya *et al.*, 1997 and Simoni & Houlsby, 2006) as:

$$\tan\psi = -\frac{\delta\varepsilon_{yy}}{\delta\gamma_{yx}} = \frac{\delta v}{\delta u} \qquad \text{Eq. 3.4}$$

where ε_{yy} and γ_{yx} are the vertical strain and shear strain, respectively.

Although the platen applying the vertical stress in the present tests was not restrained from rotation, this analysis has been used to obtain the angle of dilation ψ. From Figure 3-12 (Page 76) the average peak rate of dilation ($\delta v/\delta u$) is 0.22 giving ψ = 12.4 °. On Figure 3-14 (Page 77) the average (ignoring the test at 100 kPa) is also 0.22, giving the same value for ψ for the two materials BPQ 1 and BPQ 2.

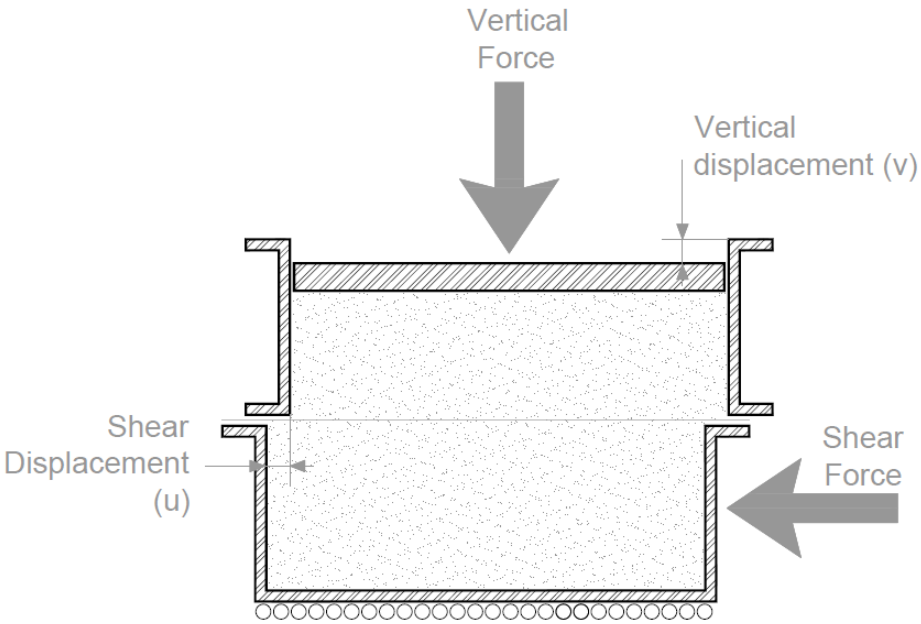


Figure 3-19: Sketch of shear displacement (u) and vertical displacement (v)

From studies on the grain size and shearing resistance characteristics of silica sand and sand gravel mixtures using a large shear box apparatus and by expressing their results after Bolton (1986) in the form $\phi' = \phi_{cv} + b\psi$, Simoni and Houlsby (2006) found that the coefficient b obtained from their results was close to the value of 0.8 reported by Bolton (1986), being in the range 0.74 to 0.84. They observed that b is not constant, but concluded that the deviations from linearity were sufficiently small that b could be taken as a constant for practical purposes. From their observations, Simoni and Houlsby (2006) also concluded that the approach used by Bolton (1986) for plane strain conditions can be used for the case of a direct shear box test.

Presenting the peak friction angle ϕ_P, the critical state friction angle ϕ_{CV} and dilatancy ψ after Bolton (1986) in the form $\phi' = \phi_{cv} + b\psi$, the following two expressions for BPQ 1 and BPQ 2 respectively were obtained using the values in Table 3-5 on Page 72 and ψ = 12.4°:

$$\phi_p = \phi_{crit} + 0.62\psi \quad \text{…(BPQ 1)} \qquad \text{Eq. 3.5}$$

$$\phi_p = \phi_{crit} + 0.21\psi \quad \text{… (BPQ 2)} \qquad \text{Eq. 3.6}$$

The expressions obtained for both BPQ 1 and BPQ 2 do not compare well with those published by Bolton (1986) and Guo & Su (2007), noting that their investigations were carried out using triaxial cells and not a shear box. Bolton (1986) also noted that soil grains in triaxial tests have considerably greater freedom to deviate laterally than those in plane strain (Shear Box) tests. It is believed that the result of BPQ 2 may be due to a lower than expected peak shear stress for the sample tested at 400 kPa (Figure 3-8 Page 74). A higher peak shear stress would have resulted in an increased peak friction angle that would lead to the b coefficient being closer to the range of 0.74 to 0.84.

CHAPTER 4

INFLUENCE OF DILATANCY ON THE LOAD CARRYING CAPACITY PREDICTED BY SAMDM

To investigate the influence of dilatancy on the load carrying capacity which is predicted by the SAMDM, three aspects were considered: firstly the principal stresses and strains in the pavement structure were calculated using the parameter values for materials BPQ 1 and BPQ 2 in two commercial Finite Element Analysis (FEA) packages and the results obtained using two constitutive models, one of which incorporates dilatancy, were compared; secondly, the sensitivity of the SAMDM input stresses which are predicted by the FEA packages to variation of the dilatancy input parameter was evaluated; and then finally the sensitivity of the Factor of Safety (FoS) and the number of load repetitions predicted by the SAMDM method to variations in the angle of dilation ψ is discussed.

4.1. Influence of dilatancy on the calculation of stresses and strains

Stresses and strains were analysed using the FEA packages SIGMA/W and PLAXIS. In both packages an axisymmetric load deformation analysis was performed and the loading, pavement geometry, material properties, constitutive models and results are described below.

4.1.1. *Loading*

Following recommendations by De Beer *et al*. (1999), the design load from dual tyres, at 350 mm spacing, each with a uniformly distributed load of 850 kPa on a circular area with radius = 96.7 mm per loading area was used. In both FEA packages the loading was applied in a single step and the induced stresses and strains are reported at two locations (See Figure 4-1 below):

- Location 1 – Centerline directly below one wheel
- Location 2 – Centerline between two wheels

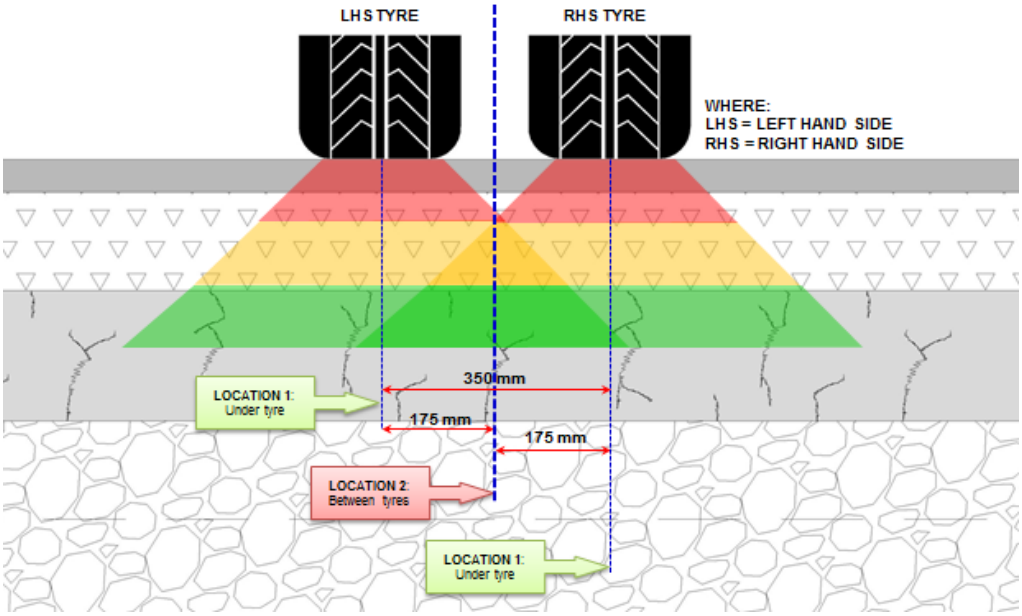


Figure 4-1: Principle of super-positioning in dual tyre loading

In pavement analysis it is standard practice to evaluate the induced stresses and strains at these two locations (Transportek, 2001). The required stress and strain input data to be obtained from the FEA packages and used in the SAMDM is shown in Table 4-1 for unbound granular materials and the subgrade. These are used to compute the Factor of Safety and in the transfer functions to determine the number of loadings to reach a predefined level of deterioration.

Table 4-1: Input parameters required in SAMDM obtained from FEA analysis

GRANULAR PAVEMENT LAYER	INPUT PARAMETER(S)
Base, Subbase, selected gravel	Major principal stress (σ_1) Minor principal stress (σ_3)
Subgrade	Vertical compressive strain ($\varepsilon 1$) at the top of the layer

Axisymmetric loading was assumed in both FEA models and in order to obtain the required stresses and strains which are induced by the dual tyres at 350 mm spacing at Locations 1 and 2, the principle of super-positioning was used (Kim *et al.,* 2009). In axisymmetric analysis only one half of one of the two tyres is analysed (See Figure 4-2 below). To obtain the total stress and strain directly below one of the wheels, i.e. Location 1, the sum of stresses/strains at a distance of 0 mm and 350 mm (Position A and C) from the axis of symmetry was used. To obtain the total stress and strain at location 2, halfway between the two tyres, the stress and strain located at a distance of 175 mm (Position B) from the axis of symmetry was multiplied by two.

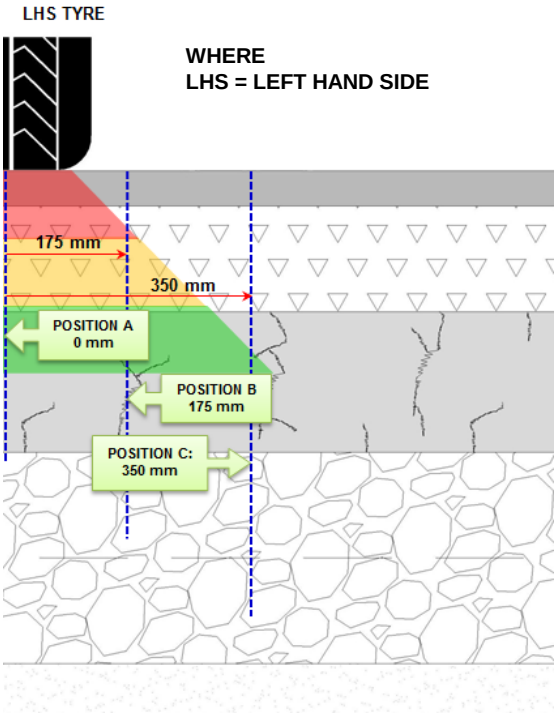
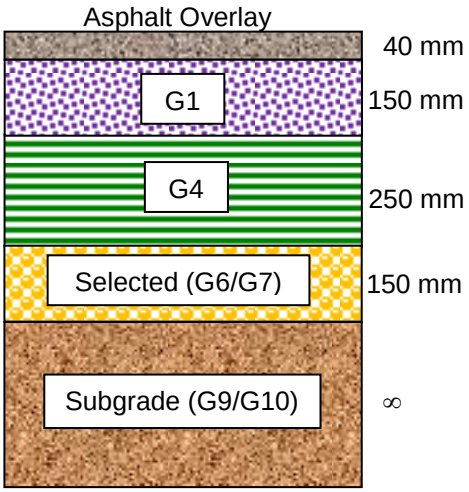


Figure 4-2: Axisymmetric analysis for dual tyre loading

4.1.2. *Pavement model geometry and material properties*

The pavement model geometry used in the FEA is shown in Figure 4-3 below, with the layer input parameters given in the adjacent table. Values for Young's modulus (E) and Poisson's ratio (ν) were obtained from published data (Jooste, 2004) and the values for cohesion, friction angle and dilatancy were obtained from the laboratory tests carried out under this investigation.



Layer	E (MPa)	ν	C (kPa)	ϕ (°)	ψ (°)
Asphalt	2 500	0.35			
G1 (BPQ 1)	650	0.35	49.3	45.2	12.4
G4 (BPQ 2)	450	0.35	40.5	48.3	12.4
Selected	140	0.35			
Subgrade	90	0.35			

Figure 4-3: Pavement model geometry

4.1.3. *Constitutive models*

The Finite Element Analysis (FEA) packages SIGMA/W and PLAXIS each include five material constitutive models with an additional option of a user defined constitutive model. The material models vary in the levels of sophistication with a corresponding increase in the number of the input variables. For the purpose of analysing the effect of dilatancy on the stresses and strains predicted, it was decided to choose the two constitutive models provided by the packages as shown in Table 4-2. The linear elastic model was chosen because it is current practice in the SAMDM to use a multi-layer linear elastic model (MLLE) to determine the stresses and strains and the elastic plastic model was chosen due to its simplicity and more importantly because in both FEA packages it incorporates dilation.

Table 4-2: Constitutive models used in finite element analysis

PROGRAM	CONSTITUTIVE MODEL	REQUIRED INPUT PARAMETERS				
		Young's Modulus (E)	Poisson's Ratio (ν)	Friction Angle (ϕ_p)	Cohesion (C)	Angle of Dilatancy (ψ)
GEO SLOPE – SIGMA/W	Linear Elastic	✓	✓	-	-	-
	Elastic Plastic	✓	✓	✓	✓	✓
PLAXIS	Linear Elastic	✓	✓	-	-	-
	Perfect Plasticity	✓	✓	✓	✓	✓

Note: The Elastic Plastic model in SIGMA/W is equivalent to the Perfect Plasticity model in PLAXIS.

4.1.4. *Finite element mesh*

The deformed (post loading) finite element mesh models that were generated in PLAXIS and SIGMA/W are shown, using exaggerated scale factors, on Figures 4-4 and 4-5. In both FEA packages axisymmetric analyses were carried out using FEA meshes generated from triangular elements. SIGMA/W allows the user to select either a 3 or 6 noded triangular element and therefore a 6 noded element was selected. PLAXIS allows for selection of either a 6 or 15 noded triangular element and the 15 noded element was selected. Since the analyses were carried out as axisymmetric, along the left hand (symmetric) side edge of the model, vertical (settlements) but not lateral (horizontal) movement was allowed. Therefore along this axis the boundary condition is fixed in the horizontal (x) direction. Along the bottom (horizontal) and right (vertical) side the boundaries were located far enough from the applied surface pressure that they could be fixed in both the horizontal (x) and vertical (y) directions without affecting the computed stresses and strains below the applied surface pressure of the tyre loading.

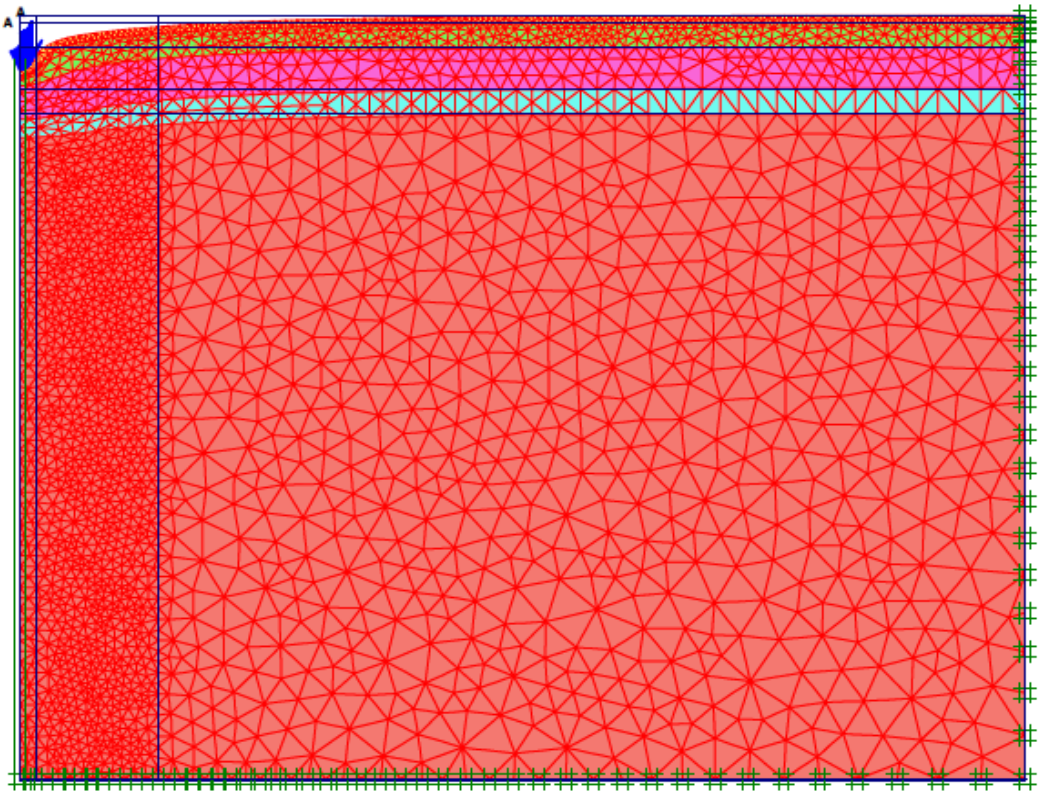


Figure 4-4: Finite Element Mesh generated in PLAXIS

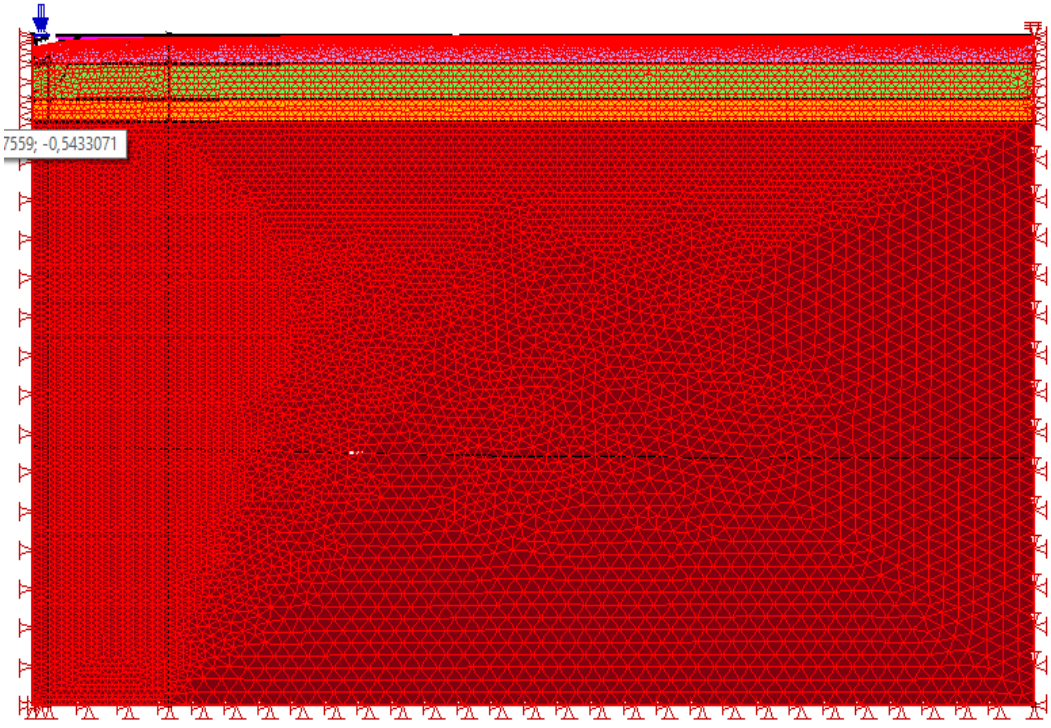


Figure 4-5: Finite Element Mesh generated in SIGMA/W

4.1.5. *Results*

Comparison and discussion of the results is presented below and only the major (σ_1) and minor (σ_3) principal stresses and the major principal strain (ε_1), which are the only input parameters required in the SAMDM from the FEA, are discussed. Firstly the PLAXIS results of the linear elastic model versus the perfectly plastic model are discussed, then the SIGMA/W FEA package results of the linear elastic model versus the elastic plastic model, followed by a comparison of the results between the two finite element models i.e. PLAXIS versus SIGMA/W.

PLAXIS – linear elastic vs. perfect plasticity

Table 4-3 shows results of σ_1 and σ_3 in the base, subbase and selected layers and the ε_1 at the top of the subgrade. These values are the input parameters used in the SAMDM method to compute the FoS and the load repetitions which can be sustained at these stresses and strains. The perfect plasticity model predicted significantly higher values of the minor principal stress (σ_3) in the base and the major principal stress (σ_1) in the subbase and selected layer. The perfect plasticity model computed lower σ_3 values in the subbase. The perfect plasticity model predicted a major principal strain (ε_1) at the top of the subgrade layer which was 3 % higher than the linear elastic model predicted strain of 317 με. In the case of σ_3 in the subbase, the linear elastic model predicted tension in the soil, while the perfectly plastic model cuts off the tensile stress and models it as zero.

Table 4-3: FEA results PLAXIS (This study)

Description		Linear Elastic	Perfect Plasticity
Base	σ_1 (kPa)	-418	-439 (+5 %)
	σ_3 (kPa)	-1	-41 (+40x)
Subbase	σ_1 (kPa)	-108	-122 (+13 %)
	σ_3 (kPa)	+28	0 [cut off] (-100 %)
Selected	σ_1 (kPa)	-52	-63 (+21 %)
	σ_3 (kPa)	-9	-3 (-67 %)
Subgrade	ε_1 (με)	-317	-327 (+3 %)

+ Tension

- Compression

SIGMA/W – Linear Elastic vs. Elastic Plastic

Table 4-4 below shows a comparison of the calculated principal stresses at the middle of the base, subbase and selected layers and the strain at the top of the subgrade layer obtained using the linear elastic and elastic plastic models in the SIGMA/W FEA package. The elastic plastic model predicted a slightly reduced value for σ_1 and significantly a higher σ_3 value in the base layer only. The major (σ_1) and minor (σ_3) principal stresses in the subbase and selected layer and the major principal strain (ε_1) at the top of the subgrade were identical for both the linear elastic and the elastic plastic models. The elastic plastic model in SIGMA/W does not have a tension cut-off formulation and both the linear elastic and elastic plastic models have predicted tensile minor principal stresses (σ_3) in the subbase layer.

Table 4-4: FEA results SIGMA/W (This study)

Description		Linear Elastic	Elastic Plastic
Base	σ_1 (kPa)	-428	-425 (-1 %)
	σ_3 (kPa)	-1	-14 (+14x)
Subbase	σ_1 (kPa)	-108	-108 (nil)
	σ_3 (kPa)	+31	+31 (nil)
Selected	σ_1 (kPa)	-52	-51 (-2 %)
	σ_3 (kPa)	-2	-2 (nil)
Subgrade	ε_1 ($\mu\varepsilon$)	-313	-313 (nil)

+ Tension

- Compression

PLAXIS vs. SIGMA/W

Table 4-5 below compares the results from the two FEA programs. These values serve as input parameters in the SAMDM method. There was generally reasonable agreement between the linear elastic model predictions from both the PLAXIS and SIGMA/W FEA packages, which should in principle be exactly the same. The differences are likely to be due to the FEA element mesh geometries which were set as irregular triangles, and the number of iterations required for achieving the required degree of accuracy. Notable differences of the linear elastic results were in the σ_1 (base), σ_3 (subbase and selected layers) and ε_1 values. The stress and strain results predicted using the elastic plastic model formulations in the two FEA packages differed more significantly. The most notable variation being the σ_3 values in the subbase layer

for which PLAXIS computed zero stresses while SIGMA/W predicted tensile stresses in the soil. The major principal strain (ε_1) computed using the PLAXIS elastic plastic formulation was notably 4.3 % higher than the SIGMA/W elastic plastic result.

Table 4-5: FEA results - PLAXIS vs. SIGMA/W (This study)

Description		Linear Elastic		Elastic Plastic	
		PLAXIS	SIGMA/W	PLAXIS	SIGMA/W
Base	σ_1 (kPa)	- 418	- 428	- 439	- 425
	σ_3 (kPa)	- 1	- 1	- 41	- 14
Subbase	σ_1 (kPa)	- 108	- 108	- 122	- 108
	σ_3 (kPa)	+ 28	+ 31	0 [cut off]	+ 31
Selected	σ_1 (kPa)	- 52	- 52	- 63	- 51
	σ_3 (kPa)	- 9	- 2	- 3	- 2
Subgrade	ε_1 ($\mu\varepsilon$)	- 317	- 313	- 327	- 313

The linear elastic model is a first order computation which is currently accepted for computing the stresses and strains that are used in pavement design for the prediction of load repetitions in South Africa. In its simplicity the model does not consider the dilation of granular materials which are used in the construction of pavements. The elastic plastic model however does account for material dilation. For c > 0, the standard Mohr Coulomb criterion in the elastic plastic model allows for tension. In reality soil can sustain little or no tensile stress. This behaviour is included in the elastic plastic formulation of the PLAXIS FEA package by incorporating a tension cut-off, in which case Mohr circles with positive principal stresses i.e. tensile stresses are not allowed. This is achieved through an iterative redistribution of the tensile stresses until equilibrium is reached and zero tensile stress exists in the soil body.

There was little difference in the stresses and strains, needed for SAMDM input, which were predicted with the SIGMA/W FEA package using the linear elastic and elastic plastic models. In fact these were identical except for the major (σ_1) and minor (σ_3) principal stresses predicted in the base layer. The elastic plastic major principal stress (σ_1) in the base was slightly lower than that predicted by the linear elastic model due to the material having yielded according to the Mohr Coulomb failure criterion. The differences between the linear elastic and the elastic plastic stress and strain values computed using the PLAXIS FEA package were bigger than for SIGMA/W. The results obtained using the linear elastic model in PLAXIS were close to the SIGMA/W results of both the linear elastic and elastic plastic models, while the elastic plastic model results differed more significantly. The elastic plastic model in PLAXIS also predicted a

higher principal strain (ε_1) at the top of the subgrade layer compared to the linear elastic results, but in SIGMA/W they were identical.

It appears that the tension cut-off formulation has a significant influence on the stresses and strains predicted by FEA packages. However, considering the results from SIGMA/W computed using the elastic plastic model, which were almost identical to the linear elastic results obtained using both SIGMA/W and PLAXIS, it is concluded that the degree to which incorporating dilation into the stress-strain computation has on the resultant stresses and strains is insignificant and can be ignored.

4.2. Influence of varying the angle of dilation ψ on SAMDM input stresses

It is current practice in pavement analysis to use a linear elastic FEA model to determine stresses and strains which are then used as input for determining the Factor of Safety (FoS) and the number of load repetitions a layer can sustain at these stresses. However, linear elasticity does not account for dilatancy in soils, and given the importance of the direct link between peak shearing resistance and dilatancy of granular soils (Rowe, 1962), which can be expressed in a practical and simplified form (Bolton, 1986) the concept of dilatancy should be incorporated in determining accurate stresses (unbound granular layers) and strains (insitu subgrade). The angle of dilation ψ is one of the required input parameters when the elastic plastic model is used. In FEA, variation in ψ should affect the size of the calculated stresses. The effect which variations in dilatancy have on the computed principal stresses is demonstrated below and the results of both SIGMA/W and PLAXIS are presented.

The formulation of the elastic-plastic model in SIGMA/W is discussed in detail in Section 2.5.2.1, and is briefly described further in this section. The elastic plastic model is implemented with both a yield (failure) surface and a plastic potential surface. The equations that describe these surfaces are the same, however the size of the plastic potential is controlled by the dilation angle ψ while the size of the failure surface is controlled by the friction angle ϕ. The vector normal to the plastic potential has (x) and (y) components that define the volumetric (x) and deviatoric (y) strain increments. The vector is vertical when the dilation angle ψ is zero; therefore, there is zero volumetric strain associated with shearing. In contrast, setting $\psi = \phi$ causes the vector normal to the plastic potential to point up and to the left on a conventional strain invariant plot; therefore the x component (i.e. volumetric strain increment) is negative (to the left). A negative volumetric strain increment is dilation; that is, volumetric expansion upon shearing (Geo Slope International Ltd, 2007).

The analysis carried out in this section is as described in Section 4.1 above. In fact the results in Section 4.1.5 are considered here as the base case. The variations on the ψ input parameter of the base layer only are considered here, and ψ was varied as shown in Table 4-6.

Table 4-6: FEA ψ input variation for base layer only (This study)

	Base Case	Variation 1	Variation 2	Variation 3	Variation 4	Variation 5
Angle of dilation (ψ)	12.40 °	12.77 ° (+ 3 %)	13.27 ° (+ 7 %)	13.64 ° (+ 10 %)	14.26 ° (+ 15 %)	14.88 ° (+ 20 %)

The results of the calculated major principal stresses σ_1 and minor principal stresses σ_3 at the center of the base layer are shown in Table 4-7 and presented graphically in Figures 4-6 and 4-7 below. From the figures it is observed that the PLAXIS FEA package predicted higher σ_1 and σ_3 stress values compared to the SIGMA/W FEA package results. The influence of variations in the angle of dilatancy differed between the two FEA packages. Gradual increases in ψ led to gradual increases in the σ_1 values predicted by SIGMA/W while increasing ψ led to decreasing values of σ_1 predicted by PLAXIS. Similarly, gradual increases in ψ led to gradual increases in SIGMA/W and gradual decreases in PLAXIS of the predicted σ_3 stress values in the base layer. In the PLAXIS model the effect of variations in dilatancy is very small on σ_3 and negligible on σ_1. A 20 % increase in ψ resulted in a decrease of the predicted major and minor principal stresses of 0.18 % and 0.97 % respectively. In SIGMA/W the influence of varying ψ is much smaller on the major principal stress σ_1 with a 20 % increase in ψ resulting in a small increase of 0.41 % in the calculated major principal stress. A 20 % increase in ψ resulted in the calculated minor principal stress increasing by 2.05 %.

The results of the stresses calculated and the discussion above illustrate that the stresses predicted by different FEA packages using the same constitutive model, in this case the elastic plastic model, differ. Small variations in ψ affect the predicted major and minor principal stresses in the base layer between the different FEA packages to varying degrees. The results indicate that the effects of small variations in the angle of dilatancy on the predicted major and minor principal stresses: 1) depend on the FEA package used to calculate the stresses; 2) the formulation of the constitutive model which is selected for the analysis i.e. the incorporation of a tension cut-off formulation; 3) are in general very small. Therefore in the elastic plastic model which incorporates dilatancy of soil, the calculated stresses are not highly sensitive to small variations, up to 20 %, in the dilatancy.

Table 4-7: Effect of variations in ψ on the calculated major and minor principal stresses in base layer only

	Base Case	Variation 1	Variation 2	Variation 3	Variation 4	Variation 5
SIGMA/W						
Major Principal Stress (σ_1) [kPa]	- 424.72	- 425.00 (+ 0.07 %)	- 425.37 (+ 0.15 %)	- 425.63 (+ 0.21 %)	- 426.06 (+ 0.45 %)	- 426.47 (+ 0.41 %)
Minor Principal Stress (σ_3) [kPa]	- 14.17	- 14.22 (+ 0.35 %)	- 14.28 (+ 0.78 %)	- 14.32 (+ 1.06 %)	- 14.39 (+ 1.55 %)	- 14.46 (+ 2.05 %)
PLAXIS						
Major Principal Stress (σ_1) [kPa]	- 439.69	- 439.58 (- 0.03 %)	- 439.42 (- 0.06 %)	- 439.30 (- 0.09 %)	- 439.10 (- 0.13 %)	- 438.91 (- 0.18 %)
Minor Principal Stress (σ_3) [kPa]	- 41.34	- 41.28 (- 0.15 %)	- 41.20 (- 0.34 %)	- 41.14 (- 0.48 %)	- 41.04 (- 0.72 %)	- 40.94 (- 0.97 %)

+ Tension

- Compression

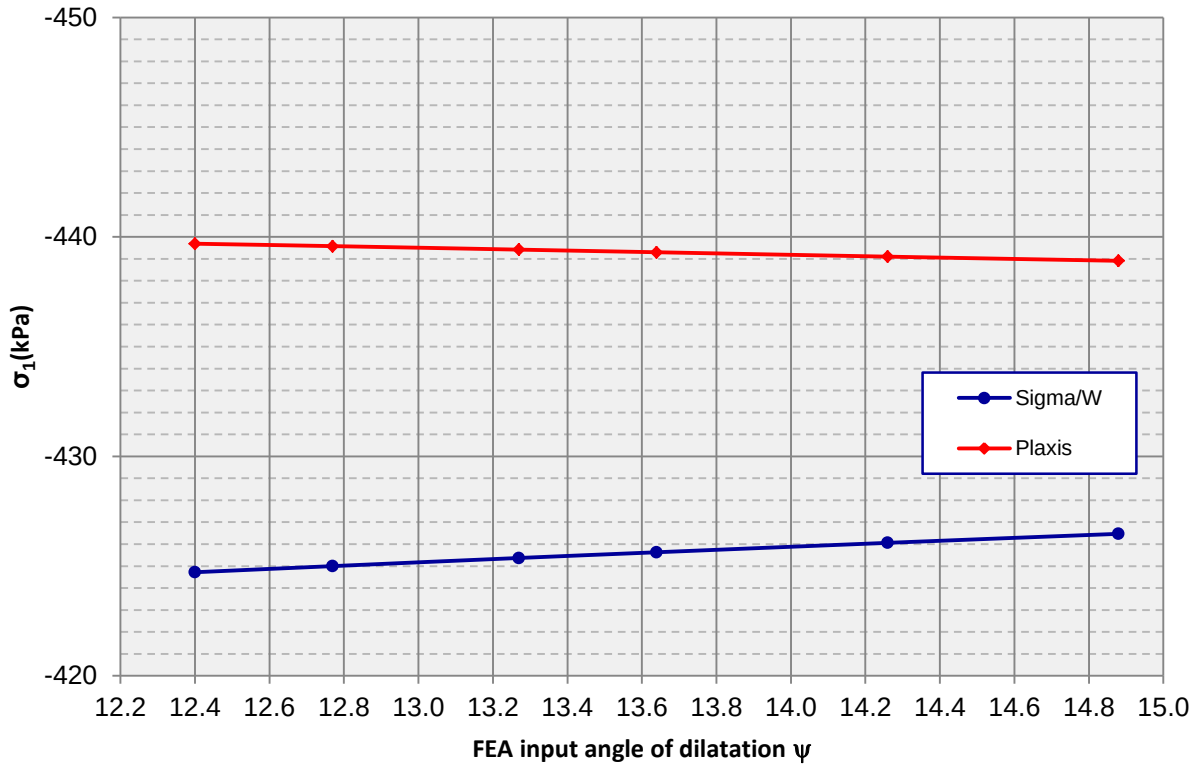


Figure 4-6: Variation of major principal stress with angle of dilation

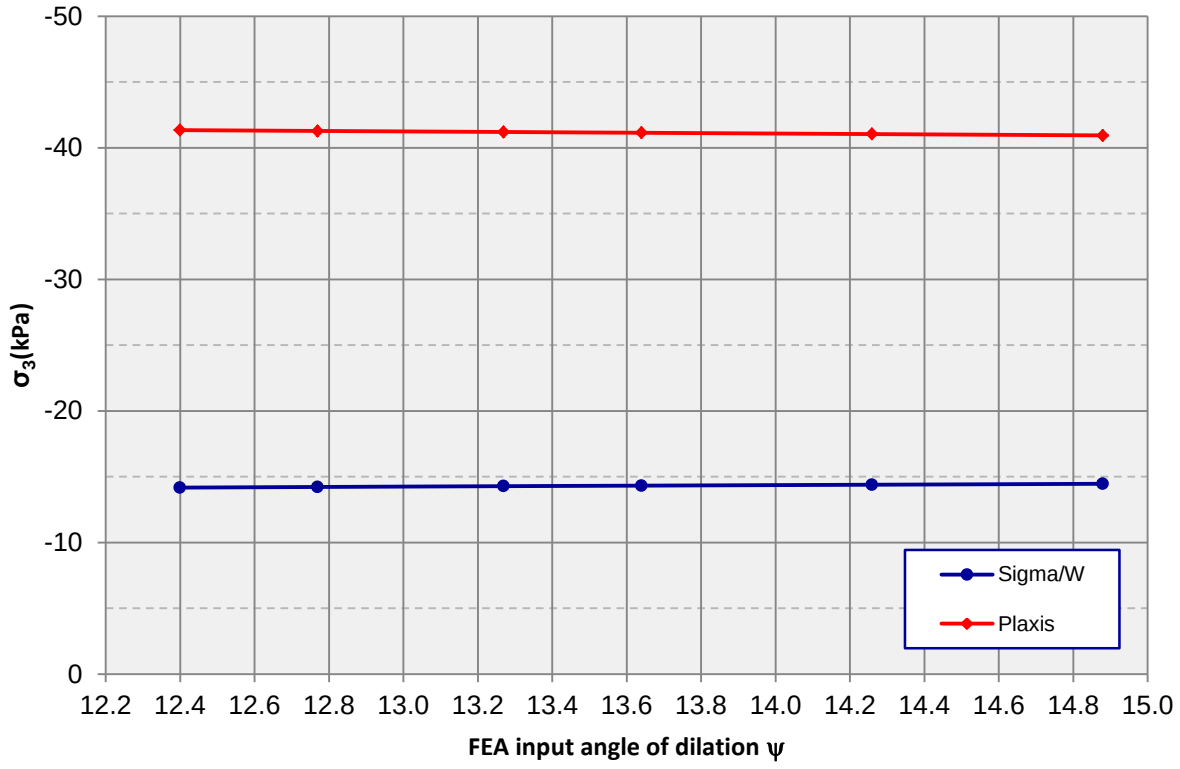


Figure 4-7: Variation of minor principal stress with angle of dilation

4.3. Influence of variations in ψ on the Factor of Safety (FoS) and predicted load repetitions

Conventional pavement engineering relies heavily on the use of the Mohr-Coulomb strength parameters, cohesion (c) and the angle of friction (ϕ_{max}) which characterise the shear strength of unbound granular material. In the SAMDM the first step is the load and material characterisation followed usually by a structural analysis based on a multilayer linear elastic model to obtain the input parameters which are then used in the FoS equation. These input parameters are the major and minor principal stresses (σ_1 and σ_3) in the base, subbase and selected granular layers and the major principal strain (ε_1) at the top of the subgrade layer. The FoS is then used as input into the selected transfer function to evaluate the number of load repetitions that the layer can sustain at these stresses and strains.

Jooste (2004) considered the sensitivity of the predicted load carrying capacity of a typical pavement designed using the SAMDM to small variations in the input parameters. He found that the SAMDM is highly sensitive to small variations of the input parameters. In the preceding Section 4.2 of this research the influence of variations of ψ on the predicted major and minor principal stresses in the base layer was evaluated using two FEA packages. The influence of variations of ψ on the predicted major and minor principal stresses was found to be very small. However, as Jooste (2004) pointed out, the sensitivity of the SAMDM to input variables may be coming from the implementation of the transfer functions. In this section the influence of variations in ψ on the Factor of Safety (FoS) and the predicted load repetitions to failure of the base layer is considered. The major and minor principal stress results obtained in the preceding section (Table 4-7 on Page 97) were used.

The FoS determined was calculated using Eq. 2.2 and the number of load repetitions were calculated using the 90 percentile confidence transfer function shown in Eq. 2.7.

The material properties used for the base layer were those obtained in the laboratory (See Table 3-5 on Page 72) and are as follows:

coheson (c)	= 49.3 kPa;
peak friction angle (ϕ_{max})	= 48.3 °.

Eq. 2.2 includes a K constant which, according to Maree (1978), is the correction factor for the saturation level of the soil. In the calculations presented below moisture condition constant (K) of 0.95 for normal moisture conditions was used.

The results of variations in the FoS and the predicted number of load repetitions due to small variations in the dilatancy ψ using SIGMA/W and PLAXIS FEA packages for the base layer only are shown in Table 4-8 and presented graphically on Figure 4-8.

Table 4-8: Variation in FoS and predicted load repetitions to failure due to variations in ψ

	Base case ψ = 12.4 º	**Variation 1** ψ = 12.77 º (+ 3 %)	**Variation 2** ψ = 13.27 º (+ 7 %)	**Variation 3** ψ = 13.64 º (+ 10 %)	**Variation 4** ψ = 14.26 º (+ 15 %)	**Variation 5** ψ = 14.88 º (+ 20 %)
SIGMA/W						
FoS	0.8228	0.8231 (+ 0.04 %)	0.8235 (+ 0.08 %)	0.8236 (+ 0.11 %)	0.8240 (+ 0.15 %)	0.8245 (+ 0.21 %)
No. of load repetitions ($N_{90\ \%}$)	709 761	711 195 (+ 0.20 %)	712 627 (+ 0.40 %)	713 467 (+ 0.52 %)	715 152 (+ 0.76 %)	717 011 (+ 1.02 %)
PLAXIS						
FoS	1.2947	1.2939 (- 0.06 %)	1.2928 (- 0.15 %)	1.2920 (- 0.21 %)	1.2907 (- 0.31 %)	1.2893 (- 0.41 %)
No. of load repetitions ($N_{90\ \%}$)	12 035 133	12 975 790 (- 0.49 %)	11 900 187 (- 1.12 %)	11 843 778 (- 1.59 %)	11 750 320 (- 2.37 %)	11 655 288 (- 3.16 %)

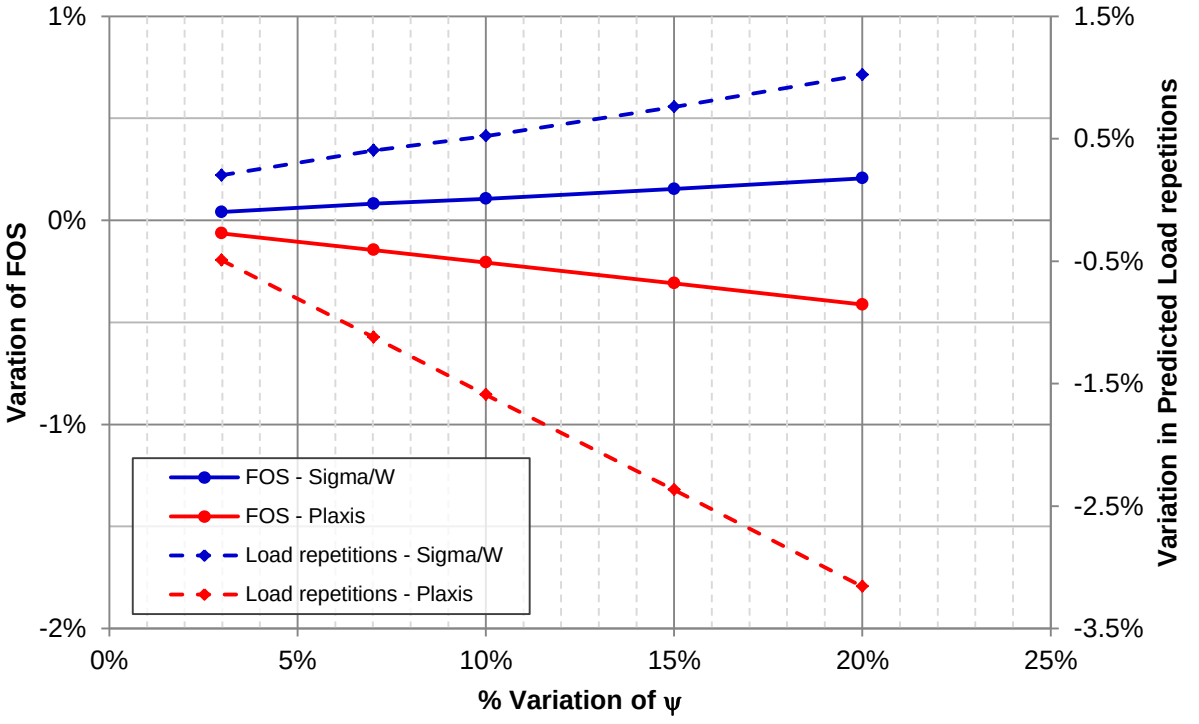


Figure 4-8: Effect of varying ψ on the calculated FoS and predicted number of load repetitions to failure

Gradually increasing ψ resulted in gradual decreasing of both the calculated Factor of Safety (FoS) and the number of load repetitions using the PLAXIS FEA package results, while the same ψ changes resulted in gradual increase of both the FoS and the load repetitions from the SIGMA/W results. In SIGMA/W a 20 % increase in ψ resulted in an increase of 0.21 % and 1.02 % for the calculated Factor of Safety and the number of load repetitions respectively. In the PLAXIS package a 20 % increase in ψ led to a decrease of the calculated Factor of Safety and the number of load repetitions of 0.41 % and 3.16 % respectively. The results indicate that variations in ψ up to 20 % have small effect on the calculated factor of safety and predicted number of load repetitions before failure of the layer. This illustrates that the SAMDM, using results from FE analysis, is not sensitive to changes in ψ.

Jooste (2004) related the problems associated with the SAMDM to the empirical element of the method, particularly the transfer functions used to predict the pavement response to applied stresses. Theyse and Kannemeyer (2010) attribute the shortcomings identified by Jooste to the incorrect calculation of the stress condition in unbound pavement layers and also pointed out that use of the FoS and Stress Ratio models in the SAMDM can yield inadmissible and counter intuitive stress conditions (FoS < 1 and SR > 1). The results in Table 4-8 show that the FoS values calculated from the stress results obtained from SIGMA/W are counter-intuitive (FoS < 1) and therefore predict almost immediate failure of the base layer. However, the FoS values calculated from the PLAXIS principal stress results are different. An average FoS of 1.13 was calculated using the PLAXIS stress results and the resulting number of load repetitions is 17 times higher than those predicted from the SIGMA/W stress results. The transfer functions are linear-logarithmic based; hence the resultant large difference in the number of load repetitions obtained from the SIGMA/W and PLAXIS FEA package calculated FOS values of ± 0.82 and ± 1.29 respectively.

This illustrates that the formulation of the constitutive model used in the selected FEA package has a large effect on the Factor of Safety and on the predicted number of load repetitions to failure. The results in the two preceding Sections (4.1 and 4.2) suggest that incorporation of the tension cut-off in PLAXIS affects the stress-strain results more than the incorporation of the dilatancy term. The formulation of the elastic plastic model in PLAXIS which incorporates tension cut-off also appears to overcome the computation of stress conditions which lead to inadmissible and counter-intuitive FoS values.

In the case of the SIGMA/W results, it may appear strange that when the calculated FoS values which are less than one were applied in the transfer function, the results

show that the pavement is capable of carrying load. Maree (1978) developed the FoS method as a safeguard against the rapid shear failure of unbound base layers by setting minimum requirements in terms of the ratio between the imposed stress and the shear strength of the material. Therefore an FoS less than one indicated that: 1) the imposed shear stress is greater than the shear strength of the soil and 2) rapid shear failure of the soil will occur. The soil does not fail immediately since the imposed stresses are cyclic and act on the soil over very short time durations. It takes a number of these cycles or repetitions (in this case approximately 710 000 wheel loads) to cause the soil to fail.

CHAPTER 5

CONCLUSIONS AND RECOMMENDATIONS

5.1. Conclusions

The research set out to study the dilatancy of granular material and the effect which dilatancy has on the load carrying capacity of pavements that is predicted by the South African Mechanistic-Empirical Design Method. It was initially postulated, in this study, that dilatancy of granular materials may be one of the mechanisms in unbound granular pavements which influence the accuracy of the predicted pavement layer life by resulting in an increase in the confinement pressure. A brief review of the SAMDM as a design tool has been presented, highlighting the method's key components and development. The SAMDM is a highly empirical design tool, and published literature shows that the SAMDM is highly sensitive to the variability of input parameters. The literature also strongly suggests, from the effect of varying Poisson's ratio of the pavement materials, that variation of the confining stress during pavement loading cycles has a significant influence on the number of load repetitions predicted by the method.

Two FEA packages, SIGMA/W and PLAXIS, were used to compute stresses and strains in a typical pavement, and two constitutive models which are supported by the FEA packages; the linear elastic model (which is the MLLE currently used in the SAMDM and does not incorporate dilation) and the elastic plastic model (which incorporates dilation of soil) were considered to assess how the incorporation of the dilatancy term in the constitutive model affects the stresses and strains required in the SAMDM for pavement analysis. Further, the influence of granular material dilation on the load carrying capacity predicted by the SAMDM was then evaluated by considering the sensitivity of the SAMDM input stresses which are predicted by the FEA packages to variation of the dilatancy input term ψ and then the sensitivity of the Factor of Safety (FoS) and the number of load repetitions predicted to variations of the dilatancy input term was evaluated.

In order to obtain input parameter values for these FEA packages, direct shear tests were conducted on road building aggregates. From the test results the dilation properties of two materials were presented and it was found that the onset of dilation commenced at very small displacements in direct shear tests: between 4.1 mm (Material 1) and 3.7 mm (Material 2). The results also indicated that at the onset of dilation an average of 64 % of the peak shear strength is mobilised, while approximately 90 % of the peak friction angle was mobilised. These results

demonstrate that dilation begins only after large proportions of the peak shear strength and friction angle have been mobilised.

The linear elastic and elastic plastic model formulations in both PLAXIS and SIGMA/W appear, from the literature describing them, to be identical, except that the elastic plastic model formulation in the PLAXIS FEA package incorporates a tension cut-off, which limits maximum tensile stresses in the soil to zero. There was good agreement between the linear elastic model results of both FEA packages. Using the SIGMA/W FEA package it was found that the major and minor principal stresses in the subbase and selected layers and the major principal strain at the top of the subgrade were identical for both the linear elastic and the elastic plastic models. Although, the results obtained using the linear elastic model in PLAXIS were similar to the SIGMA/W results, the elastic plastic model results differed significantly. The elastic plastic model in PLAXIS also predicted a much higher principal strain at the top of the subgrade layer compared to the linear elastic results. The linear elastic model (both PLAXIS and SIGMA/W) and the elastic plastic model (PLAXIS) predicted tensile minor principal stresses in the subbase layer while the elastic plastic model in PLAXIS predicted zero stresses at the same location due to the tension cut-off formulation.

It appears that the tension cut-off formulation has a significant impact on the stresses and strains predicted by FEA packages. Incorporating dilation into the stress-strain computation affected the resultant stresses and strains to a lesser degree.

Small variations in the dilation angle ψ affect the major and minor principal stresses predicted by the elastic plastic constitutive model formulations in the PLAXIS and SIGMA/W FEA packages in different ways. Gradual increases in ψ led to gradual increases in σ_1 values predicted by SIGMA/W while increasing ψ led to decreasing values of σ_1 predicted by PLAXIS. Similarly, gradual increases in ψ led to gradual increases of the predicted σ_3 stress values in the base layer in SIGMA/W and gradual decreases in PLAXIS. In the PLAXIS model the effect of variations in ψ is very small on σ_3 and negligible on σ_1. A 20 % increase in ψ resulted in a decrease of the predicted major and minor principal stresses of 0.18 % and 0.97 % respectively. In SIGMA/W the influence of varying ψ is much smaller on the major principal stress σ_1 with a 20 % increase in ψ resulting in a small increase of 0.41 % in the calculated major principal stress. A 20 % increase in ψ resulted in the calculated minor principal stress increasing by 2.05 %.

The results indicate that the effects of small variations in the angle of dilatancy on the predicted major and minor principal stresses: 1) depend on the FEA package used to

calculate the stresses; 2) the formulation of the constitutive model which is selected for the analysis; 3) are in general very small. Therefore in the elastic plastic model which incorporates dilatancy of soil, the calculated stresses are not highly sensitive to small variations in the dilatancy within the context and scope of this study.

The influence of small variations in ψ (via the FEA calculated stresses and strains, and the SAMDM) on the Factor of Safety (FoS) and the load repetitions to failure was also considered and it was demonstrated that variations in ψ up to 20 % have a relatively small effect on the calculated Factor of Safety and predicted number of load repetitions before failure of the base layer. Gradually increasing ψ resulted in gradual decreasing of both the calculated FoS and the number of load repetitions using results from the PLAXIS FEA package, while it resulted in gradual increase of both the FoS and the load repetitions using the SIGMA/W results. In the PLAXIS package a 20 % increase in ψ led to a decrease of the calculated factor of safety and the number of load repetitions of 0.41 % and 3.16 % respectively. In SIGMA/W a 20 % increase in ψ resulted in an increase of 0.21 % and 1.02 % for the calculated Factor of Safety and the number of load repetitions respectively. The current SAMDM is therefore not overly sensitive to small variations in the dilatancy input parameter.

Comparison of the calculated FoS and load repetitions to failure due to the stresses computed with the elastic plastic model formulation of the SIGMA/W and PLAXIS FEA packages illustrated that the incorporation of a tension cut-off in the FEA package has a significant effect on the FoS and predicted load repetitions to failure. The FoS calculated from the stress results obtained using SIGMA/W were inadmissible due to the FoS value being less than one while the FoS values obtained from the PLAXIS stress results were greater than one resulting in load repetitions which are up to 17 times larger than those predicted from the SIGMA/W results. The transfer functions are linear-logarithmic based; hence the resultant large difference in the number of load repetitions obtained from the SIGMA/W and PLAXIS FEA package calculated FoS values of ±0.82 and ±1.29 respectively. The formulation of the elastic plastic model in PLAXIS which incorporates tension cut-off also appears to overcome the computation of stress conditions which lead to inadmissible and counter-intuitive FoS values.

It is therefore concluded that according to this study the effect of dilation in unbound granular pavement materials on the load carrying capacity of flexible pavements predicted by the South African Mechanistic-Empirical Design Method is small and may therefore be ignored. The higher order elastic plastic constitutive model did not yield stresses and strains, required in the SAMDM, which were significantly different to those computed using the first order linear elastic model. Incorporating a tension cut-

off formulation in the FEA model, however, had a more significant effect on the calculated stresses and strains and also overcame the computation of in-admissible stresses and strains which predict almost immediate failure of the pavement layer.

5.2. Recommendations

The Road Traffic Act of 1996 (Act No. 93 of 1996) and the Road Traffic Regulations legislate the maximum legal mass limits of vehicles used on South African public roads. The regulations are concerned with protecting the pavement by limiting the legal mass of vehicles to a value that the pavement can support without being overstressed. In terms of the Act and the Regulations the maximum permissible axle load is 88 kN. However according to the technical recommendation on traffic loading and rehabilitation design TRH 14 (CSRA, 1985) the design standard is 80 kN. There is an apparent incoherence between legislation and design recommendations. Researchers (De Beer et al. (1991, 2004) and Morton et al. (2004) have published large quantities of traffic data including actual tyre/pavement contact pressures. It is crucial that these data are used in design and adequately incorporated in design methods and practice. De Beer et al. (1995) and Kim et al. (2005) also found that the prevalence of super single tyres is gaining momentum and that these tyres apply higher vertical and transverse contact stresses to the pavement, which means that updated and appropriate regulation is necessary to control the number of passages of super single tyres as well. It is therefore important that legislation is kept updated and in line with developments in traffic trends and pavement loading.

This research set out to investigate dilation of granular pavement materials and to evaluate the effects of incorporation of the dilatancy term on the calculated stresses and strains and on the factor of safety and predicted load repetitions to failure. The findings indicated that the results are dependent on the FEA package used and the formulation of the constitutive model which, according to the software literature of the two packages reviewed in this study, should be almost the same. The only difference being that the PLAXIS elastic plastic formulation incorporates the tension cut off. Detailed evaluation of how the FEA packages model and incorporate the dilatancy term in the computation of the stresses and strains was not included in the scope of this report. However, the results shown in Table 4-7 and Figure 4-7 lead to the following questions: 1) whether these FEA package really model shear induced dilation and 2) exactly how this is achieved since the increases in ψ only result in very small changes to σ_3 stress values. It is therefore recommended that further studies should investigate deeper into the FEA package constitutive model formulations and evaluate comprehensively how the dilatancy term is considered in each case.

REFERENCES

AASHTO (1972) Interim guide for Design of Pavement Structures, American Association of State Highway and Transport Officials, Washington D.C.

AASHTO (1993) AASHTO guide for Design of Pavement Structures, American Association of State Highway and Transport Officials, Washington D.C., pp. 1 – 640.

ABAQUS (1997) Finite Element Computer Program, Theory Manual, Version 6.7, Habbit, Karlsson and Sorrenson Inc., Pawtucket, USA.

Ackerman, D. (1969) An application of the A.A.S.H.O. Road Test findings to South African Roads, Proceedings of the First conference on asphalt pavements for Southern Africa, Secretary Birds (Pty) Ltd, Durban, Jul-Aug,1970, pp. 3A/1-3A/9.

Adu-Osei, A. (2001) Characterisation of unbound granular layers in flexible pavements, Project No. 404001, Report No. 502-3, Texas Transport institution, Texas A&M University, Texas, Dec 2001, pp. 1-219.

Ahlborn, G. (1960) Elysm 5, Computer program for Determining Stresses and Deformations in a Five Layer Elastic System, University of California, Berkely.

Asphalt Academy (2009) Technical guideline: Bituminous Stabilised Materials – A guideline for the design and construction of bitumen emulsion and foamed bitumen stabilised materials, 2nd edition, May 2009.

Atkinson, J.H. and Bransby, P.L. (1978) The mechanics of soils: An introduction to critical state soil mechanics, McGraw-Hill, Berkshire, England, pp. 15-26, 28-44.

Been, K. and Jefferies, M. (2004) Stress dilatancy in very loose sand, Canadian Geotechnical Journal, No. 41, Oct 2004, pp. 972-989.

Bolton, M.D. (1986) The strength and dilatancy of sands, Geotechnique, 36, No. 1, pp. 65 -78.

Boussinesq, J. (1883) Application des Potentials a L'Etude de L'Equilibri et due Mouvement des Solides Elastiques, Gauthier- Villars, Paris.

Boyce, J. R. (1976) The behavior of a granular material under repeated load." Ph.D. Thesis, Department of Civil Engineering, University of Nottingham, U.K.

Brink, A.B.A. (1983) Engineering geology of Southern Africa, Karoo Sequence, vol. 3, Building Publications, South Africa, pp. 179-199.

Brinkgreve et al. (2002) PLAXIS – 2D –Version 8 (Material Models), A.A. Balkema Publisher, the Netherlands, 2002, pp.1-1 to 9-10.

Brown, S.F. (1969) The “structural design” approach to flexible pavement Design, Proceedings of the first conference on asphalt pavements for Southern Africa, Secretary Birds (Pty) Ltd, Durban, Jul-Aug,1970, pp. 5A/1-5D/11.

Burmister, D. M. (1943) The Theory of Stresses and Displacements in Layered Soil Systems and applications to the Design of Airport Runways, Proceedings, Highway Research Board, Vol. 23, pp. 126-144.

Burmister, D. M. (1945) The General Theory of Stresses and Displacements in Layered Soil Systems, Journal of Applied Physics, Vol. 16, pp. 84-94, 126- 127 and 296-302.

Burt, M.E. (1969) Research on Pavement Design, Proceedings of the first conference on asphalt pavements for Southern Africa, Secretary Birds (Pty) Ltd, Durban, Jul-Aug,1970, pp. 5D/1-5D/15.

Cleaver, J.A.S, Nedderman, R.M. and Thorpe, R.B. (2000) Accounting for granular material dilation during the operation of an annular shear cell, Advanced Powder Technology, Vol. 11, No. 4, pp. 385-399.

CSRA (1985) Traffic Guidelines for road construction materials, Technical Recommendations for Highways TRH 14, Department of Transport, Committee of State Road Authorities, Pretoria, South Africa, 1991, pp. 1-33.

CSRA (1991) Traffic loading and rehabilitation design, Technical Recommendations for Highways Draft TRH 16, Department of Transport, Committee of State Road Authorities , Pretoria, South Africa, 1991, pp. 1-33.

CSRA (1996) Structural design of flexible pavements for interurban and rural roads, Technical Recommendations for Highways Draft TRH 4, Department of Transport, Committee of State Road Authorities, Pretoria, South Africa, 1996, pp. 1-101.

Craig, R.F. (2004) Craig’s Soil Mechanics, Seventh Edition, Spon Press, London and New York pp. 71 -105.

Davis, R.O.E. and Bennett, H.H. (1927) Grouping of soils on the basis of mechanical analysis, circular no. 419, U.S. Department of Agriculture, Jan 1927.

De Beer, M. (1991) Use of the Dynamic Cone Penetrometer (DCP) in the design of road structures, Research Report DPVT-187, Division of Roads and Transport Technology, CSIR, Pretoria.

De Beer, M., Fisher, C., Jooste, F. (1997) Determination of pneumatic tyre/pavement interface contact stresses under moving loads and some effect on pavements with thin asphalt surfacing layers, Proceedings of 8th International Conference on Asphalt Pavement, Seattle, USA, Aug, 1997, pp. 179-227.

De Beer, M., Kannemeyer, L., and Ficher C. (1999) Towards improved mechanistic design of thin asphalt layer surfacing based on actual tyre/pavement contact stress-in-motion (SIM) data in South Africa, Proceedings of the 7th conference on asphalt pavements for South Africa, Sun City, South Africa, 1999, pp. 1 – 33.

De Beer, M., Fisher, C. and Kannemeyer, L (2004) Tyre-pavement interface contact stress on flexible pavements – quo vadis?, Proceedings of the 8th Conference of Asphalt Pavements of Southern Africa (CAPSA), Sun City, South Africa, Sept. 2004, pp. 1-26.

Dehlen, G.L (1969) Limitations to the use of thin surfacing and unbound aggregate bases for pavements, Proceedings of the First conference on asphalt pavements for Southern Africa, Secretary Birds (Pty) Ltd, Durban, Jul-Aug,1970, pp. 3B/1-3B/9.

De Josselin de Jong, G. (1976) Rowe's stress-dilatancy relation based on friction, Geotechnique 26, No. 3, pp. 527 – 534.

Duncan, J.M. and Chang, C.Y. (1970) Nonlinear analysis of stress and strain in soils, Journal of the Soil Mechanics and Foundations Division, Vol. 96, No. SM5, Sept/Oct 1970, pp. 1629-1653.

Freeme, C. R. (1983) Evaluation of Pavement Behaviour for Major Rehabilitation of Roads, Technical Report RP/19/83, National Institute for Transport and Road Research, CSIR, Pretoria, South Africa, 1983.

Fuller, W. and Thompson, S.E. (1907) The laws of proportioning concrete, Transactions of the American Society of civil Engineers, paper no. 1053, pp. 67 – 143.

GEO-SLOPE International Ltd (2007) Stress-deformation modeling with SIGMA/W 2007, Second Edition, GEO-SLOPE International ltd, Calgary, Alberta, Canada, May 2007, pp. 107 -152.

Government Printer (1981), Geological map: Sheet no. 2526 - Rustenburg, 1: 250 000 scale, Government Printer, Pretoria, South Africa, 1981.

Guo, P. and Su, X. (2007) Shear strength, interparticle locking, dilatancy of granular materials, Canadian Geotechnical Journal, No. 44, Jun 2007, pp. 579-591.

Head, K.H. (1992a) Manual of Soil Laboratory Testing, Volume 1: Soil Classification and Compaction Tests, 2nd Edition, Prentech Press Limited, London, pp.59-109, 116-149, 159-205, 302-356.

Head, K.H. (1992b) Manual of Soil Laboratory Testing, Volume 2: Permeability, Shear strength and Compression Tests, 2nd Edition, Prentech Press Limited, London, pp. 148-159, 189-248.

Hicks, R. G. and Monismith, C. L. (1971) Factors Influencing the Resilient Properties of Granular Materials, Transportation Research Record 345, Transportation Research Board, National Research Council, Washington, DC, 15-31.

Highway Research Board (1961) The AASHO Road test, History and description of the project, Special Report No. 61A, National Academy of Science, National Research Council, 1961, pp i – v.

Hill, R. (1950) The mathematical theory of plasticity, Oxford university press, London UK.

Hoffman, C. (2008) *Loads*
INTERNET: http://www.pavementinteractive.org/index.php?title=Loads
Last Cited: 3 April 2011

Horak, E. (2008) Benchmarking the structural condition of flexible pavements with deflection bowl parameters, Journal of the South African Institute of Civil Engineering, vol. 50, No. 2, Jun 2008.

Huang, Y. H., (2004). Pavement Analysis and Design. 2nd Edition, Prentice Hall, Inc., New Jersey, USA, 2004 pp. 1 - 652.

Jooste, F.J (2004) A Re-evaluation of some aspects of the Mechanistic-Empirical Design Approach, Proceedings of the 8th Conference on Asphalt Pavements for Southern Africa, Sun City (CAPSA), Sun City, South Africa, 2004.

Jordaan, G. J. (1989) Guidelines towards the use of the Asphalt Institute's Method for Pavement Rehabilitation Design, Technical Report DPVT 55, Division for Roads and Transport Technology, CSIR, Pretoria.

Kim, D., Salgado, R. and Altschaeffl, G. (2005) Effects of super single tyre loadings on pavements, Journal of Transportation Engineering, ASCE, Oct 2005 pp. 732-742.

Kim, YR, Ban, H. and Im, S (2009) Impact of Truck Loading on Design Analysis of Asphaltic Pavement Structures, Report No 25-1121-0001-223, Mid-American Transport Center, University of Nebraska-Lincoln, Dec 2009.

Kleyn, E.G. (1984) Aspects of pavement evaluation and design as determined with the Dynamic Cone Penetrometer (DCP), Report L6/84, Transvaal Roads Department, Material Branch, Pretoria.

Kleyn, E.G. (2012) Successful G1 crushed stone base-course construction, proceedings of the 31st Southern African Transport Conference, Pretoria, South Africa, Jul. 2012, pp. 110 – 118.

Lekarp, F., Isaacson, U. and Dawson, A. (2000a) State of the Art. I: Resilient Response of Unbound Aggregates, Journal of Transportation Engineering, ASCE, Vol. 126, No. 1, 66-75.

Lekarp, F., Isaacson, U. and Dawson, A. (2000b) State of the Art. II: Permanent Strain response of Unbound Aggregates, ASCE, Vol. 126, No. 1, 76-83.

Li, X.S. and Dafalias, Y.F. (2000) Dilatancy of cohesionless soils, Geotechnique, 50 (4) pp. 449 – 460.

Lytton, R. L. (1995) Foundations and Pavements on Unsaturated Soils, 1st International Conference on Unsaturated Soils. Paris.

Maina, J. W., Denneman, E., De Beer, M., (2008) Introduction of new road pavement response modelling software by means of benchmarking, Proceedings of the 27th Annual Southern African Transport Conference, South Africa, July 7–11, 2008. ISBN: 978-1-920017-34-7.

Marais, G.P. (1969) The design of lightly trafficked roads in the Transvaal, Proceedings of the first conference on asphalt pavements for Southern Africa, Secretary Birds (Pty) Ltd, Durban, Jul-Aug,1970, pp. 1A/1-1A/11.

Maree, J. H. (1978) Design Parameters for Crushed Stone in Pavements (Afrikaans) M Eng thesis, Department of Civil Engineering, Faculty of Engineering, University of Pretoria, South Africa, 1978.

Maree, J.H. and Freeme, C.R. (1981) The Mechanistic Design Method used to evaluate the pavement structures in the catalogue of the Draft TRH4 1980, Technical report RP/2/81, National Institute for Transport and Road Research, CSIR, Pretoria, South Africa, Mar 1981, pp. 1-27.

Maree, J.H. (1990) Structural classification of pavement structures using measured deflection bowl parameters, The IDMP program, Scott & de Waal Inc, Sandton.

Morton, B.S., Luttig, E., Horak, E. and Visser, A.T. (2004) The effect of axle load spectra and tyre inflation pressures on standard pavement design methods, Proceedings of the 8th Conference of Asphalt Pavements of Southern Africa (CAPSA), South Africa, Sun City Sept, 2004, pp. 1-26.

NATIONAL ROAD TRAFFIC ACT, 1996 (South African Act No. 93 of 1996), Notice 1359 of 2008.

Nova, R. (91982) A constitutive model under monotonic and cyclic loading, Soil Mechanics – transient and cyclic loads, ed. Pande, G. and Zienkiewicz, O.C., John Wiley & Sons Ltd., New York. Pp. 343 – 373.

Perret, J. (2002) The effect of loading conditions on pavement responses calculated using a linear elastic model. Proceedings of the 3rd International Symposium on 3D Finite Element for Pavement Analysis, Design and Research, Amsterdam, The Netherlands, 2002, pp. 283-303
INTERNET: http://infoscience.epfl.ch/record/115364/files/3DFEM-Perret.pdf
Last Cited: 3 April 2011.

Porter, O.J. (1943) Foundations for flexible pasvements, Proceedings of the 22nd annual meeting of the Highway Research Board, Washington, D.C., Dec 1942, pp. 100 – 143.

Reynolds, O. (1885) On the dilatancy of media composed of rigid particles in contact, Philosophical magazine and journal of science, fifth series, Vol. 20, No.127, Dec 1885 pp. 469-281.

Rohde, G.T. (1994) Determining pavement structural number from FWD testing, Transport Research Record 1448, Transport Research Board, National Research Council, Washington DC, USA.

Roscoe, K.H. and Burland, J.B. (1968) On the generalized stress-strain behaviour of wet clay, Engineering Plasticity, ed. Heyman, J. and Leckie, F.A., Cambridge University Press, London, UK, pp. 535 – 609.

Rowe, P.W. (1962) The stress-dilatancy relation for static equilibrium of an assembly of particles in contact, Proceedings of the Royal Society of London, Series A, Mathematical and Physical Sciences, Vol. 269,No. 1339, Oct 1962, pp. 500 – 527.

Sampson, L.R. (1984) Investigation of the correlation between CBR and DCP, Technical Note TS/33/84, Division of Roads and Transport Technology, CSIR, Pretoria.

SANRAL (2013) South African Pavement Engineering Manual: Chapter 9 – Materials utilization and design, South African National Roads Agency Revision 1, RSA.

Schanz, T. and Vermeer, P.A. (1996) Angles of Friction and Dilatancy of Sand. Geotechnique 46, pp. 145 – 151.

Schanz, T. et al. (1999) Formulation and verification of the hardening soil model, In. Brinkgreve, Beyond 2000 in Computational Geotechniques, Balkema, Rottedam, pp. 281 – 290.

Schofield, A. and Wroth, C.P. (1987) Critical state soil mechanics, McGraw-Hill, London, UK.

Seed, H. B., Chan, C. K. and Monismith, C. L. (1955) Effects of Repeated Loading on the Strength and Deformation of Compacted Clay, Proceedings, Highway Research Board, 34, Washington, DC, pp. 541 – 558.

Semmelink, C. and Visser, A.T. (1994) Effect of material properties on compactibility and bearing capacity, Journal of Transportation Engineering, Vol. 120, No. 4, Jul. 2004 pp. 570 – 589.

Simoni, A. and Houlsby, G.T. (2006) The direct shear strength and dilatancy of sand-gravel mixtures, Geotechnical and Geological Engineering, Vol. 24, Issue No. 3 pp. 523 – 549.

Shibuya, S., Mitachi, T. and Tamante, T.A. (1997) Interpretation of direct shear box testing of sands as quasi-simple shear, Geotechnique, volume 47, issue no. 4, pp 57 – 86.

Tatsuoka, F., Nakamura, S., Huang, C and Tani, K. (1990) Strength anisotropy and shear band direction in plane strain tests in sand, Soil foundations, volume 30, issue no, 1, pp. 35 – 54.

Taylor, D.W. (1948) Fundamentals of Soil Mechanics, John Wiley & Sons, New York, USA, pp. 311 – 362.

Terzaghi, K., Peck, R.B. and Mesri, G. (1996) Soil mechanics in engineering practice, 3rd edition, John Wiley & Sons Inc., New York, USA, pp. 138 – 139.

TMH (1986) TMH 1: Standard Methods of testing road construction materials, 2nd Edition, Technical Methods for Highways, Pretoria, South Africa, 1985, pp 1 – 232.

Theyse, H.L. *et al.* (1995) TRH4 Revision (1995): Phase I: Updating the South African Mechanistic Design Method, National Service Contract NSC24/1, Report No. I/PA/13/95, Department of Transport, Division of Roads and Transport, CSIR, Pretoria, 1995, pp. 1.1 – 7.4.

Theyse, H.L. *et al.* (1996) Overview of the South African Mechanistic pavement Design Analysis Method, DP96/005, presented at the 75th Annual Transport Research Board Meeting, Washington D.C. , Paper No.961294 Mar 1996, pp. 1 – 40.

Theyse H.L. (2000) The development of mechanistic-empirical permanent deformation design models for unbound pavement materials from laboratory and accelerated pavement test data, Proceedings of the 5th International Symposium on Pavement unbound, Nottingham, England, July 2000, pp. 285 – 293.

Theyse, H.L. (2004) Empirical shear strength models for unbound road building materials, Proceedings of the 6th International Symposium on Pavement unbound (UNBAR 6), Nottingham, England, July 2004, pp. 250 – 262.

Theyse, H.L. (2007) A Mechanistic-Empirical design model for unbound granular pavement layers, PHD Thesis, University of Johannesburg, Johannesburg, South Africa.

Theyse, H L. and Kannemeyer, L. (2010) New directions in the design of unbound granular layers in road pavements, Civil Engineering, SAICE, Midrand, South Africa Volume 18, No 8, Sept 2010 pp. 34 – 42.

Transportek (2001), Overview of the South African Mechanistic Pavement Design Method, mePADS Software, CSIR, Pretoria, 2001.

Uzan, J. (1985) Characterisation of Granular Material, Transportation Research Record 1022, TRB, National Research Council, Washington DC, pp. 52-59.

Van Niekerk, A.A. and Huurman, M. (1995) Establishing complex behaviour of unbound road building materials from simple material testing, report no. 7-95-200-16, Delft University of Technology, Delft, The Netherlands, pp. 57.

Van Vuuren, D. J. Otte, E. and Paterson, W.D.O (1974) The structural Design of Flexible Pavement in South Africa, Proceedings of the 2nd Conference on Asphalt Pavements in South Africa, Durban, 1974.

Vokas, C. A. and Stoll D. S. (1985) Reinforced Elastic Layered System, Transportation Research Record, Issue No. 1153, pp. 1-7.

Walker, R. N., Paterson, W. D. O., Freeme, C. R. and Marais, C. P. (1977) The South African Mechanistic Pavement Design Procedure. Proceedings of the fourth International Conference on the Structural Design of Asphalt Pavements, University of Michigan, Ann Arbor, Michigan, U S A.

Werkmeister, S. (2003) Permanent deformation behaviour of unbound granular materials in pavement construction, PHD Thesis, University of Dresden, Apr. 2003 pp. 2-1 to 2-25.

Wolff, H. (1996) Elasto-plastic modeling of granular layers, Research no. 92/312, Report No. 92/312, Department of Transport, Division of Roads and Transport, CSIR, Pretoria, Mar 1996, pp. 1-1 to 5-22.

Yoder, E.J. and Witczak, M.W. (1975) Principles of pavement Design, Second Edition, John Wiley & Son Inc., New York, USA, pp. 24 – 76.

BIBLIOGRAPHY

Paterson, W.D.O. (1977a) Evaluating the structural response of a pavement and the moduli of Materials – a review, Report No. RP/1/74, National Institute for transport and road research, South Africa, May 1977.

Paterson, W.D.O. (1977b) Considering the pavement as a mechanism, Technical Report RP/3/77, National Institute for Transport and Road Research, South Africa, Dec 1977, pp1 - 35.

APPENDIX 1

Transfer Functions of continuously graded and gap graded asphalt, cemented materials, thick asphalt and subgrade

Table A1: Transfer Functions for continuously graded and gap graded asphalt, cemented materials, thick asphalt and subgrade (after Theyse *et al.*, 1995).

	50% Transfer function	80% Transfer function	90% Transfer function	95% Transfer function
CONTINUOUSLY GRADED ASPHALT	$N_f = 10^{17.71\left(1-\frac{Log\epsilon_t}{3.46}\right)}$ $\epsilon_t = 10^{\left(3.46-\frac{LogN_f}{5.11931}\right)}$	$N_f = 10^{17.54\left(1-\frac{Log\epsilon_t}{3.42}\right)}$ $\epsilon_t = 10^{\left(3.42-\frac{LogN_f}{5.11931}\right)}$	$N_f = 10^{17.46\left(1-\frac{Log\epsilon_t}{3.41}\right)}$ $\epsilon_t = 10^{\left(3.41-\frac{LogN_f}{5.11931}\right)}$	$N_f = 10^{17.40\left(1-\frac{Log\epsilon_t}{3.40}\right)}$ $\epsilon_t = 10^{\left(3.40-\frac{LogN_f}{5.11931}\right)}$
GAP GRADED ASPHALT	$N_f = 10^{16.09\left(1-\frac{Log\epsilon_t}{3.774}\right)}$ $\epsilon_t = 10^{\left(3.774-\frac{LogN_f}{4.26265}\right)}$	$N_f = 10^{15.93\left(1-\frac{Log\epsilon_t}{3.736}\right)}$ $\epsilon_t = 10^{\left(3.736-\frac{LogN_f}{4.26265}\right)}$	$N_f = 10^{15.85\left(1-\frac{Log\epsilon_t}{3.719}\right)}$ $\epsilon_t = 10^{\left(3.719-\frac{LogN_f}{4.26265}\right)}$	$N_f = 10^{15.79\left(1-\frac{Log\epsilon_t}{3.705}\right)}$ $\varepsilon_t = 10^{\left(3.705-\frac{LogN_f}{4.26265}\right)}$
CEMENTED MATERIAL CRUSH INITIATION	$N_{Ci} = 10^{8.216\left(1-\frac{\sigma_v}{1.21UCS}\right)}$ $\frac{\sigma_v}{UCS} = 1.21 - \frac{logN_{ci}}{6.8016}$	$N_{Ci} = 10^{7.706\left(1-\frac{\sigma_v}{1.13UCS}\right)}$ $\frac{\sigma_v}{UCS} = 1.13 - \frac{logN_{ci}}{6.8016}$	$N_{Ci} = 10^{7.506\left(1-\frac{\sigma_v}{1.10UCS}\right)}$ $\frac{\sigma_v}{UCS} = 1.10 - \frac{logN_{ci}}{6.8016}$	$N_{Ci} = 10^{7.386\left(1-\frac{\sigma_v}{1.09UCS}\right)}$ $\frac{\sigma_v}{UCS} = 1.09 - \frac{logN_{ci}}{6.8016}$
CEMENTED MATERIAL ADVANCED CRUSHING	$N_{ca} = 10^{8.894\left(1-\frac{\sigma_v}{1.31UCS}\right)}$ $\frac{\sigma_v}{UCS} = 1.31 - \frac{logN_{ca}}{6.8016}$	$N_{ca} = 10^{8.384\left(1-\frac{\sigma_v}{1.23UCS}\right)}$ $\frac{\sigma_v}{UCS} = 1.23 - \frac{logN_{ca}}{6.8016}$	$N_{ca} = 10^{8.184\left(1-\frac{\sigma_v}{1.20UCS}\right)}$ $\frac{\sigma_v}{UCS} = 1.20 - \frac{logN_{ca}}{6.8016}$	$N_{ca} = 10^{8.8064\left(1-\frac{\sigma_v}{1.19UCS}\right)}$ $\frac{\sigma_v}{UCS} = 1.19 - \frac{logN_{ca}}{6.8016}$
CEMENTED MATERIAL EFFECTIVE FATIGUE	$N_{eff} = 10^{7.06\left(1-\frac{\epsilon}{7.86\epsilon_b}\right)}$ $\frac{\epsilon}{\epsilon_b} = 7.86 - 1.114logN_{eff}$	$N_{eff} = 10^{6.87\left(1-\frac{\epsilon}{7.66\epsilon_b}\right)}$ $\frac{\epsilon}{\epsilon_b} = 7.66 - 1.114logN_{eff}$	$N_{eff} = 10^{6.84\left(1-\frac{\epsilon}{7.63\epsilon_b}\right)}$ $\frac{\epsilon}{\epsilon_b} = 7.63 - 1.114logN_{eff}$	$N_{eff} = 10^{6.72\left(1-\frac{\epsilon}{7.49\epsilon_b}\right)}$ $\frac{\epsilon}{\epsilon_b} = 7.49 - 1.114logN_{eff}$
THICK ASPHALT BASES	$N_f = 10^{A\left(\frac{1\times Loge_t}{B}\right)}$			
SUBGRADE	$N_f = 10^{A\times Loge_v}$			

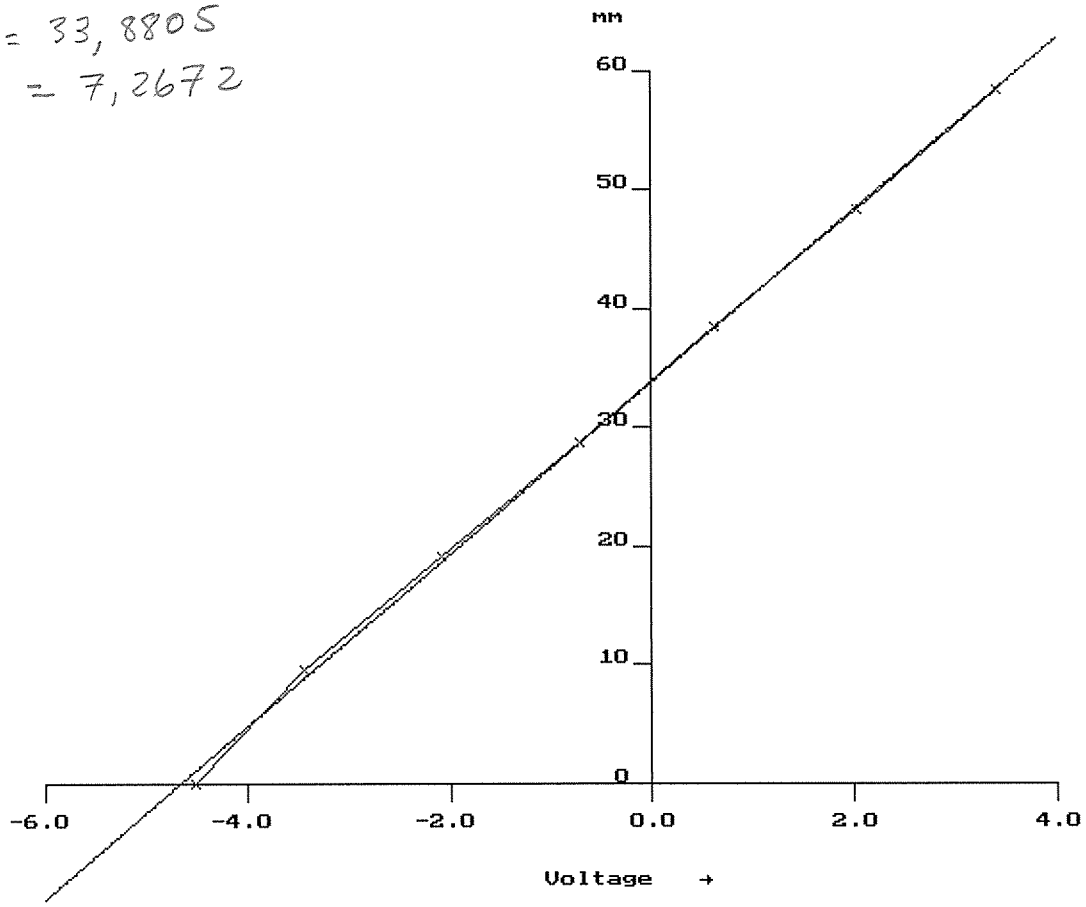
APPENDIX 2

Calibration Results for converting data logger output from volts (V) and millivolts (mV) to millimeters (mm) and kiloNewtons (kN)

==========
Least-squares straight line fit: y = a + bx
==========

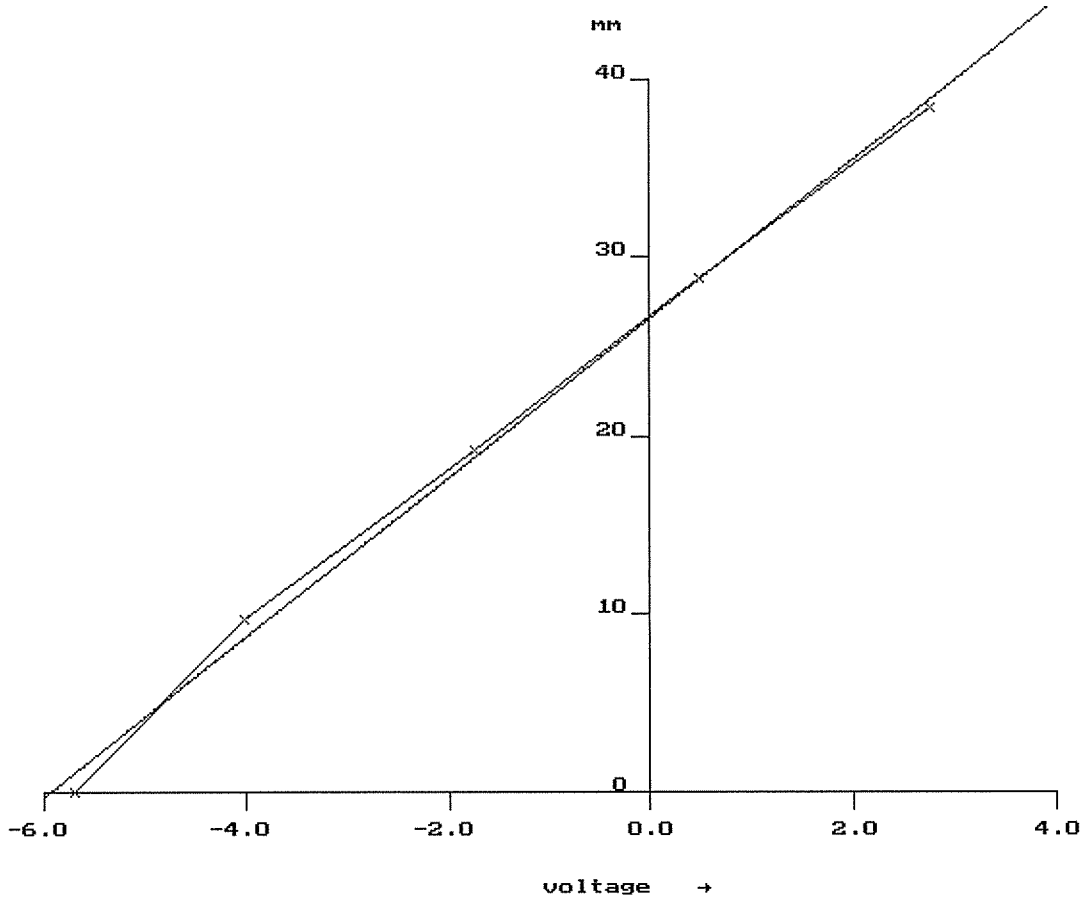
LVDT 1033

a = 33,8805
b = 7,2672



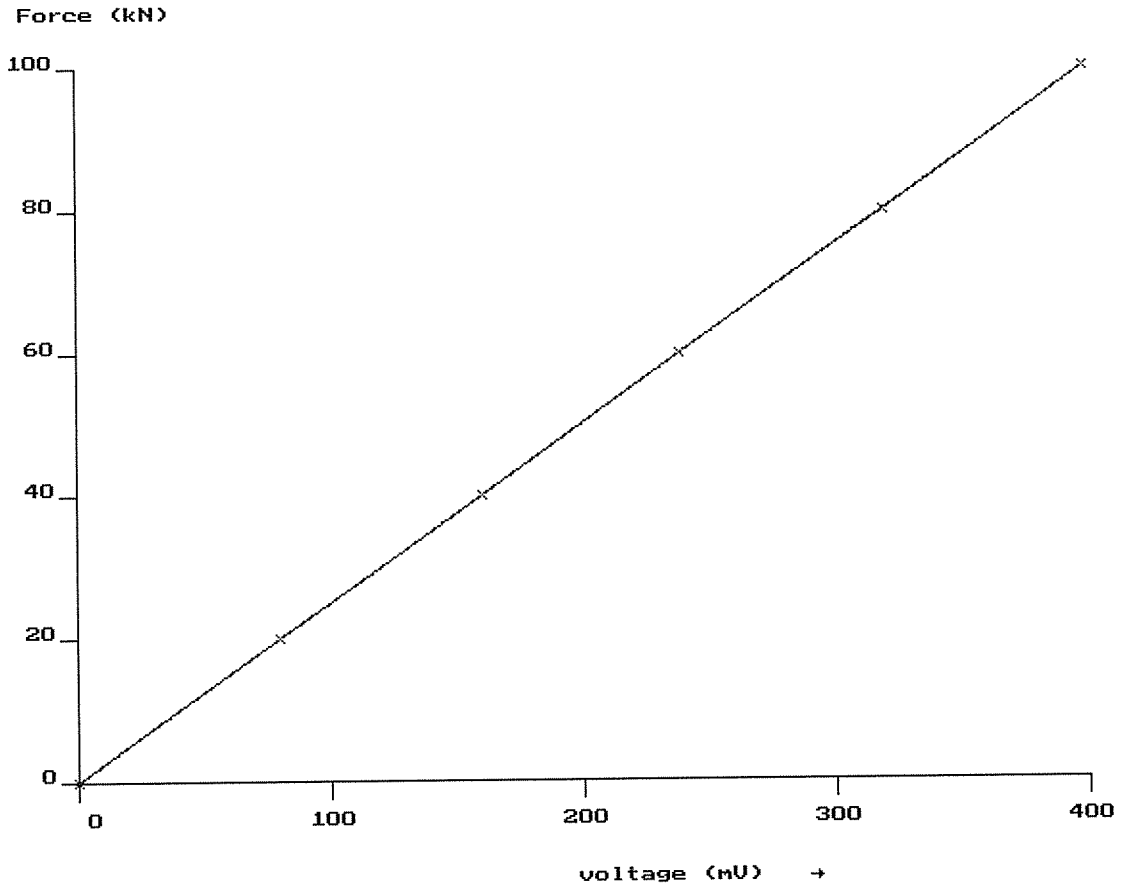
==========
Least-squares straight line fit: y = a + bx
==========

LVDT 587



==========
Least-squares straight line fit: y = a + bx
==========

Horizontal load cell : 44927



==========
Least-squares straight line fit: y = a + bx
==========

Vertical Load Cell 921169

